Finite element mesh optimization using the partial p-adaptive method for stress analysis of underground excavations

Diego Fernando Garcia Rosero

A Thesis

in

The Department

of

Building, Civil and Environmental Engineering

Presented in Partial Fulfillment of the Requirements

For the Degree of Master of Applied Science (Civil Engineering) at

Concordia University

Montreal, Quebec, Canada

November 2011

CONCORDIA UNIVERSITY

School of Graduate Studies

This is to certify that the thesis prepared

By: Diego Fernando GARCIA ROSERO

Entitled: Finite element mesh optimization using the partial p-adaptive

                                   method for stress analysis of underground excavations

and submitted in partial fulfillment of the requirements for the degree of

Master of Applied Science (Civil Engineering)

complies with the regulations of the University and meets the accepted standards with

respect to originality and quality.

Signed by the final examining committee:

_____ - Dr. Ali DOLATABADI (MIE)

_____ - Dr. Adel HANNA (BCEE)

_____ - Dr. S Samuel LI (BCEE)

_____ - Dr. Attila M. ZSAKI (BCEE) – Supervisor

Approved by   _____

                                  Dr. Maria Elektorowicz

                                  Graduate Program Director

October 10th 2011   _____

                                  Dr. Robin A. L. Drew

                                  Dean of Faculty

ABSTRACT

Finite element mesh optimization using the partial p-adaptive method for stress analysis of underground excavations

Diego Garcia Rosero, MASc

Concordia University, 2011

Savings in computational resources have become a main subject of study in geomechanics due to the complexity of the problems analyzed. This thesis develops and evaluates the performance of a partial p-adaptive mesh optimization method for stress analysis of underground excavations. The method uses transition finite elements in order to connect a mesh of quadratic (triangular or quadrilateral) elements with a mesh of linear (triangular or quadrilateral) elements. The analysis is performed using SIMFEM, a computer program that solves plane strain problems and is able to handle this type of mixed meshes. After the formulation of 4 types of transition elements (5-node, 7-node quadrilateral, 4-node and 5-node triangle), which were incorporated into the code, 57 models (including the analysis of a pressurized cavity) were run, analyzed and for some of the models, the results obtained were compared to commercial software, as to ensure the correct behaviour of these elements in a finite element mesh. A final application was performed modeling a continuum with two circular excavations, surrounded by a linear elastic material in a biaxial stress field, obtaining favourable results. The global stiffness matrix size was reduced by 85.4% and by 74.1% for the models using triangles and quadrilaterals respectively, as a result, the calculation times were considerably reduced. The average percentage of error with respect to the models without optimization, measured at eight critical points, was 0.15% and 2.63% in the case of triangular and quadrilateral elements respectively.

ACKNOWLEDGEMENTS

It is a pleasure to thank those who made this thesis possible, especially my supervisor, Dr. Attila Zsaki, whose guidance, wisdom and knowledge were essential to route this research project from the initial to the final stage. Probably, without his help the overwhelming amount of information obtained from the models run and the theoretical background would have become an assembly of numbers without sense, but his way to channel all the ideas and concepts towards the final objective was even a lifelong learning lesson.

Lastly, I offer my regards, blessings and gratitude to all those who supported me and walked beside me during this amazing period of my life, my friends in Montreal and especially my parents and the rest of my family in Colombia who were there supporting and encouraging me and being a special part in this important enterprise in my life.

"Make everything as simple as possible, but not simpler" – Albert Einstein

TABLE OF CONTENTS

Page

LIST OF FIGURES

Page

LIST OF TABLES

Page

NOMENCLATURE

A	Equilibrium matrix
a	Radius of a circular opening (m)
B	Compatibility, deformation-displacement, strain-displacement matrix
D	Disturbance
E	Modulus of Elasticity (MPa)
f	Vector of forces
h	Depth of overburden (m)
K	Stress ratio (horizontal stress/vertical stress)
K	Stiffness matrix
N_i	Shape function for the i-th node
r	Radial distance from center of an opening (m)
S	Rigidity, material, constitutive matrix
U	Vector of displacements (m)
γ	Unit Weight (kN/m³)
ρ	Density of rock mass (kg/m³)
ζ	Natural coordinate for quadrilateral elements
η	Natural coordinate for quadrilateral elements
ζ_i	Natural coordinate for triangular elements, i = 1, 2 or 3
ν	Poisson's ratio
σ_r	Radial stress (MPa)
σ_θ	Tangential stress (MPa)
σ_H	γh = Horizontal pressure *in situ* (MPa)
σ_V	Geostatic overburden pressure (MPa)
σ_1	Major principal stress in a biaxial stress field (MPa)
σ_3	Minor principal stress in a biaxial stress field (MPa)
σ_{xx}	Horizontal stress (MPa)
σ_{yy}	Vertical stress (MPa)
θ	Central angle with x-axis (CCW is positive)
$\tau_{r\theta}$	Shear stress related to σ_r and σ_θ (MPa)
τ_{HV}	Shear stress related to σ_H and σ_V (MPa)
U_x	Displacement in horizontal direction (m)
U_y	Displacement in vertical direction (m)
U_T	Total displacement (m)

1. INTRODUCTION

The optimization of resources in computational sciences has been an important concern since the beginning of their application in engineering, and will be a matter of discussions and new developments as long as the science continues advancing. The application of methods and theories, especially the latest developments in the field of engineering imply the usage of important quantities of computational resources, which in some cases do not seem to evolve as fast as the theory requires.

In order to solve problems in geomechanics, a considerable amount of computational resources is required by all the different numerical methods available, due to the nature of these problems, which imply *"involving nonlinear and time dependent material behaviour, arbitrary geometries, initial or in situ conditions, multi-phase media, different loadings (static, quasi-static, cyclic and dynamic), and such environmental factors as temperature, fluids and pollutant movement" (Desai, and Gioda, 1990)*. Thus, the implementation of these numerical methods has taken place progressively, starting by the least expensive method in terms of computational resources to the most complex and complete. For better understanding of this thesis, a very brief and conceptual explanation of the most popular numerical methods in geomechanics are stated in chapter 2.

All these approaches have been implemented to describe the behaviour of geomaterials throughout engineering's history and a good example is the Finite Element Method (FEM), which is the method used in this thesis. The FEM, whose first developments were done in early 1940s by Hernnikoff and Courant, who proposed radically opposite approaches of the discretization of a domain. However, it was only a few decades ago, when the computer capacity required became available, that these works caught the attention of the engineering community (Rao, 2011).

Despite undeniable advances of computer science and software engineering, complex and large problems in geomechanics, especially those involving 3 dimensions require a considerable amount of memory and the use of state-of-the-art processors to be run, nevertheless the processing times are in the order of magnitude of days or even weeks, which leads to endless calculations an extremely high engineering cost.

Due to the nature of the geotechnical engineering, repetitive calculations or ever changing conditions and parameters are always obstacle for the engineer, long calculation times are seldom afforded by the projects and it is reflected either in delays

1

or last minute decision-making meetings, where the expert staff involved comes up with a design solution taking as criteria only the experience and a good judgement, setting aside the advantages of a calculation tool.

Aiming to implement these extensive models that can provide invaluable forecasting in geotechnical problems, several methods were developed to reduce the calculation times by essentially reducing the number of nodes and/or elements which subsequently decreases the size of the matrices and vectors required to solve the problem.

One of the ways to reduce the size of the problem without affecting the accuracy or the quality of the solution is the adaptive re-meshing. This method modifies an existing mesh used to discretize a given media either by changing the elements, the nodes or the order of the elements. The types of mesh refinement are listed at this stage nonetheless are further elaborated on subsequent pages;

- r-adaptivity
- h-adaptivity

- p-adaptivity
- hp-adaptivity

In this thesis, a p-refinement process is implemented through the modeling of plane strain problems that included as main test the modeling of two excavations assumed to be of circular shape in a continuum of elastic medium; and the stresses in the elastic medium caused by these openings were calculated following the analytical solution given by Kirsch (1898) (Ramamurthy, 2007) for infinite plates with circular holes. The elements changing their order were those where the percentage of disturbance caused by the excavation was below a defined value (Zsaki et al, 2005).
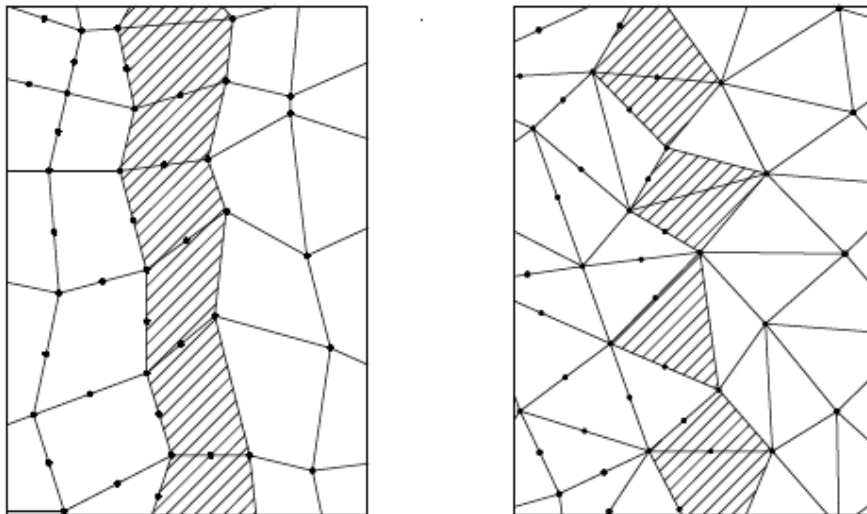
Figure 1. Transition elements (shaded) in meshes with quadrilateral and triangular elements

2

The elements used to discretize the zone were assumed as linear order (with respect to displacement) and in zones where the percentage of disturbance was above the set value, the elements were assumed as quadratic order (with respect to displacement); this criterion implied the formulation of transition elements, which are located in the zones where the quadratic order elements meet with the linear order elements (Figure 1).

To execute this process, the formulation of transition elements was necessary and eventually these elements intended to perform the stress analysis were tested for their accuracy and behaviour through several tests whose characteristics and results are shown and discussed in chapter 5.

Since there is no relevant commercial software in the context of geomechanics, that is able to include in a given FEM both linear and quadratic order elements and the transition elements, the development of a new tool was necessary. The SIMFEM (Zsaki, 2010) code is program written in C++ intended for research purposes that solves plane strain problems and allows including the formulation of transition elements within the code.

Some of the main features of the SIMFEM code include the capability to output all the results of the calculation including stresses and displacements either by text files or graphic files. The results obtained are shown throughout this thesis.

1.1 THESIS OBJECTIVE

The objective of this thesis is to evaluate the possibility in the reduction of the calculation times and the computer memory usage by reducing the degrees of freedom used to solve a finite element model, without affecting the quality of the solution. This is achieved by removing a certain amount of nodes in the elements comprising the model. Evidently, in order to maintain the mathematical coherence of matrices and vectors involved in the operations, this process has to comply with a set of criteria.

1.2 DETAILED OBJECTIVES

- Implement and test the accuracy of the transition elements. The elements to be included in this formulation and later testing are: a 7-node quadrilateral element,

a 5-node quadrilateral element, a 5-node triangular element and 4-node triangular element (Gupta, 1975, Felippa, 2010).

- Define a disturbance percentage in the media assumed. This parameter is used to define the boundary where quadrilateral elements are replaced by linear elements and, consequently, define the location of the band of transition elements.

- Use the analytical solution given by Kirsch (1898) for an infinite plate with circular holes in order to define the Excavation Disturbed Zones (EDZ) and therefore define transition zones from quadratic order to linear order elements. This is applied with the modelling of two circular excavations in an elastic continuum.

- Change the amount of nodes and the types of elements (quadrilateral, linear and transition) by applying the mesh optimization process, in order to compare the quality and memory usage of several numerical solutions.

2. LITERATURE REVIEW – NUMERICAL STRESS ANALYSIS IN GEOMECHANICS

In order to create a context for this thesis, the main concepts necessary to understand the algorithm applied to improve the stress analysis for underground excavations are compiled in this chapter. The review will cover the numerical techniques for finding approximate solutions to Partial Differential Equations (PDE) in geomechanics and presents an overview of mesh optimization techniques.

The numerical techniques summarized are: Finite Difference Method (FDM), Discrete Element Method (DEM), Boundary Element Method (BEM) and Finite Element Method (FEM). The method implemented in this thesis is the FEM, thus an extensive description is provided and includes most of main concepts of the method.

The versatility of the FEM to solve partial differential equations over complex domains makes it one of the best choices in geomechanics, still, complex domains imply the usage of a considerable number of elements in a mesh (refer to chapter 2.4), which is closely related to the computational cost. In order to reduce the computational cost, mesh optimization techniques are often applied. These are summarized as well in the subsequent pages.

2.1 FINITE DIFFERENCE METHOD (FDM)

The FDM, along with the FEM, this is one of the often-used methods to solve PDE's and also was the first one applied to solve problems in geomechanics (Desai, 1977). It consists of the division of a continuum into several parts and the nodes comprising these parts must have the same distance between each other (magnitude of Δx and Δy shown in Figure 2). This dictates one of the most important restrictions of the method as a result of the existence of irregular geometries often seen in geomechanics. This implies the requirement of a special treatment of the points not coinciding exactly with the boundary of the problem, thus adding a procedure to alter the finite difference equation.

The procedure consists of transforming the partial derivatives of the PDE by the ratio of change in a variable over a small, but finite increment, as shown in equation (1).

$$\frac{du}{dx} = lim_{\Delta x \to 0} \frac{\Delta u}{\Delta x} \approx \frac{\Delta u}{\Delta x} \qquad\qquad (1)$$

After this substitution, a differential equation is converted into a difference equation that can be evaluated by three approximations, as it is presented for the first derivative in the direction of the x-axis:

Central difference $\qquad \dfrac{du}{dx} = \dfrac{u_{i+1,j}-u_{i-1,j}}{2\Delta x} + O(\Delta x)^2$

Forward difference $\qquad \dfrac{du}{dx} = \dfrac{u_{i+1,j}-u_{i,j}}{\Delta x} + O(\Delta x)$ $\qquad\qquad$ (2)

Backward difference $\qquad \dfrac{du}{dx} = \dfrac{u_{i,j}-u_{i-1,j}}{\Delta x} + O(\Delta x)$

Equation (2) can then be arranged in matrix form including all the points of interest and then solved obtaining the values of u (displacements) at all the points.
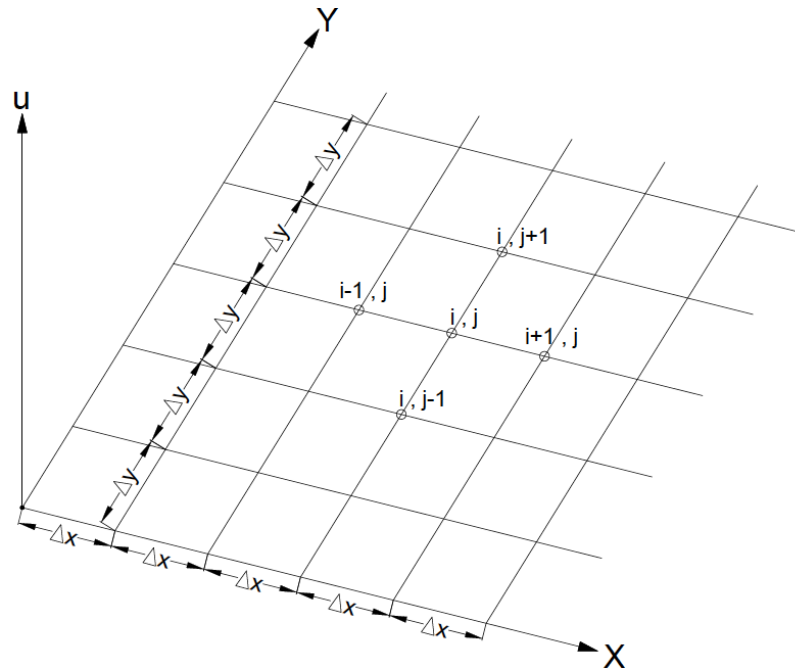
Figure 2. A Finite Difference Mesh

2.2 DISCRETE ELEMENT METHOD (DEM)

The DEM is often applied in geomechanics as well, especially when the problem considers materials found in nature as a discontinuous granular medium (soils) or bonded medium, such as sandstone (Figure 3).

The DEM allows treating the media as discontinuous and emphasizes the mechanics of the contact between distinct blocks. Therefore, each element can possess different displacements and rotations, and also might be assumed as rigid or deformable. The method requires the repeated application of Newton's laws of motion

to each particle and contact surface, while constantly updating the location of the elements.
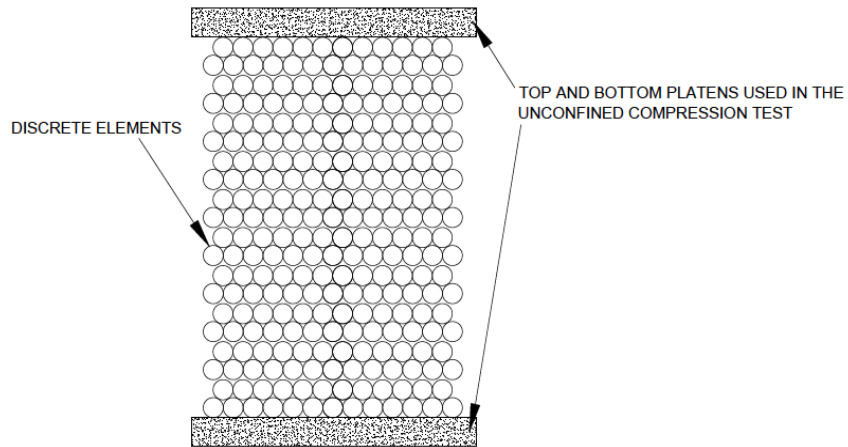
Figure 3. Idealized sandstone modeled with DEM in an unconfined compressive strength test

2.3 BOUNDARY ELEMENT METHOD (BEM)

This method solves a set of integral equations that connect the boundary. Considering its formulation, only the boundaries of the problem are required to be discretized (Figure 4) and the solution is only found at the boundary in the first stage reducing the dimensions of the problem by one; then the solutions within the body or domain are obtained numerically (Bekker, 1992).

This implies less data preparation time, faster re-meshing (if it is required), less calculation time and less storage space. Yet, in BEM, the element integrals are harder to evaluate and require a fundamental solution of the PDE, as a starting point for the rest of the solution.
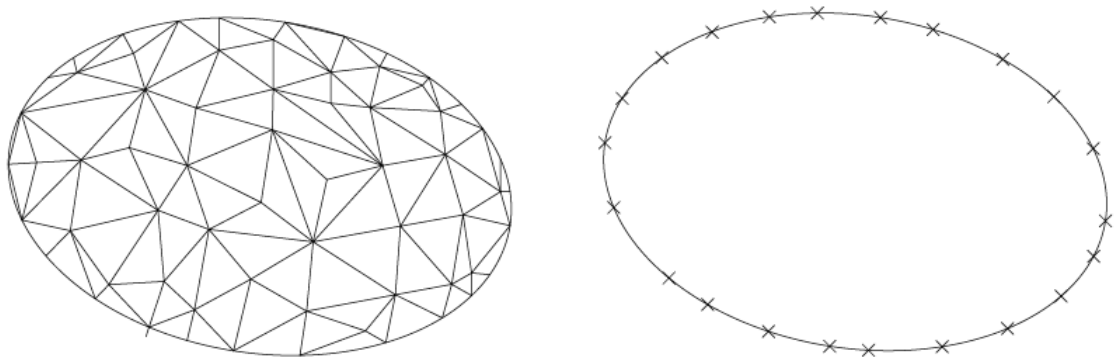
Figure 4. a) Discretization in FEM (left) and b) BEM (right)

2.4 FINITE ELEMENT METHOD (FEM)

The FEM is one of the most popular methods to solve problems in continuum geomechanics that are described by a PDE. The main principle of the FEM consists of dividing a domain into a finite number of elements (discretization). These elements are interconnected by a number of nodes (Figure 1 and Figure 4a).

The points where the variable under consideration has known values across the domain are introduced in the model (boundary conditions) and the variation of the variable is solved across each element using the stiffness matrices based on a particular set of shape functions (also called interpolation functions).

2.4.1 SHAPE FUNCTIONS

The essence of the FEM is the approximation of the PDE that govern the problem. This approximation has to be done locally on each element by shape functions and can be summarized with the following mathematical expression:

$$u \approx \sum_{i=1}^{n} N_i \cdot a_i = \boldsymbol{N} \cdot \boldsymbol{a} \qquad (3)$$

where N corresponds to the interpolating or shape functions and a is a set of unknown parameters. In the case of stress analysis, these functions represent the element geometry and the unknowns by interpolating the internal displacements directly from the nodal values. Specifically, they are responsible for representing any displacement in the elements and also provide the required consistency in the model (Felippa, 2010).

Rigid Body Translation   Rigid Body Rotation   Deformation
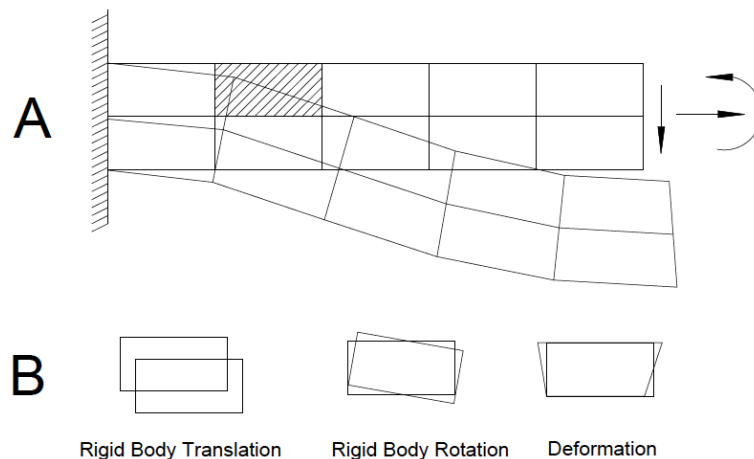
Figure 5. Different behaviors that must be represented by the shape functions. A) Deformed cantilever beam B) Behavior of hatched element

In order to obtain a difference as small as possible between the analytical solution (called exact solution) and the result obtained from the FEM, three requirements must be satisfied: proper set of shape or interpolation functions which represent adequately the behaviour of the object modeled (Figure 5), consistency and stability. These are the so-called convergence requirements.

2.4.2   REQUIREMENTS FOR CONSISTENCY

To achieve consistency in a FEM, it is required to fulfill the compatibility and completeness requirements that are explained as follows:

COMPATIBILITY: Has to be attained at two locations in the element, its boundary and within the element. Compatibility at the edge is achieved when the sharing edges of two elements have the same polynomial order and the same displacements (piecewise differentiable), so they do not leave a gap between them; for instance, when a load is applied (Figure 6). Changing the shape functions allowing displacement continuity between the elements repairs this. As an axiom of compatibility, *"the node displacements for several elements meeting in the same node must be the same"* (Felippa, 2010).
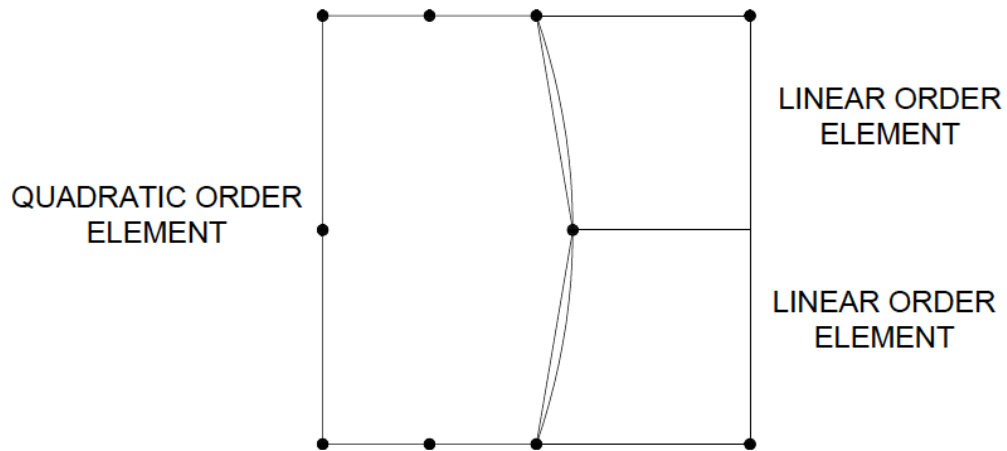
Figure 6 "Gap or penetration occurs along a transition element edge if quadratic displacement interpolation is employed by the transition element along the transition edge" (Rao, 2010)

Compatibility within the element is when the shape functions are single-valued and continuous. An easy way to verify the compatibility is by ensuring that any side of the element that has a polynomial order m must contain m+1 nodes. The elements satisfying

this requirement are called conforming. For two neighbouring elements sharing an edge, compatibility is formulated as follows:

$$\{a_i^A\} = \{a_i^B\} + \{a_i^0\}$$ (4)

Where a_i^0 is the vector of clearances, and a_i^B and a_i^A are the vectors of displacement of reaction points, vector of displacements at contact points and the vector of displacement where external forces are applied all together for elements A and B.

COMPLETENESS: It is defined as the approximation power of the shape functions to the behavior of the mathematical model. Thus, these must be able to represent the rigid body displacement and the constant strain state, implying by this that the shape function must represent all polynomial terms of order m (Felippa, 2010). If this is satisfied, the shape functions are called m-complete. In order to satisfy the completeness of the shape functions, the sum of these must be unity and the element must be compatible. The sum may be verified, once the formulation of the elements is derived and evaluated for every node in one element.

$$u_x = \sum_{i=1}^{n} (\alpha_0 + \alpha_1 x_i + \alpha_2 y_i)\, N_i^e$$

$$u_x = \alpha_0 \sum_{i=1}^{n} N_i^e + \alpha_1 \sum_{i=1}^{n} x_i N_i^e + \alpha_2 \sum_{i=1}^{n} y_i N_i^e$$ (5)

$$u_x = \alpha_0 + \alpha_1 x \quad + \alpha_2 y$$

$$1 = \sum_{i=1}^{n} N_i^e, \qquad x = \sum_{i=1}^{n} x_i N_i^e \qquad y = \sum_{i=1}^{n} y_i N_i^e$$

2.4.3 STABILITY

The stability of a system of finite element equations involves two aspects: rank sufficiency and a positive Jacobian.

RANK SUFFICIENCY: It is an aspect of the element stiffness matrix. An element "is considered to be rank sufficient if its only zero-energy modes are rigid-body modes" (Felippa, 2010).

POSITIVE JACOBIAN: The determinant of the Jacobian matrix must be positive within the element. This quantity relates the natural and the Cartesian coordinates.

2.5 MESH OPTIMIZATION DURING MESH GENERATION

Mesh optimization includes all the methods to improve the quality *(the convergence of the computational schemes and the accuracy of the results (Pascal et al. 2008))* of a mesh. Usually, some form of *a priori* optimization takes place in all the commercial software as a part of the mesh generation process.

The criteria used to optimize a finite element mesh may include changing the size of the elements uniformly or only in certain areas and the aspect ratio control (Section 2.6.2) in order to avoid extremely acute or obtuse angles in the elements.

The mesh optimization may include changing the shape and size of the elements; also the removal of certain amount of nodes, thus changing the number of elements in the mesh and the mesh adaptivity techniques, which are covered in the following section.

2.6 MESH ADAPTIVITY TECHNIQUES

More advanced implementations (adaptive finite element methods) utilize a method to assess the quality of the results (based on error estimation theory) and modify the mesh during the solution. This aims to achieve an approximate solution within some bounds from the 'exact' solution of the continuum problem. Mesh adaptivity may apply various techniques, of which the most popular are:

- Moving nodes (r-adaptivity)
- Refining (and coarsening) elements (h-adaptivity)
- Changing order of base functions (p-adaptivity)
- Combination of the above two (hp-adaptivity)

2.6.1   p-ADAPTIVITY

The p-refinement or p-adaptivity technique only increases the order of the interpolation functions when the convergence error is large; the size and location of element remains unaltered. This technique may also be implemented in certain areas of a finite element mesh where the error obtained is greater than a reference value, however, when this technique is not applied to all the elements, an incompatibility between two elements is caused and the addition of transition elements is necessary (Figure 1).

This method has a limitation as the number of increases available in the order of the functions. If a mesh is not fine enough, the convergence error might not be reduced below a reference value. The p-adaptive technique is identified for increasing the ability of the elements to capture more deformations in large elements, but it is also expensive in computational terms.

2.6.2   r-ADAPTIVITY

In r-adaptive methods the nodes are relocated. Essentially, more nodes are placed in regions of larger error. The amount of nodes and subsequently, the amount of elements, in the mesh is kept unaltered. This method is sometimes found in literature as a sub-class of the h-refinement, due to the fact that there are no changes in the number of degrees of freedom in the problem.

Since there are no increases in the degrees of freedom, at first glance, this method optimizes the usage of resources. However, extreme changes in the location of the nodes may lead to elements with high aspect ratios (Defined as the ratio between the largest and smallest dimension of the elements) (Figure 7). *"As a rough guideline, elements with aspect ratios exceeding 3 should be viewed with caution"* (Felippa, 2010).
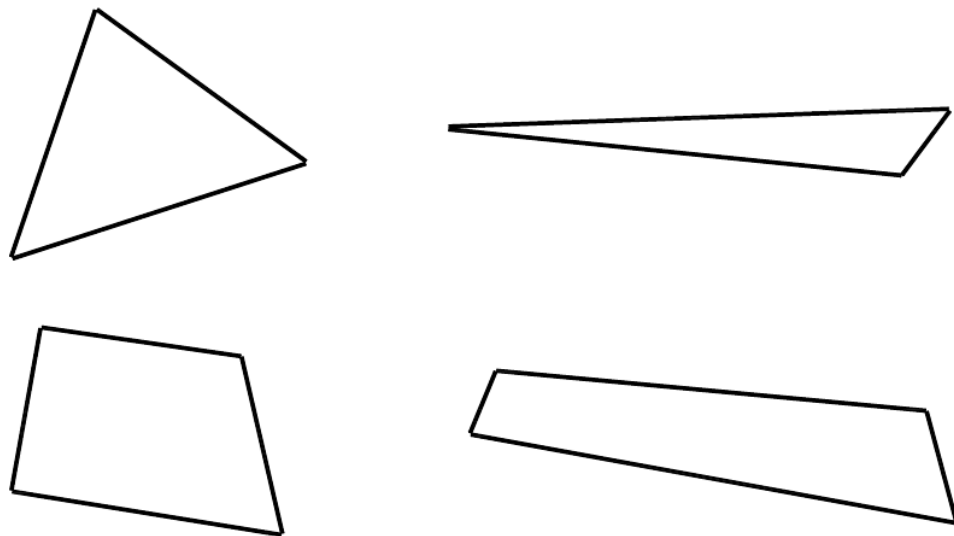
Figure 7. Good (left) and bad (right) aspect ratios in finite elements

2.6.3 h-ADAPTIVITY

This method involves the modification of the finite element mesh. This is achieved by subdividing the medium into smaller elements at the zones where a better accuracy is preferred, which increases the amount of degrees of freedom in the global stiffness matrix. However, the order of the interpolation functions has to remain unchanged.

The subdivision is either performed by diving the existing elements in a fixed number of new elements or by generating a completely new mesh.

2.6.4 hp-ADAPTIVITY

In this case, the size of the elements and the polynomial degree of the interpolation functions are changed. This is a combination of the h-refinement and the p-refinement method. Generally, this is implemented in stages by first obtaining an acceptable accuracy using h-refinement methods and then by using p-adaptive methods to acquire precise results in specific regions. All the methods might be summarized schematically on Figure 8.
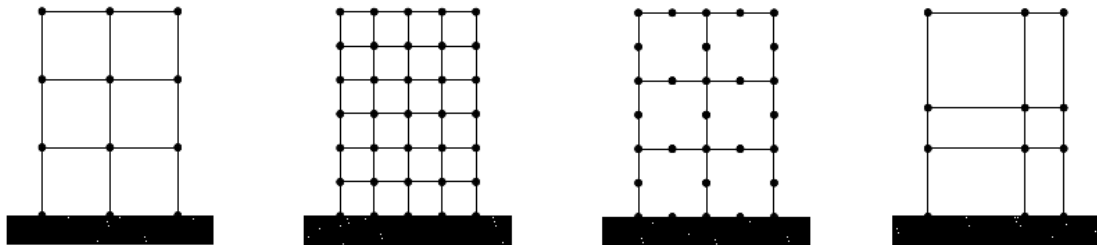
Figure 8. Mesh refinement methods. From left to right 1) Original mesh 2) Uniform h-refinement 3) Uniform p-refinement 4) An r-refinement

2.7 EXCAVATION DISTURBED ZONE (EDZ)

In order to apply the concept of partial p-adaptivity, which is extensively covered in chapter 3, it is compulsory to mention at this point that this type of refinement considers the change in the order of the interpolation functions of the elements in certain areas of the continuum. A higher order of the functions will be maintained in zones where higher accuracy is required, in the specific case of this thesis; this zone is referred to as Excavation Disturbed Zone.

The EDZ is defined as the region in the FEM where the excavation(s) induce(s) a change in the initial conditions of the model. In this thesis, the boundaries of an EDZ are

defined using the percentage of disturbance with respect to the *in situ* biaxial stress field defined in the model (Martin et. al., 1992).

The method of adaptive meshing proposed in this thesis, considers the EDZ's as the zones where accurate results are sought and therefore these correspond to the locations where the elements with higher polynomial order must be placed. The threshold that defines whether a linear order or a quadratic order element must be located depends on the percentage of disturbance.

2.8 PERCENTAGE OF DISTURBANCE

It is defined as the change in the initial conditions as an effect of the modification in any of the variables taken into account (e.g. in situ stresses, geometry, etc.) in the model. In this thesis, the sources of disturbance are the excavations and the percentage is evaluated with respect to the stresses after these are computed, compared to the *in situ* stresses. This percentage of disturbance (Zsaki, 2005) is defined as:

$$\Delta\sigma_i = \left| \frac{\sigma_i^{in-situ} - \sigma_i^{computed}}{\sigma_i^{in-situ}} \right| \cdot 100 \qquad (6)$$

Where i = 1, 2, 3 denotes the major, intermediate and minor principal stresses.

Since a theoretical formulation taking into consideration the interaction between two circular openings is not available, the disturbance caused by these is assessed individually.

3. PARTIAL P-ADAPTIVE MESH OPTIMIZATION PROCEDURE

This research applies a partial p-adaptive method to stress analysis problems. Therefore, after the optimization is executed, the only changes that are reflected in the mesh are the total number of nodes and, consequently, the existence of quadratic, transition and linear elements.

The process starts from a mesh completely composed of quadratic elements (8-node quadrilaterals or 6-node triangles) and, after applying an algorithm, some of the mid-side nodes are removed, converting quadratic into linear order elements and generating a band of transition elements (Section 3.2). As an example, the mesh optimization procedure implemented in this thesis is comprised of a partial p-adaptivity refinement applied to a continuum containing two excavations of different radii (Table 2) which represent a typical tunnel construction where a main tunnel is excavated at a relatively close distance from the service tunnel. The geomechanical properties of the final application are listed in Table 1 and the geometric properties are shown in Figure 9.

PROPERTIES	UNIT	VALUE
W	kN/m^3	0
E	kPa	1.0E+06
υ	-	0.3
σ_1	kPa	10
σ_3	kPa	7.5
σ_z	kPa	10
θ	°	20

Table 1 Application to underground excavations - Model material properties

The initial mesh is changed by reducing the order of the interpolation functions of some elements, thus a controlled quantity of these are reduced to a linear order, and a determined quantity of elements are formulated as a transition from quadratic to linear order elements. These elements are necessary to make a changeover between the two main types of elements aforementioned and are called transition elements (Figure 1).

	LEFT EXCAVATION		RIGHT EXCAVATION	
	Excavation 1		Excavation 2	
	X (m)	Y (m)	X (m)	Y (m)
Coordinates Center	43	18	61.0	13.0
Radius (m)	2.6		5.4	

Table 2 Location and radii of the excavations modeled

The partial p-adaptive refinement, considers the modification of the order of the interpolation functions in the elements found outside the EDZ of each excavation. The threshold defining the EDZ will be set as a percentage of disturbance of 5% (Zsaki, 2005), calculated as mentioned in section 2.8. The EDZ's are considered to be zones where less accuracy in the solution is accepted since it is located at points where the excavations have inappreciable or no effect in the medium.

3.1 DETERMINING EDZ's

The distribution of stresses around each circular excavation are found using the analytical solution for holes in infinite plates proposed by Kirsch (1898) (Figure 10 and Figure 11), the values obtained from the analytical solution are compared to the biaxial stress field thus finding the distance from the center of each excavation where a percentage of disturbance is achieved.
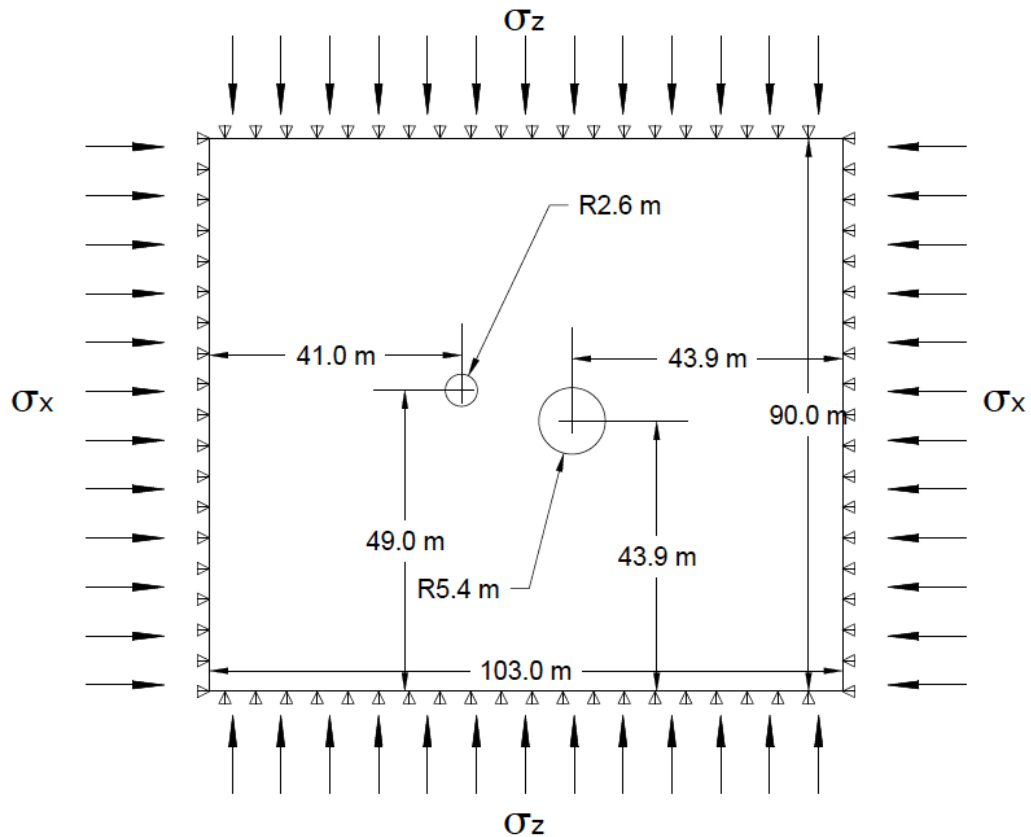
Figure 9 Scheme of the example problem

The EDZ's are defined by those nodes that are located in the elastic medium undergoing more than 5% of the disturbance, with respect to the initial stresses given by the biaxial

stress field (principal stresses). These zones are determined by using the analytical solution formulated by Kirsch (1898). The stresses generated around the excavation are governed by the following equations (Figure 10).

$$\sigma_r = \frac{1}{2}(\sigma_H + \sigma_V)\left(1 - \frac{a^2}{r^2}\right) + \frac{1}{2}(\sigma_H - \sigma_V)\left(1 + \frac{3a^4}{r^4} - \frac{4a^2}{r^2}\right)\cos 2\theta \qquad (7)$$

$$\sigma_\theta = \frac{1}{2}(\sigma_H + \sigma_V)\left(1 + \frac{a^2}{r^2}\right) - \frac{1}{2}(\sigma_H - \sigma_V)\left(1 + \frac{3a^4}{r^4}\right)\cos 2\theta \qquad (8)$$

$$\tau_{r\theta} = -\frac{1}{2}(\sigma_H - \sigma_V)\left(1 - \frac{3a^4}{r^4} + \frac{2a^2}{r^2}\right)\sin 2\theta \qquad (9)$$
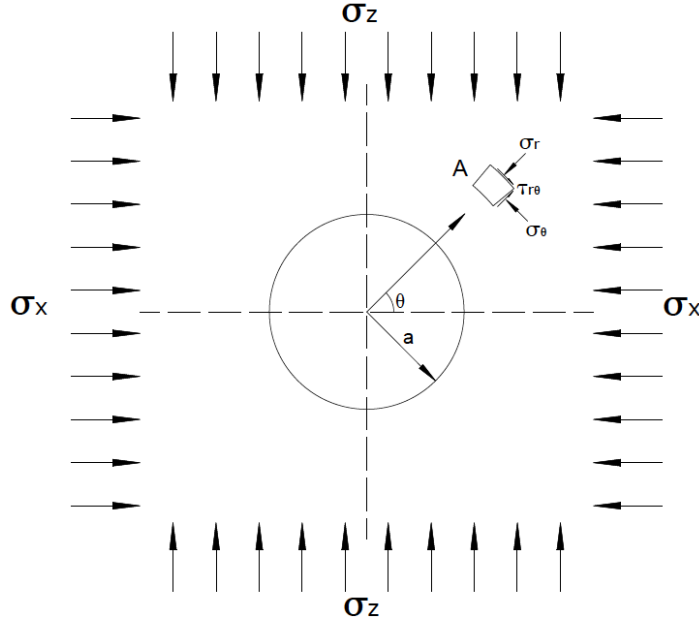
Figure 10. Circular hole in an infinite plate (Kirsch, 1898)

The radial (σ_r), the tangential (σ_θ) and the shear stresses ($\tau_{r\theta}$) are evaluated for each excavation. This evaluation is done for a quarter of each circular excavation (First quadrant) due to symmetry. For each 10ª, from 0ª to 90ª iterating the value taken by r from a to 15*a (ensuring a value large enough to find minimum disturbances) in equations (7), (8) and (9). The values previously obtained are then converted from polar coordinates system to Cartesian coordinate system with the following stress transformation equations:

$$\sigma_{xx} = \sigma_r \cos^2\theta + \sigma_\theta \sin^2\theta - \tau_{r\theta}\sin\theta\cos\theta \qquad (10)$$

$$\sigma_{zz} = \sigma_r \sin^2\theta + \sigma_\theta \cos^2\theta - \tau_{r\theta}\sin\theta\cos\theta \qquad (11)$$

$$\tau_{xz} = (\sigma_r - \sigma_\theta)\sin\theta\cos\theta + \tau_{r\theta}(\cos^2\theta - \sin^2\theta) \qquad (12)$$

The radii where σ_{xx} is equivalent to 0.95σ_H or 1.05σ_H , and where σ_{YY} is equivalent to 0.95σ_V or 1.05σ_V (where σ_H and σ_V correspond to the horizontal and vertical stresses

caused by the initial biaxial stress field) are stored, then the largest value from the previous four is chosen to be the distance from the center of the excavation where the band of transition elements will be located. The value τ_{XZ} was neglected in the comparison since, it tends to reach any percentage of disturbance at a more distant point (approximately 7 times the radius of the excavation for 5% of disturbance) compared to σ_{XX} or σ_{YY}, which would lead to a less significant optimization.

Therefore, a transition zone (from quadratic to linear elements) can be defined and a new mesh including quadratic, transition and linear elements can be generated with quadratic order elements positioned where a percentage of disturbance is higher than 5%; the rest of the continuum will be comprised of transition and linear order elements, and will be considered as the area where less accuracy in the solution is accepted since it is outside the EDZ.
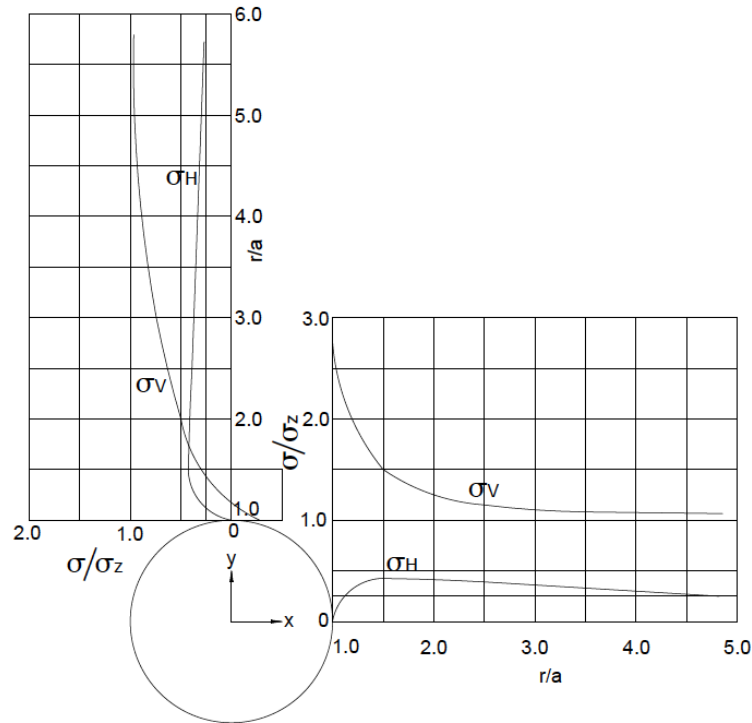
Figure 11 Stress distribution around a circular opening K = 0.25 (Ramamurthy, 2007).

3.2 MESH OPTIMIZATION ALGORITHM

As mentioned, the partial p-adaptive method proposed involves the application of an analytical solution to the problem before the optimized models are generated. The complete procedure passing through the mesh generation until the full recovery of

results is explained step by step along the next lines and might be summarized in the algorithm shown in Figure 12:
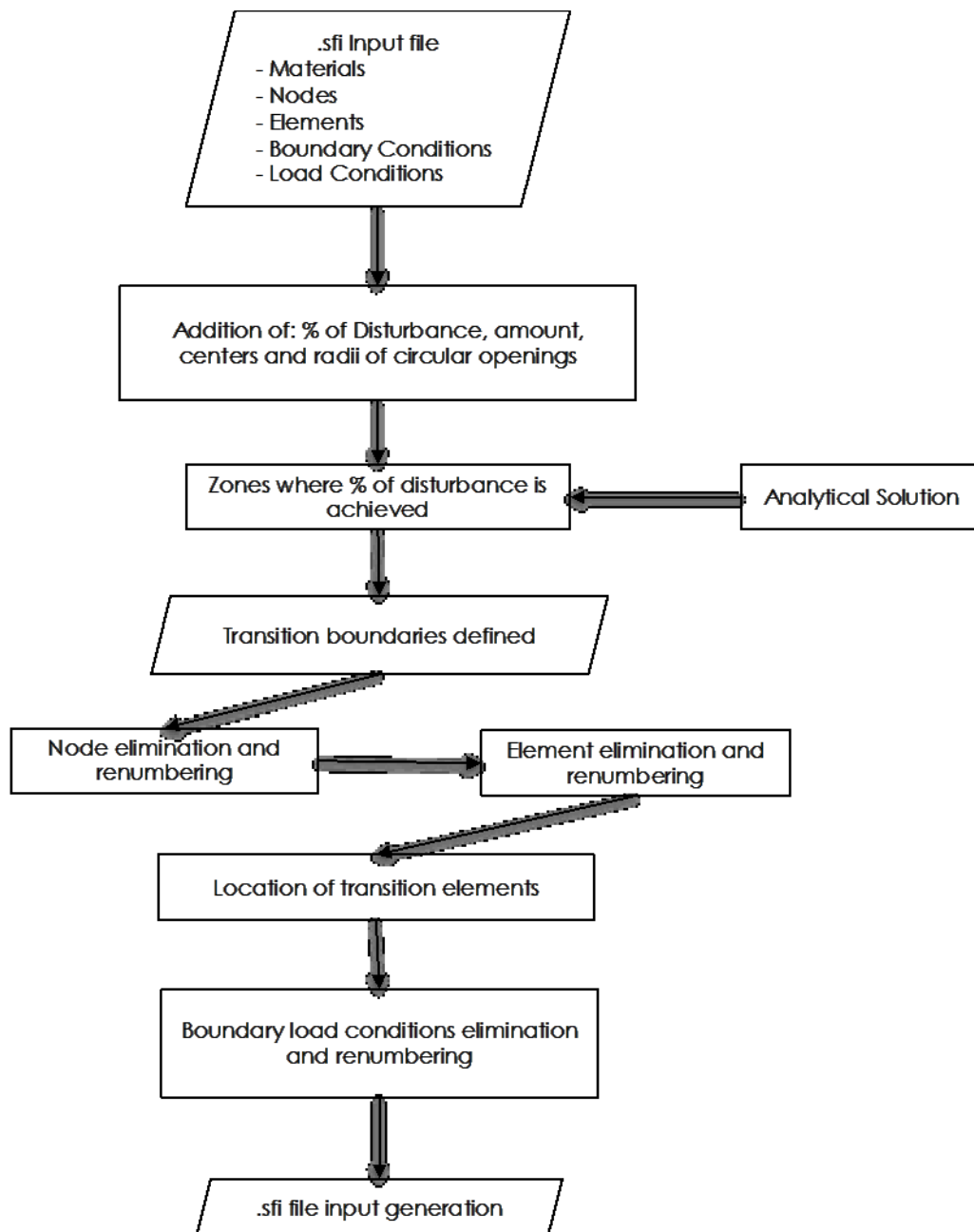
Figure 12. P-adaptive method proposed for circular underground excavations

1. PROBLEM GENERATION: Using Phase^2 (Rocscience, 2007), the geometry, load conditions, boundary conditions and mesh used to discretize the medium are generated. In this specific case, two circular excavations of different size were included (Figure 9). The size of the model was defined large enough to avoid any boundary effects on both

excavations. The input file generated by Phase^2 is then subjected to several modifications.

2. FILE ALTERATION: The original input file includes all the elements, including those that have to be removed in the excavation. In addition to that, several changes in the file syntax are necessary in order to make the file readable by SIMFEM. These changes were carried out with the help of spreadsheets:

- *Element elimination:* Corresponding to the elements present in the excavations.

- *Element renumbering:* The element elimination requires a renumbering.

- *Node renumbering:* All the internal elements belonging to the excavations were eliminated. Therefore, the nodes composing these elements, had to be removed as well and a node renumbering had to take place.

- *Boundary Conditions renumbering:* The boundary conditions list had to be rearranged, as a consequence of the elimination done in the previous step.

- *Addition of excavations characteristics:* This is required to execute the analytical solution and the subsequent determination of the regions disturbed. The characteristics added were: amount of excavations, center of the excavations (coordinates) and radii of the excavations.

- *Addition of percentage of disturbance:* Set to determine the extent of the EDZ's.

- *.Sfi File Generation:* An .sfi file is generated. This file is read by the UNDEROPT code in order to determine the EDZ's and the location of the band(s) of transition elements.

3. UNDEROPT: This is a fragment of code especially developed for circular openings in infinite plates. Using the .sfi generated before, this code is in charge of determining the EDZ's and determines where to locate linear, transition and quadrilateral elements. It has to undertake activities related to element, nodes and boundary conditions renumbering and rearrangement.

4. FINAL .sfi GENERATION: An .sfi file is generated and it is completely ready to be run by SIMFEM. This file includes the linear, transition and quadratic elements.

In order to formulate a transition element, a proper set of shape functions must be implemented recalling that these govern the displacements at the element level and hence the stresses in it.

The elements to be formulated are isoparametric, that is to say that the element shape coordinates and displacements are given by using the same shape functions, mainly because of their versatility, since with these functions is possible to have curved boundaries by only introducing a natural coordinate system.

4. FORMULATION OF FULL ORDER AND TRANSITION ELEMENTS

The transition elements will allow the interconnection of linear order elements with quadratic order elements. The formulations of the transition quadrilateral and triangular elements are found throughout the literature (Felippa, 2010; Gupta, 1975) and are compiled in this chapter.

The element formulation, programming and how they are included into the solution algorithm of the FEM for the plane-strain stress problem are shown, although no extensive treatment has been given to the mathematical procedure necessary to achieve the solution in FEM problems.

4.1 TRIANGULAR ELEMENTS

The formulation for isoparametric 6-node quadratic triangular elements, 5-node isoparametric transition triangular elements, 4-node isoparametric transition triangular elements and 3-node isoparametric linear triangular elements are presented in this section. For convenience, the complete formulation of the elements is given only for the quadratic elements. The transition elements are derived from this one, and the only change is found in their shape functions. The shape functions and the partial derivatives of the shape functions for the triangular elements are summarized in Table 3.

ELEMENT	SHAPE FUNCTIONS AT EACH NODE	SHAPE FUNCTIONS DERIVATIVES		
		$\frac{\partial N_i}{\partial \zeta_1}$	$\frac{\partial N_i}{\partial \zeta_2}$	$\frac{\partial N_i}{\partial \zeta_3}$
6-NODE QUADRATIC TRIANGLE				
	$N_1 = (2\zeta_1 - 1)\zeta_1$	$4\zeta_1 - 1$	0	0
	$N_2 = (2\zeta_2 - 1)\zeta_2$	0	$4\zeta_2 - 1$	0
	$N_3 = (2\zeta_3 - 1)\zeta_3$	0	0	$4\zeta_3 - 1$
	$N_4 = 4\zeta_1\zeta_2$	$4\zeta_2$	$4\zeta_1$	0
	$N_5 = 4\zeta_2\zeta_3$	0	$4\zeta_3$	$4\zeta_2$
	$N_6 = 4\zeta_3\zeta_1$	$4\zeta_3$	0	$4\zeta_1$
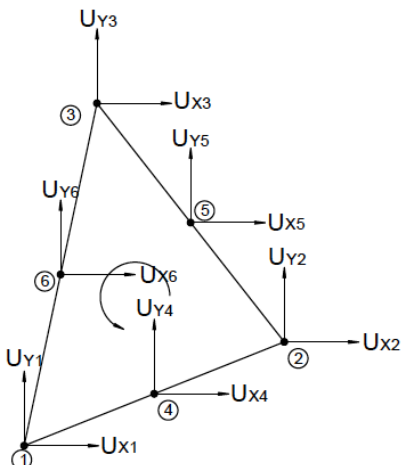
ELEMENT	SHAPE FUNCTIONS AT EACH NODE	SHAPE FUNCTIONS DERIVATIVES		
5-NODE TRANSITION TRIANGLE				
	$N_1 = \zeta_1 - 2\zeta_1\zeta_2$	$1 - \zeta_2$	$-2\zeta_1$	0
	$N_2 = 2\zeta_2\zeta_2 - \zeta_2$	0	$4\zeta_2 - 1$	0
	$N_3 = \zeta_3 - 2\zeta_2\zeta_3$	0	$-2\zeta_3$	$1 - 2\zeta_2$
	$N_4 = 4\zeta_1\zeta_2$	$4\zeta_2$	$4\zeta_1$	0
	$N_5 = 4\zeta_2\zeta_3$	0	$4\zeta_3$	$4\zeta_2$
4-NODE TRANSITION TRIANGLE				
	$N_1 = \zeta_1 - 2\zeta_1\varepsilon_2$	$1 - \zeta_2$	$-2\zeta_1$	0
	$N_2 = \zeta_2 - 2\zeta_1\varepsilon_2$	$-2\zeta_2$	$2\zeta_1 + 1$	0
	$N_3 = \zeta_3$	0	0	1
	$N_4 = 4\zeta_1\zeta_2$	$4\zeta_2$	$4\zeta_1$	0
3-NODE LINEAR ORDER TRIANGLE				
	$N_1 = \zeta_1(2\zeta_1 - 1)$	$4\zeta_1 - 1$	0	0
	$N_2 = \zeta_2(2\zeta_2 - 1)$	0	$4\zeta_2 - 1$	0
	$N_3 = \zeta_3(2\zeta_3 - 1)$	0	0	$4\zeta_3 - 1$
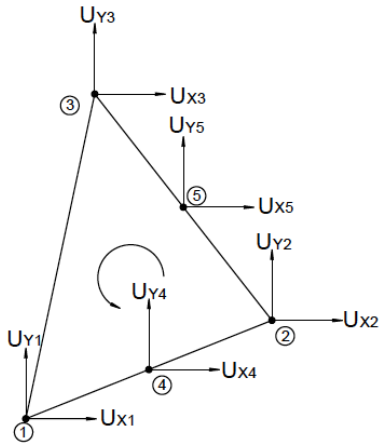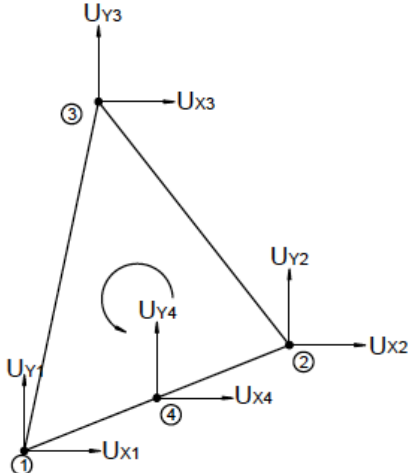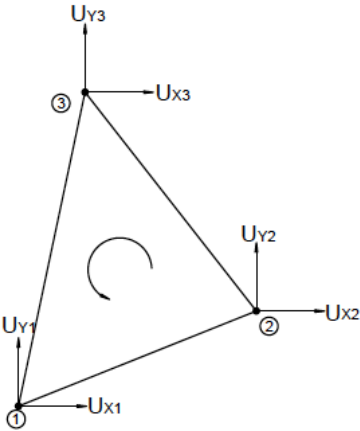
Table 3 Shape functions and partial derivatives of shape functions - Triangular Elements

22

Let us consider the shape functions $\sum_{i=0}^{n} N_i$, where n correspond to the number of nodes representing any triangular element. Be the shape functions partial derivatives $\frac{\partial N_i}{\partial \zeta_1}$, $\frac{\partial N_i}{\partial \zeta_2}$ and $\frac{\partial N_i}{\partial \zeta_3}$ with respect to each one of the axis in the triangular coordinate system. Let us consider a generic scalar function $\omega(\zeta_1 + \zeta_2 + \zeta_3)$ that is interpolated over the triangle by:

$$\omega = \omega_1 N_1 + \omega_2 N_2 + \omega_3 N_3 + \omega_4 N_4 + \omega_5 N_5 + \omega_6 N_6 \qquad (13)$$

ω may stand for any element-varying quantity such as thickness, temperature, etc. In the case of the plane strain problem, this quantity is the displacements. Finding the partial derivatives of the shape functions with respect to x and y and applying the chain rule, we obtain:

$$\frac{\partial \omega}{\partial x} = \sum_{i=0}^{n} \frac{\partial N_i}{\partial x} = \sum_{i=0}^{n} w_i \left(\frac{\partial N_i}{\partial \zeta_1} \frac{\partial \zeta_1}{\partial x} + \frac{\partial N_i}{\partial \zeta_2} \frac{\partial \zeta_2}{\partial x} + \frac{\partial N_i}{\partial \zeta_3} \frac{\partial \zeta_3}{\partial x} \right) \qquad (14)$$

$$\frac{\partial \omega}{\partial y} = \sum_{i=0}^{n} \frac{\partial N_i}{\partial y} = \sum_{i=0}^{n} w_i \left(\frac{\partial N_i}{\partial \zeta_1} \frac{\partial \zeta_1}{\partial y} + \frac{\partial N_i}{\partial \zeta_2} \frac{\partial \zeta_2}{\partial y} + \frac{\partial N_i}{\partial \zeta_3} \frac{\partial \zeta_3}{\partial y} \right)$$

Where n is the number of node. Equation (14) in matrix form is:

$$\begin{bmatrix} \frac{\partial w}{\partial x} \\ \frac{\partial w}{\partial y} \end{bmatrix} = \begin{bmatrix} \frac{\partial \zeta_1}{\partial x} & \frac{\partial \zeta_2}{\partial x} & \frac{\partial \zeta_3}{\partial x} \\ \frac{\partial \zeta_1}{\partial y} & \frac{\partial \zeta_2}{\partial y} & \frac{\partial \zeta_3}{\partial y} \end{bmatrix} \begin{bmatrix} \sum_{i=0}^{n} w_i \frac{\partial N_i}{\partial \zeta_1} \\ \sum_{i=0}^{n} w_i \frac{\partial N_i}{\partial \zeta_2} \\ \sum_{i=0}^{n} w_i \frac{\partial N_i}{\partial \zeta_3} \end{bmatrix} \qquad (15)$$

If we choose w=1, x, y and transposing both sides of equation (15) yields:

$$\begin{bmatrix} \sum_{i=0}^{n} \frac{\partial N_i}{\partial \zeta_1} & \sum_{i=0}^{n} \frac{\partial N_i}{\partial \zeta_2} & \sum_{i=0}^{n} \frac{\partial N_i}{\partial \zeta_3} \\ \sum_{i=0}^{n} x_i \frac{\partial N_i}{\partial \zeta_1} & \sum_{i=0}^{n} x_i \frac{\partial N_i}{\partial \zeta_2} & \sum_{i=0}^{n} x_i \frac{\partial N_i}{\partial \zeta_3} \\ \sum_{i=0}^{n} y_i \frac{\partial N_i}{\partial \varepsilon_1} & \sum_{i=0}^{n} y_i \frac{\partial N_i}{\partial \zeta_2} & \sum_{i=0}^{n} y_i \frac{\partial N_i}{\partial \zeta_3} \end{bmatrix} \begin{bmatrix} \frac{\partial \zeta_1}{\partial x} & \frac{\partial \zeta_1}{\partial y} \\ \frac{\partial \zeta_2}{\partial x} & \frac{\partial \zeta_2}{\partial y} \\ \frac{\partial \zeta_3}{\partial x} & \frac{\partial \zeta_3}{\partial y} \end{bmatrix} = \begin{bmatrix} \frac{\partial 1}{\partial x} & \frac{\partial 1}{\partial y} \\ \frac{\partial x}{\partial x} & \frac{\partial x}{\partial y} \\ \frac{\partial y}{\partial x} & \frac{\partial y}{\partial y} \end{bmatrix} \qquad (16)$$

Since $\frac{\partial 1}{\partial x} = \frac{\partial 1}{\partial y} = 0$ because x and y are independent coordinates and $\frac{\partial x}{\partial x} = \frac{\partial y}{\partial y} = 1$, therefore:

$$\begin{bmatrix} \frac{\partial 1}{\partial x} & \frac{\partial 1}{\partial y} \\ \frac{\partial x}{\partial x} & \frac{\partial x}{\partial y} \\ \frac{\partial y}{\partial x} & \frac{\partial y}{\partial y} \end{bmatrix} = \begin{bmatrix} 0 & 0 \\ 1 & 0 \\ 0 & 1 \end{bmatrix} \qquad (17)$$

23

If $\sum_{i=0}^{n} 1$, then the first row is equal to a constant C and since the right side of the matrix equation is null, this C can be replaced by unity, obtaining a linear system of equations of order 3, which is called the Jacobian matrix Eq. 19

$$
\begin{bmatrix}
1 & 1 & 1 \\
\sum_{i=0}^{n} x_i \frac{\partial N_i}{\partial \zeta_1} & \sum_{i=0}^{n} x_i \frac{\partial N_i}{\partial \zeta_2} & \sum_{i=0}^{n} x_i \frac{\partial N_i}{\partial \zeta_3} \\
\sum_{i=0}^{n} y_i \frac{\partial N_i}{\partial \zeta_1} & \sum_{i=0}^{n} y_i \frac{\partial N_i}{\partial \zeta_2} & \sum_{i=0}^{n} y_i \frac{\partial N_i}{\partial \zeta_3}
\end{bmatrix}
\begin{bmatrix}
\frac{\partial \zeta_1}{\partial x} & \frac{\partial \zeta_1}{\partial y} \\
\frac{\partial \zeta_2}{\partial x} & \frac{\partial \zeta_2}{\partial y} \\
\frac{\partial \zeta_3}{\partial x} & \frac{\partial \zeta_3}{\partial y}
\end{bmatrix}
=
\begin{bmatrix}
0 & 0 \\
1 & 0 \\
0 & 1
\end{bmatrix}
\tag{18}
$$

$$
JP =
\begin{bmatrix}
1 & 1 & 1 \\
J_{x1} & J_{x2} & J_{x3} \\
J_{y1} & J_{y2} & J_{y3}
\end{bmatrix}
\begin{bmatrix}
\frac{\partial \zeta_1}{\partial x} & \frac{\partial \zeta_1}{\partial y} \\
\frac{\partial \zeta_2}{\partial x} & \frac{\partial \zeta_2}{\partial y} \\
\frac{\partial \zeta_3}{\partial x} & \frac{\partial \zeta_3}{\partial y}
\end{bmatrix}
=
\begin{bmatrix}
0 & 0 \\
1 & 0 \\
0 & 1
\end{bmatrix}
\tag{19}
$$

In equation (19), if J ≠ 0 and solving for P we have:

$$
\begin{bmatrix}
\frac{\partial \zeta_1}{\partial x} & \frac{\partial \zeta_1}{\partial y} \\
\frac{\partial \zeta_2}{\partial x} & \frac{\partial \zeta_2}{\partial y} \\
\frac{\partial \zeta_3}{\partial x} & \frac{\partial \zeta_3}{\partial y}
\end{bmatrix}
= \frac{1}{2J}
\begin{bmatrix}
J_{y23} & J_{x32} \\
J_{y31} & J_{x13} \\
J_{y12} & J_{x21}
\end{bmatrix}
= P
\tag{20}
$$

$J_{xji} = J_{xj} - J_{xi}$ and $J_{yji} = J_{yj} - J_{yi}$

The Jacobian $J \quad = \frac{1}{2} detJ = \frac{1}{2}\left(J_{x21}J_{y31} - J_{y12}J_{y13}\right)$
$\tag{21}$

Substituting into equation (14), we get:

$$
\frac{\partial \omega}{\partial x} = \sum_{i=0}^{n} \omega_i \frac{\partial N_i}{\partial x} = \sum_{i=0}^{n} \frac{\omega_i}{2J}\left(\frac{\partial N_i}{\partial \zeta_1}J_{y23} + \frac{\partial N_i}{\partial \zeta_2}J_{y31} + \frac{\partial N_i}{\partial \zeta_3}J_{y12}\right)
\tag{22}
$$

$$
\frac{\partial \omega}{\partial y} = \sum_{i=0}^{n} \omega_i \frac{\partial N_i}{\partial y} = \sum_{i=0}^{n} \frac{\omega_i}{2J}\left(\frac{\partial N_i}{\partial \zeta_1}J_{y32} + \frac{\partial N_i}{\partial \zeta_2}J_{y13} + \frac{\partial N_i}{\partial \zeta_3}J_{y21}\right)
$$

Weights and coordinates for numerical integration at the Gauss points in two different cases for triangular elements:

1 point $w_i = 1.0$

$\zeta_1 = \frac{1}{3}, \zeta_2 = \frac{1}{3}, \zeta_3 = \frac{1}{3}$

3 points $w_i = \frac{1}{3}$ (23)

$\zeta_1 = \frac{2}{3}, \zeta_2 = \frac{1}{6}, \zeta_3 = \frac{1}{6}$

$\zeta_1 = \frac{1}{6}, \zeta_2 = \frac{2}{3}, \zeta_3 = \frac{1}{6}$

$\zeta_1 = \frac{1}{6}, \zeta_2 = \frac{1}{6}, \zeta_3 = \frac{2}{3}$

The Stiffness matrix for these elements, after the formulation is done, a procedure that allows a program to form and evaluate the integrated stiffness matrix in global coordinates is executed. The numerically integrated stiffness matrix is:

$$K = \int_{\Omega} hB^T EBd\Omega \approx \sum_{j=1}^{P} w_i \cdot f(\zeta_1, \zeta_2, \zeta_3) = \sum_{j=1}^{P} w_i \cdot hB^T EBJ$$ (24)

p indicates the number of sample points of the Gauss rule used. ω_i is the integration weight for the ith sample point. h indicates the thickness of the element, which in this case is taken over the element and corresponds to unity (plane strain). The integration over two-dimensional element areas consists of evaluating the integrand at optimally selected integration points within the element (Gauss points), and forming a weighted summation of the integrand values at these points.

The solution is computed at the Gaussian integration points. Therefore, in order to recover the stresses at the nodes of the elements (corner or mid-side nodes), an extrapolation function given by a matrix equation must be implemented.

4.2 QUADRILATERAL ELEMENTS

The formulation of isoparametric 8-node quadratic quadrilateral elements, 7-node isoparametric transition quadrilateral elements, 5-node isoparametric transition quadrilateral elements and 4-node isoparametric linear quadrilateral elements are presented in this section. For convenience, the complete formulation of the elements is given only for the quadratic elements; the transition and linear elements are derived from this one, and the only change is found in their shape functions. This formulation is following Gupta (1975). The shape functions and the partial derivatives of the shape functions for the quadrilateral elements are summarized in Table 4.

ELEMENT	SHAPE FUNCTIONS AT EACH NODE	SHAPE FUNCTIONS DERIVATIVES	
		$\dfrac{\partial N_i}{\partial \zeta}$	$\dfrac{\partial N_i}{\partial \eta}$
8-NODE QUADRATIC ORDER QUADRILATERAL			
	$N_1 = \dfrac{1}{4}(1+\zeta)(1+\eta) - \dfrac{1}{2}N_8 - \dfrac{1}{2}N_5$	$\dfrac{1}{4}(1+\eta)(2\zeta+\eta)$	$\dfrac{1}{4}(1+\zeta)(\zeta+2\eta)$
	$N_2 = \dfrac{1}{4}(1-\zeta)(1+\eta) - \dfrac{1}{2}N_5 - \dfrac{1}{2}N_6$	$\dfrac{1}{4}(2\zeta-\eta)(1+\eta)$	$\dfrac{1}{4}(\zeta-1)(\zeta-2\eta)$
	$N_3 = \dfrac{1}{4}(1-\zeta)(1-\eta) - \dfrac{1}{2}N_6 - \dfrac{1}{2}N_7$	$-\dfrac{1}{4}(\eta-1)(2\zeta+\eta)$	$-\dfrac{1}{4}(\zeta-1)(\zeta+2\eta)$
	$N_4 = \dfrac{1}{4}(1+\zeta)(1-\eta) - \dfrac{1}{2}N_7 - \dfrac{1}{2}N_8$	$-\dfrac{1}{4}(2\zeta-\eta)(\eta-1)$	$-\dfrac{1}{4}(\zeta-1)(\zeta-2\eta)$
	$N_5 = \dfrac{1}{2}(1-\zeta^2)(1+\eta)$	$-\zeta(1+\eta)$	$\dfrac{1}{2}(1-\zeta^2)$
	$N_6 = \dfrac{1}{2}(1-\zeta)(1-\eta^2)$	$\dfrac{1}{2}(\eta^2-1)$	$-\eta(1-\zeta)$
	$N_7 = \dfrac{1}{2}(1-\zeta^2)(1-\eta)$	$-\zeta(1-\eta)$	$\dfrac{1}{2}(\zeta^2-1)$
	$N_8 = \dfrac{1}{2}(1+\zeta)(1-\eta)$	$\dfrac{1}{2}(1-\eta^2)$	$-\eta(1+\zeta)$

ELEMENT	SHAPE FUNCTIONS AT EACH NODE	SHAPE FUNCTIONS DERIVATIVES	
		$\dfrac{\partial N_i}{\partial \zeta}$	$\dfrac{\partial N_i}{\partial \eta}$
7-NODE TRANSITION QUADRILATERAL			
	$N_1 = \dfrac{1}{4}(1+\zeta)(1+\eta) - \dfrac{1}{2}N_5$	$\dfrac{1}{4}(1+\eta) - \dfrac{1}{2}\zeta(1-\eta)$	$\dfrac{1}{4}(1+\zeta) - \dfrac{1}{4}(1-\zeta^2)$
	$N_2 = \dfrac{1}{4}(1-\zeta)(1+\eta) - \dfrac{1}{2}N_5 - \dfrac{1}{2}N_6$	$\dfrac{1}{4}(2\zeta-\eta)(1+\eta)$	$\dfrac{1}{4}(\zeta-1)(\zeta-2\eta)$
	$N_3 = \dfrac{1}{4}(1-\zeta)(1-\eta) - \dfrac{1}{2}N_6 - \dfrac{1}{2}N_7$	$-\dfrac{1}{4}(\eta-1)(2\zeta+\eta)$	$-\dfrac{1}{4}(\zeta-1)(\zeta+2\eta)$
	$N_4 = \dfrac{1}{4}(1+\zeta)(1-\eta) - \dfrac{1}{2}N_7$	$\dfrac{1}{4}(1-\eta) + \dfrac{1}{2}\zeta(1-\eta)$	$-\dfrac{1}{4}(1+\zeta) + \dfrac{1}{4}(1-\zeta^2)$
	$N_5 = \dfrac{1}{2}(1-\zeta^2)(1+\eta)$	$-\zeta(1+\eta)$	$\dfrac{1}{2}(1-\zeta^2)$
	$N_6 = \dfrac{1}{2}(1-\zeta)(1-\eta^2)$	$\dfrac{1}{2}(\eta^2-1)$	$-\eta(1-\zeta)$
	$N_7 = \dfrac{1}{2}(1-\zeta^2)(1-\eta)$	$-\zeta(1-\eta)$	$\dfrac{1}{2}(\zeta^2-1)$
5-NODE TRANSITION QUADRILATERAL			
	$N_1 = \dfrac{1}{4}(1+\zeta)(1+\eta) - \dfrac{1}{2}N_5$	$\dfrac{1}{4}(1+\eta) - \dfrac{1}{2}\zeta(1+\eta)$	$\dfrac{1}{4}(1-\zeta) - \dfrac{1}{4}(1-\zeta^2)$
	$N_2 = \dfrac{1}{4}(1-\zeta)(1+\eta) - \dfrac{1}{2}N_5$	$-\dfrac{1}{4}(1+\eta) + \dfrac{1}{2}\zeta(1+\eta)$	$\dfrac{1}{4}(\zeta-1)(\zeta-2\eta)$
	$N_3 = \dfrac{1}{4}(1-\zeta)(1-\eta)$	$-\dfrac{1}{4}(1-\eta)$	$-\dfrac{1}{4}(1-\zeta)$
	$N_4 = \dfrac{1}{4}(1+\zeta)(1-\eta)$	$\dfrac{1}{4}(1-\eta)$	$-\dfrac{1}{4}(1+\zeta)$
	$N_5 = \dfrac{1}{2}(1-\zeta^2)(1+\eta)$	$-\zeta(1+\eta)$	$\dfrac{1}{2}(1-\zeta^2)$

ELEMENT	SHAPE FUNCTIONS AT EACH NODE	SHAPE FUNCTIONS DERIVATIVES	
		$\dfrac{\partial N_i}{\partial \zeta}$	$\dfrac{\partial N_i}{\partial \eta}$
4-NODE LINEAR ORDER QUADRILATERAL			
	$N_1 = \dfrac{1}{4}(1 + \zeta)(1 + \eta)$	$\dfrac{1}{4}(\eta - 1)$	$\dfrac{1}{4}(\zeta - 1)$
	$N_2 = \dfrac{1}{4}(1 - \zeta)(1 + \eta)$	$\dfrac{1}{4}(1 - \eta)$	$\dfrac{1}{4}(-1 - \zeta)$
	$N_3 = \dfrac{1}{4}(1 - \zeta)(1 - \eta)$	$\dfrac{1}{4}(1 + \eta)$	$\dfrac{1}{4}(1 + \zeta)$
	$N_4 = \dfrac{1}{4}(1 + \zeta)(1 - \eta)$	$\dfrac{1}{4}(-1 - \eta)$	$\dfrac{1}{4}(1 - \zeta)$

Table 4 Shape functions and partial derivatives of shape functions - Quadrilateral Elements

Let us assume the shape functions $\sum_{i=0}^{n} N_i$, where n correspond to the amount of nodes present in any triangular element. Be the shape functions derivatives $\frac{\partial N_i}{\partial \zeta}$ and $\frac{\partial N_i}{\partial \eta}$. Finding the Jacobian and inverse Jacobian (J and J^T)

$$\begin{bmatrix} dx \\ dy \end{bmatrix} = \begin{bmatrix} \dfrac{\partial x}{\partial \zeta} & \dfrac{\partial x}{\partial \eta} \\ \dfrac{\partial y}{\partial \zeta} & \dfrac{\partial y}{\partial \eta} \end{bmatrix} \begin{bmatrix} d\zeta \\ d\eta \end{bmatrix} = J^T \begin{bmatrix} d\zeta \\ d\eta \end{bmatrix} \qquad \begin{bmatrix} d\zeta \\ d\eta \end{bmatrix} = \begin{bmatrix} \dfrac{\partial x}{\partial \zeta} & \dfrac{\partial x}{\partial \eta} \\ \dfrac{\partial y}{\partial \zeta} & \dfrac{\partial y}{\partial \eta} \end{bmatrix} \begin{bmatrix} dx \\ dy \end{bmatrix} = J^T \begin{bmatrix} dx \\ dy \end{bmatrix} \qquad (\,25\,)$$

$$J = \begin{bmatrix} \dfrac{\partial(x,y)}{\partial(\zeta,\eta)} \end{bmatrix} = \begin{bmatrix} \dfrac{\partial x}{\partial \zeta} & \dfrac{\partial y}{\partial \zeta} \\ \dfrac{\partial x}{\partial \eta} & \dfrac{\partial y}{\partial \eta} \end{bmatrix} = \begin{bmatrix} J_{11} & J_{12} \\ J_{21} & J_{22} \end{bmatrix} \qquad J^{-1} = \begin{bmatrix} \dfrac{\partial(\zeta,\eta)}{\partial(x,y)} \end{bmatrix} = \begin{bmatrix} \dfrac{\partial \zeta}{\partial x} & \dfrac{\partial \eta}{\partial x} \\ \dfrac{\partial \zeta}{\partial y} & \dfrac{\partial \eta}{\partial y} \end{bmatrix} = \dfrac{1}{J}\begin{bmatrix} J_{22} & -J_{12} \\ -J_{21} & J_{11} \end{bmatrix} \qquad (\,26\,)$$

$$detJ = J_{11}J_{22} - J_{12}J_{21} \qquad (\,27\,)$$

Finding the shape function derivatives by the chain rule

$$\frac{\partial N_i}{\partial x} = \frac{\partial N_i}{\partial \zeta} \cdot \frac{\partial \zeta}{\partial x} + \frac{\partial N_i}{\partial \eta} \cdot \frac{\partial \eta}{\partial x} \qquad \frac{\partial N_i}{\partial y} = \frac{\partial N_i}{\partial \zeta} \cdot \frac{\partial \zeta}{\partial y} + \frac{\partial N_i}{\partial \eta} \cdot \frac{\partial \eta}{\partial y} \qquad (\,28\,)$$

$$J = PX \qquad (\,29\,)$$

$$J = \begin{bmatrix} \dfrac{\partial x}{\partial \zeta} & \dfrac{\partial y}{\partial \zeta} \\ \dfrac{\partial x}{\partial \eta} & \dfrac{\partial y}{\partial \eta} \end{bmatrix} = \begin{bmatrix} \dfrac{\partial N_i}{\partial \zeta} & \cdots & \dfrac{\partial N_n}{\partial \zeta} \\ \dfrac{\partial N_i}{\partial \eta} & \cdots & \dfrac{\partial N_n}{\partial \eta} \end{bmatrix}_{2xn} \begin{bmatrix} x_i & y_i \\ \vdots & \vdots \\ x_n & y_n \end{bmatrix}_{nx2} = PX \qquad (\,30\,)$$

Differentiating with respect to the quadrilateral coordinates, where n is the number of nodes:

$$x = \sum_{i=1}^{n} N_i\,(\zeta,\eta) \cdot x_i \qquad\qquad y = \sum_{i=1}^{n} N_i\,(\varepsilon,\eta) \cdot y_i \tag{31}$$

$$\frac{\partial x}{\partial \zeta} = \sum_{i=1}^{n} \frac{\partial N_i}{\partial \zeta} \cdot x_i \qquad\qquad \frac{\partial y}{\partial \zeta} = \sum_{i=1}^{n} \frac{\partial N_i}{\partial \varepsilon} \cdot y_i \tag{32}$$

$$x = \sum_{i=1}^{n} N_i\,(\zeta,\eta) \cdot x_i \qquad\qquad y = \sum_{i=1}^{n} N_i\,(\zeta,\eta) \cdot y_i \tag{33}$$

$$\frac{\partial x}{\partial \eta} = \sum_{i=1}^{n} \frac{\partial N_i}{\partial \eta} \cdot x_i \qquad\qquad \frac{\partial y}{\partial \eta} = \sum_{i=1}^{n} \frac{\partial N_i}{\partial \eta} \cdot y_i \tag{34}$$

$$\frac{\partial N_i}{\partial x} = \frac{\partial N_i}{\partial \zeta}\frac{\partial \zeta}{\partial x} + \frac{\partial N_i}{\partial \eta}\frac{\partial \eta}{\partial x} \qquad\qquad \frac{\partial N_i}{\partial y} = \frac{\partial N_i}{\partial \zeta}\frac{\partial \zeta}{\partial y} + \frac{\partial N_i}{\partial \eta}\frac{\partial \eta}{\partial y} \tag{35}$$

Thus,

$$\begin{bmatrix} \dfrac{\partial N_i}{\partial \zeta} \\[2mm] \dfrac{\partial N_i}{\partial \zeta} \end{bmatrix} = \begin{bmatrix} \dfrac{\partial x}{\partial \zeta} & \dfrac{\partial y}{\partial \zeta} \\[2mm] \dfrac{\partial x}{\partial \zeta} & \dfrac{\partial y}{\partial \zeta} \end{bmatrix} \cdot \begin{bmatrix} \dfrac{\partial N_i}{\partial x} \\[2mm] \dfrac{\partial N_i}{\partial y} \end{bmatrix} = J \cdot \begin{bmatrix} \dfrac{\partial N_i}{\partial x} \\[2mm] \dfrac{\partial N_i}{\partial y} \end{bmatrix} \tag{36}$$

The determinant of J (Jacobian)

$$det \quad J = \frac{\partial x}{\partial \zeta} \cdot \frac{\partial y}{\partial \eta} - \frac{\partial y}{\partial \zeta} \cdot \frac{\partial x}{\partial \eta} \tag{37}$$

Inverse of J

$$= \frac{1}{det \quad J} \begin{bmatrix} \dfrac{\partial y}{\partial \eta} & -\dfrac{\partial y}{\partial \zeta} \\[2mm] -\dfrac{\partial x}{\partial \eta} & \dfrac{\partial x}{\partial \zeta} \end{bmatrix} \tag{38}$$

$$\therefore \frac{\partial \varepsilon}{\partial x} = \frac{1}{det \quad J}\frac{\partial y}{\partial \eta} \qquad\qquad \therefore \frac{\partial \eta}{\partial x} = -\frac{1}{det \quad J}\frac{\partial y}{\partial \zeta} \tag{39}$$

$$\therefore \frac{\partial \varepsilon}{\partial y} = -\frac{1}{det \quad J}\frac{\partial x}{\partial \eta} \qquad\qquad \therefore \frac{\partial \eta}{\partial y} = -\frac{1}{det \quad J}\frac{\partial x}{\partial \zeta} \tag{40}$$

In the case of small strains in plane strain conditions, the strain-displacement relation is given by the Strain Displacement Matrix (n corresponds to the number of nodes in the element)

$$e = Bu == \begin{bmatrix} e_{xx} \\ e_{yy} \\ e_{xy} \end{bmatrix} = \begin{bmatrix} \dfrac{\partial N_1}{\partial x} & 0 & \ldots\ldots & \dfrac{\partial N_n}{\partial x} & 0 \\ 0 & \dfrac{\partial N_1}{\partial y} & \ldots\ldots & 0 & \dfrac{\partial N_n}{\partial y} \\ \dfrac{\partial N_1}{\partial y} & \dfrac{\partial N_1}{\partial x} & \ldots\ldots & \dfrac{\partial N_n}{\partial y} & \dfrac{\partial N_n}{\partial x} \end{bmatrix} u \qquad (41)$$

Weight and coordinates of Gaussian points for numerical integration in three different cases for quadrilateral elements:

1 point $\qquad w_i = 2.0$

$\qquad\qquad\qquad \zeta = \eta = 0.0$

4 points $\qquad w_i = 1.0$

$$\zeta = -\frac{1}{\sqrt{3}}, \frac{1}{\sqrt{3}} \qquad (42)$$

$$\eta = -\frac{1}{\sqrt{3}}, \frac{1}{\sqrt{3}}$$

9 points $\qquad w_i = \frac{5}{9}, \frac{8}{9}, \frac{5}{9}$

$$\zeta = -\sqrt{\frac{3}{5}}, 0, \sqrt{\frac{3}{5}}$$

$$\eta = -\sqrt{\frac{3}{5}}, 0, \sqrt{\frac{3}{5}}$$

The canonical form of the Gaussian quadrature for isoparametric quadrilateral elements is given as:

$$\iint_{-1}^{1} f(\zeta,\eta) d\zeta d\eta \approx \sum_{i=1}^{P_1} \sum_{j=1}^{P_2} w_i \cdot w_j f(\zeta_i, \eta_j) \qquad (43)$$

Where:

$$f = K = \int_{\Omega} hB^T EB d\Omega \qquad (44)$$

$$d\Omega = dxdy = detJ \ d\varepsilon d\eta \qquad (45)$$

$$f(\zeta,\eta) = hB^T EB \ detJ \qquad (46)$$

$$K = \int_{\Omega} hB^T EB d\Omega \approx \sum_{j=1}^{P} w_i \cdot f(\zeta_1,\zeta_2,\zeta_3) = \sum_{j=1}^{P} w_i \cdot hB^T EBJ \qquad (47)$$

$$m_t = w_i \cdot \left(\frac{\partial N_i}{\partial x} \cdot \frac{\partial N_j}{\partial x} + \frac{\partial N_i}{\partial y} \cdot \frac{\partial N_j}{\partial y} \right) \cdot det \quad J \qquad (48)$$

For all Gauss integration points the program must:

1) Evaluate $\frac{\partial N_i}{\partial \varepsilon}$ and $\frac{\partial N_i}{\partial \eta}$

2) Evaluate $\frac{\partial x}{\partial \varepsilon}, \frac{\partial x}{\partial \eta}, \frac{\partial y}{\partial \varepsilon}, \frac{\partial y}{\partial \eta}$

3) Evaluate det J $= \dfrac{\partial x}{\partial \varepsilon} \cdot \dfrac{\partial y}{\partial \eta} - \dfrac{\partial y}{\partial \varepsilon} \cdot \dfrac{\partial x}{\partial \eta}$

4) Evaluate

$$\frac{\partial \varepsilon}{\partial x} = \frac{1}{\det\ J}\frac{\partial y}{\partial \eta} \qquad\qquad \frac{\partial \eta}{\partial x} = -\frac{1}{\det\ J}\frac{\partial y}{\partial \zeta}$$

$$\frac{\partial \varepsilon}{\partial y} = -\frac{1}{\det\ J}\frac{\partial x}{\partial \eta} \qquad\qquad \frac{\partial \eta}{\partial y} = -\frac{1}{\det\ J}\frac{\partial x}{\partial \zeta}$$

5) Evaluate

$$\frac{\partial N_i}{\partial x} = \frac{\partial N_i}{\partial \varepsilon}\frac{\partial \zeta}{\partial x} + \frac{\partial N_i}{\partial \eta}\frac{\partial \eta}{\partial x} \qquad\qquad \frac{\partial N_i}{\partial y} = \frac{\partial N_i}{\partial \varepsilon}\frac{\partial \zeta}{\partial y} + \frac{\partial N_i}{\partial \eta}\frac{\partial \eta}{\partial y}$$

6) Assemble the stiffness matrix (eq (43))

5. PERFORMANCE EVALUATION OF TRANSITION ELEMENTS

Once the theoretical formulation and the subsequent addition of these elements into the SIMFEM code was carried out, a testing process to assess the performance of several configurations of the elements was done using three different FEM programs SAP2000® (CSI Inc., 2007), Phase2 and SIMFEM. Since stresses and forces are derived quantities from the general matrix stiffness equation (49), the displacements at several points of the geometry of the element were chosen to be the parameter of performance of the elements.

$$f = Ku \hspace{5cm} (49)$$

All the tests are subdivided into two categories:

Type I Models: These models contain 1 or 2 elements, depending on whether triangles or quadrilaterals were used. Further specifications are given throughout the next pages.

Type II Models: These models contain 9 or 18 elements, depending on whether triangles or quadrilaterals were used. Further specifications are given through the next pages.

5.1 TYPE I MODELS

All the type I models were designed with the same geometric and material properties. For the lower edge, where the base is located, fixed type supports were assumed. In the case of quadratic edges, three supports were installed; two at the extremes and one at the midside node. In the case of linear edges, two fixed type supports were installed; one at each extreme (Figure 13). The vertical distributed load applied in the upper part of the models was 2 kN/m/m had to be transformed into an equivalent nodal load (Nikishov, 2007). This transformation depends on what type of edge the load is being applied on and can be better explained as follows.
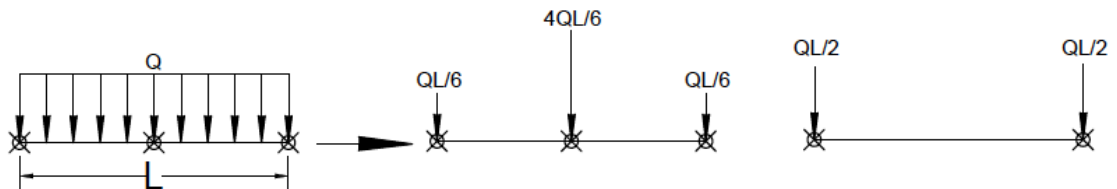
Figure 13 Nodal equivalent forces for quadratic and linear edges

It is also necessary to take into account the Gauss integration points, which are mandatory to perform the numerical integration. These points are used to evaluate the stresses in the element stiffness integration, which are later extrapolated to the element node points. The triangular elements were tested assuming 3 integration points and in the case of quadrilateral elements, the amount of integration points was set to be 9. The SIMFEM code has the capacity to consider 1 or 3 integration points in triangular elements and 1, 4 or 9 integration points in quadrilateral elements.
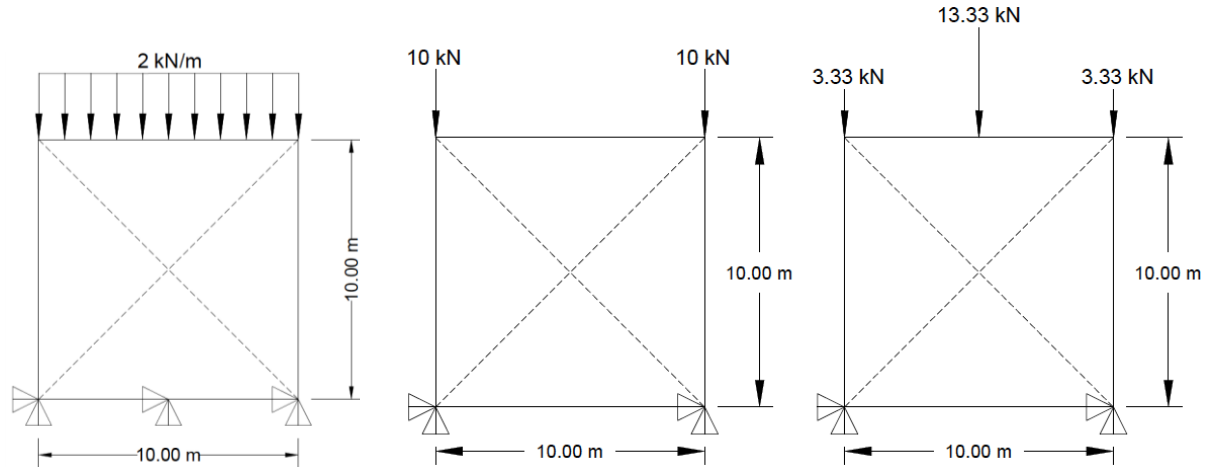
Figure 14. Type I model - General sketch (a) and Equivalent nodal loads (b)

The dimensions of all the arrangements of elements are of 10 m by 10 m and the material constituting the continuum was assumed to be linear elastic. Other properties are listed in the following table:

PROPERTY	UNIT	VALUE
γ	kN/m³	0.02
E	kPa	1000
ν	-	0.3

Table 5. Type I and type II models properties

5.1.1   TYPE I MODELS USING TRIANGLES – RESULTS

A total of 32 type I models were evaluated, taking into account several geometric configurations of the nodes along the models as is shown in the column "scheme" in the APPENDIX 2. TYPE I MODELS USING TRIANGULAR ELEMENTS - RESULTS for a better understanding of the appendix presented, the column named "LOC" indicates at what corner or midside points the displacement is measured. As a key, the reader must use: UR

(Upper Right), UM (Upper Medium), UL (Upper Left), C (Center), ML (Medium Left), MR (Medium Right), LL (Lower Left), LM (Lower Medium) and LR (Lower Right). The results of the calculations are shown in Table 6 through Table 9. By plotting the displacements of the upper nodes of the models, the behaviour of the elements under same load and support conditions can be compared.

Due to the large number of results to be plotted, three plots were necessary. In the first two plots, only the models done with 3-node and 6-node triangles are included.
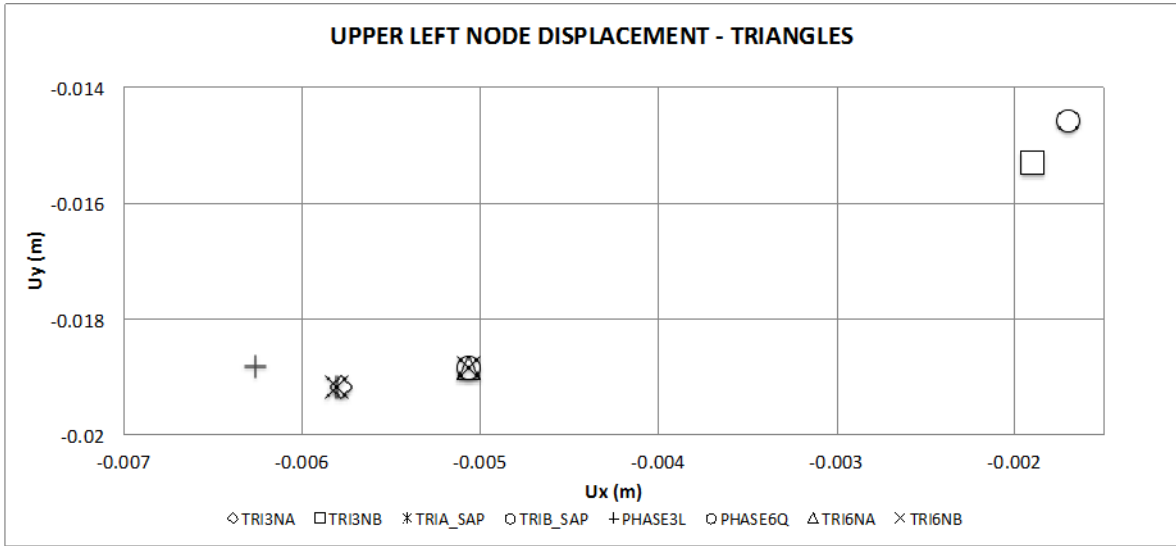
Figure 15. Models using elements with 3 and 6 nodes. Displacements at the upper edge – Left corner.
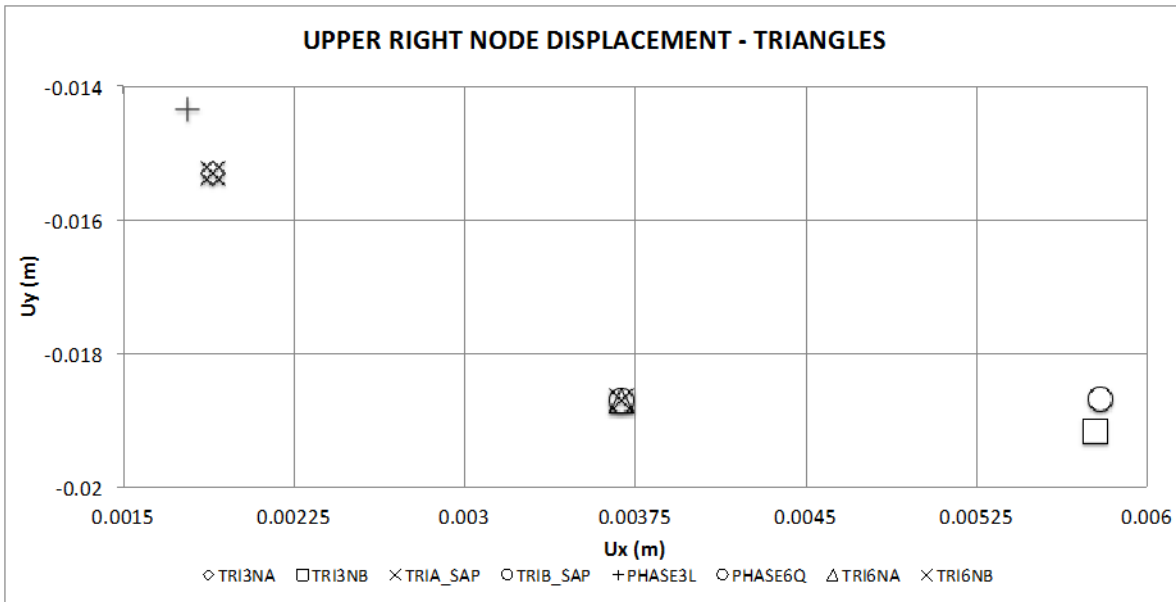
Figure 16. Models using elements with 3 and 6 nodes. Displacements at the upper edge – Right corner

In Figure 15 and Figure 19 only the linear models TRI3NB and TRIB_SAP, which are modeled with a diagonal edge in a different direction (refer to APPENDIX 2. TYPE I MODELS USING TRIANGULAR ELEMENTS - RESULTS), present a different behavior. Yet, their displacements are very close, despite using two different programs for the modeling (Figure 17 and Figure 18) (SAP2000® and SIMFEM). The effect of the direction of the diagonal seems to disappear in the quadratic elements, since all the models using them present comparable displacements (PHASE6Q, TRI6NA and TRI6NB), as shown on Figure 15 and Figure 16.
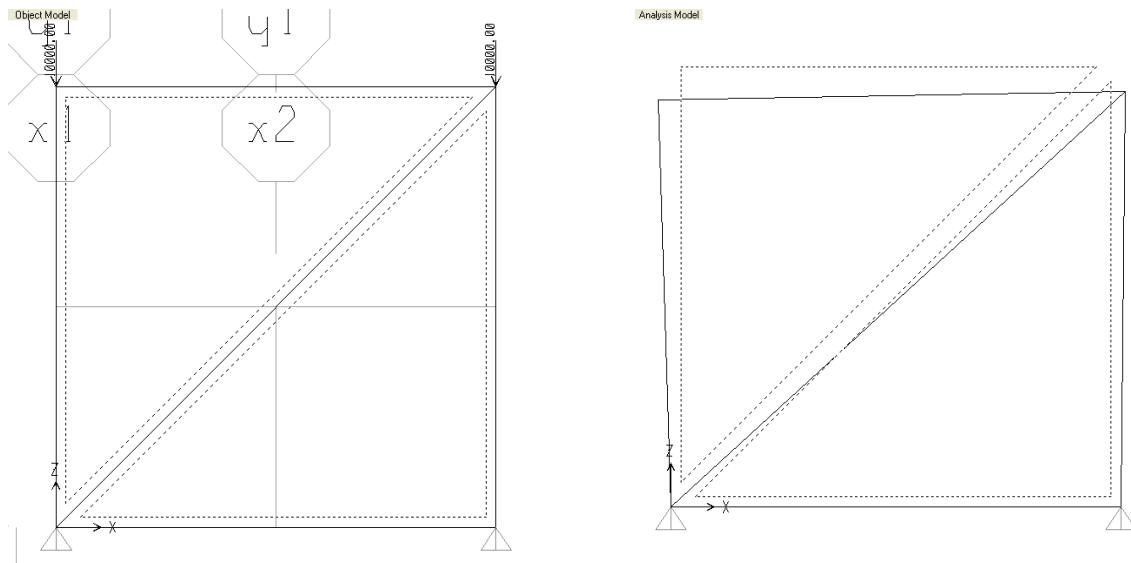
Figure 17 Model TRIA_SAP (Left: Loads assignments - Right: Deformed model) (Units kN, m)
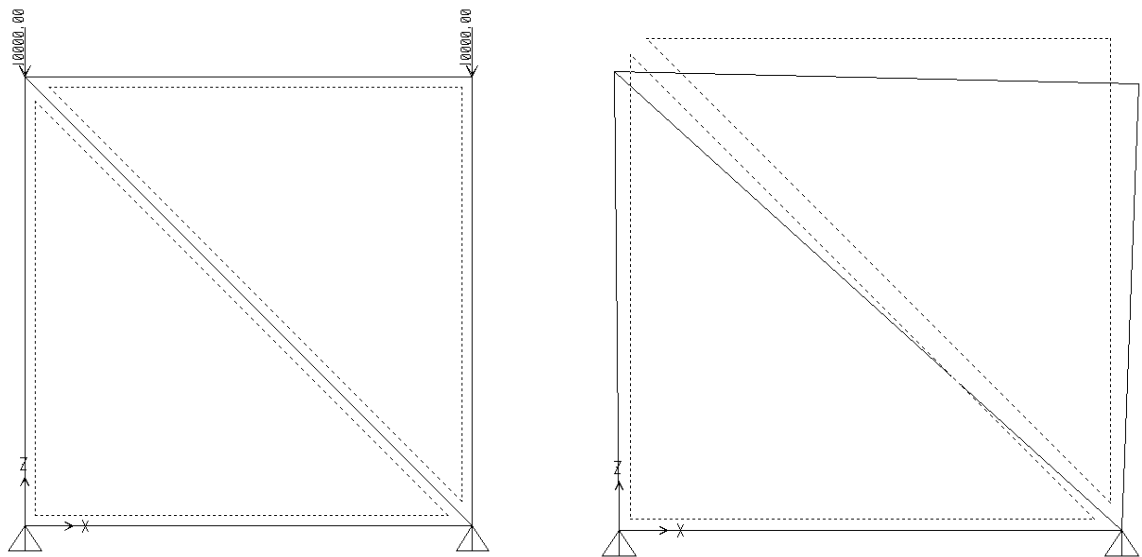
Figure 18 Model TRIB_SAP (Left: Loads assignments - Right: Deformed model) (Units kN, m)

After evaluating all the displacements of the model, it was inferred that the dispersion in the results at the upper part of the model is the most evident. Therefore the comparison is also based on this edge of the model. Specifically, the displacements of the nodes were compared at the upper left node of the models. There was also the possibility of evaluating the displacements at the mid-part of the element, but as can be observed in the displacements results, the dispersion is not as evident as at the other location, provoking non-representative percentage errors. Besides, some of the models were not assigned mid-side nodes as is shown in the scheme column of appendix 1 and 2, which would lead to an incomplete evaluation of results.

The performance evaluation was done based on the displacements at certain points. These displacements were normalized with respect to results obtained in Phase[2], a FEA software intended for geotechnical engineering with the capability of formulate either linear or quadratic elements. The other software package used was SAP2000®; this program allows only the use of linear elements. The percent error in X and Y directions were derived using the following:

$$\%error = \frac{(Experimental\ \ Value - Benchmark\ \ Value)}{Benchmark\ \ Value}$$

(50)

ELEMENTS	Ux (m)	Uy (m)
TRI3NA	-0.00578	-0.019186
TRI3NB	-0.0018992	-0.015304
TRIA_SAP	-0.0058	-0.0192
TRIB_SAP	-0.0017	-0.0146
WITH RESPECT TO		
PHASE3L	-0.0062603	-0.018818
AT	UL	
	ERROR IN X	**ERROR IN Y**
% E TRI3NA WRT PHASE3L	7.67%	1.96%
% E TRI3NB WRT PHASE3L	69.66%	18.67%
% E TRIA_SAP WRT PHASE3L	7.35%	2.03%
% E TRIB_SAP WRT PHASE3L	72.84%	22.41%

Table 6 Comparison of linear triangles in SIMFEM, Phase[2] and SAP2000®

In Table 6, only the models with linear triangular elements are analyzed. The effect of the inverted diagonal may dictate the tendency of the displacements at Figure 19, Figure 16 and Figure 23, where we can appreciate the two zones (left and right side of the plot) where these are located. When the same geometry was modeled in different programs the greatest error found was around 7.5%.

ELEMENTS	Ux (m)	Uy (m)
TRI6NA	-0.005064	-0.01885
TRI6NB	-0.005064485	-0.018856
WITH RESPECT TO		
PHASE6Q	-0.0050645	-0.018856
AT	UL	
	ERROR IN X	ERROR IN Y
% E TRI6NA WRT PHASE6Q	0.01%	0.03%
% E TRI6NB WRT PHASE6Q	0.00%	0.00%

Table 7 Comparison of quadratic triangles in SIMFEM and Phase[2]

Only the quadrilateral triangles were evaluated in the previous table. In this case, for two different programs replicating the same model the displacements are almost identical. In the next two figures only the models using 4-node triangles are plotted.
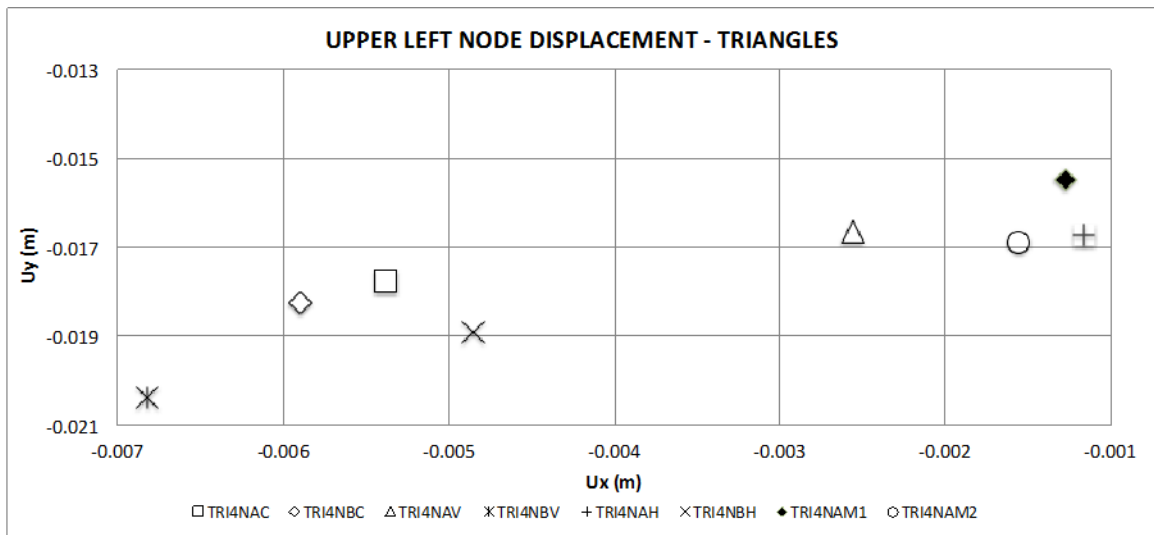
Figure 19. Models using elements with 4 nodes. Displacements at the upper edge – Left corner.
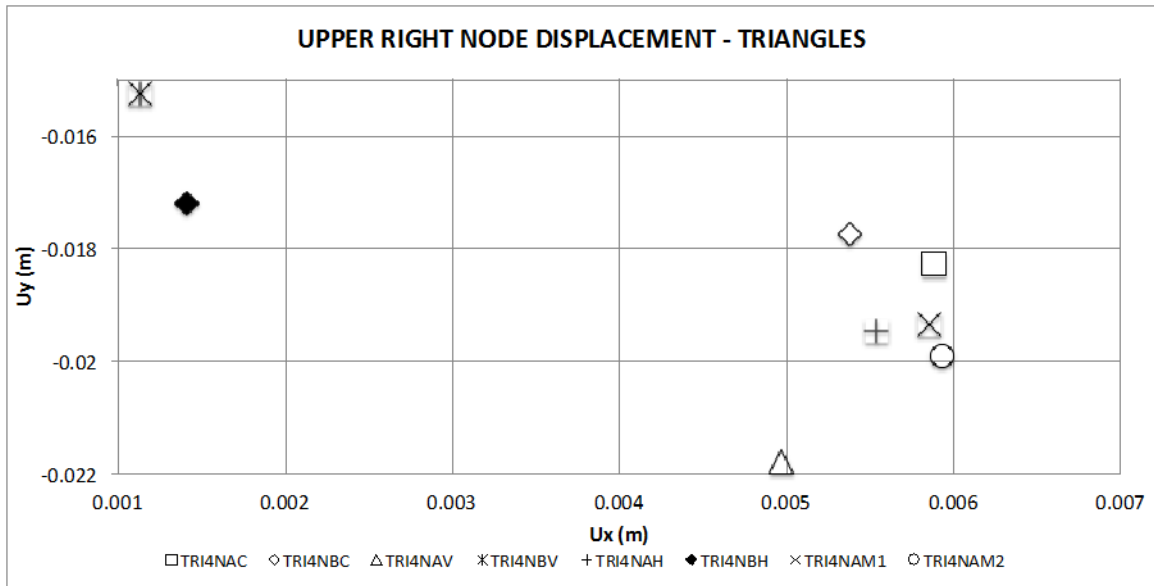
Figure 20. Models using elements with 4 nodes. Displacements at the upper edge – Right corner.

Figure 19 and Figure 20 show a disperse behavior of the displacements not as defined as in the previous figures, let us recall that only 4-node transition elements are included, in addition to the position of the fourth node or transition edge and the direction of the diagonal change in each model. Although the tendency of similar models to tilt towards the same directions and with the same order of magnitude of displacements is observed, for instance the models with the forth node located in the center of the model (TRI4NAC and TRI4NBC) tend to have similar displacements. The same analysis might be depicted for the models TRI4NAH, TRI4NAM1 and TRI4NAM2 that have their diagonal edge in the same direction and present similar tendency. Models TRI4NBV and TRI4NBH, that have the diagonal edge in the same direction, also show similar tendencies, located in similar zones at upper left and upper right node.

ELEMENTS	Ux (m)	Uy (m)
TRI4NBC	-0.005895	-0.01827
TRI4NBV	-0.006819	-0.0204
TRI4NBH	-0.002553	-0.01665
WITH RESPECT TO		
PHASE3L	-0.0062603	-0.018818
AT	UL	
	ERROR IN X	ERROR IN Y
% E TRI4NBC WRT PHASE3L	5.84%	2.91%
% E TRI4NBV WRT PHASE3L	8.92%	8.41%
% E TRI4NBH WRT PHASE3L	59.22%	11.52%

Table 8 4-node triangular transition elements – Inverted edge

The element TRI4NBH shows the largest errors, even though, the values obtained remain within the same order of magnitude. These large errors lead to the design of further tests on the elements with the objective of performing a further evaluation of the transition elements.

ELEMENTS	Ux (m)	Uy (m)
TRI4NAC	-0.00538	-0.01776
TRI4NAV	-0.00538	-0.01776
TRI4NAH	-0.00538	-0.01776
WITH RESPECT TO		
TRI3NA	-0.00578	-0.019186
AT	UL	
	ERROR IN X	ERROR IN Y
% E TRI4NAC WRT TRI3NA	6.92%	7.43%
% E TRI4NAV WRT TRI3NA	6.92%	7.43%
% E TRI4NAH WRT TRI3NA	6.92%	7.43%

Table 9. 4-node triangular transition elements compared to linear triangular elements

As can be seen in the data tables listed in the appendix, there is also a tendency for all the triangular transition elements formulated to behave similarly as the models where

triangular quadratic elements were used. The results obtained from the models developed only using quadrilaterals are shown on the next section.
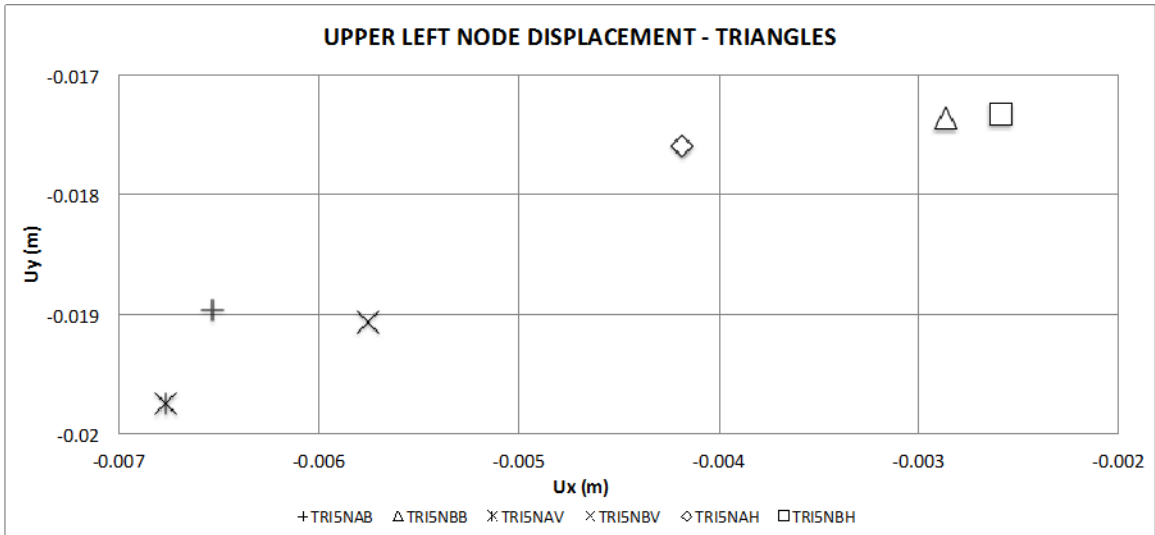
Figure 21. Models using elements with 5 nodes. Displacements at the upper edge – Left corner.

In Figure 21 the models TRI5NAB, TRI5NBV, TRI5NAV, that have quadratic edges in the base and the upper part of the models (edge carrying the distributed load) tend to behave similarly and their displacements are located in the left side of the graph. The other models, that either have a linear edge at the base or at the upper part, display similar displacements located at the right side of the previous chart.
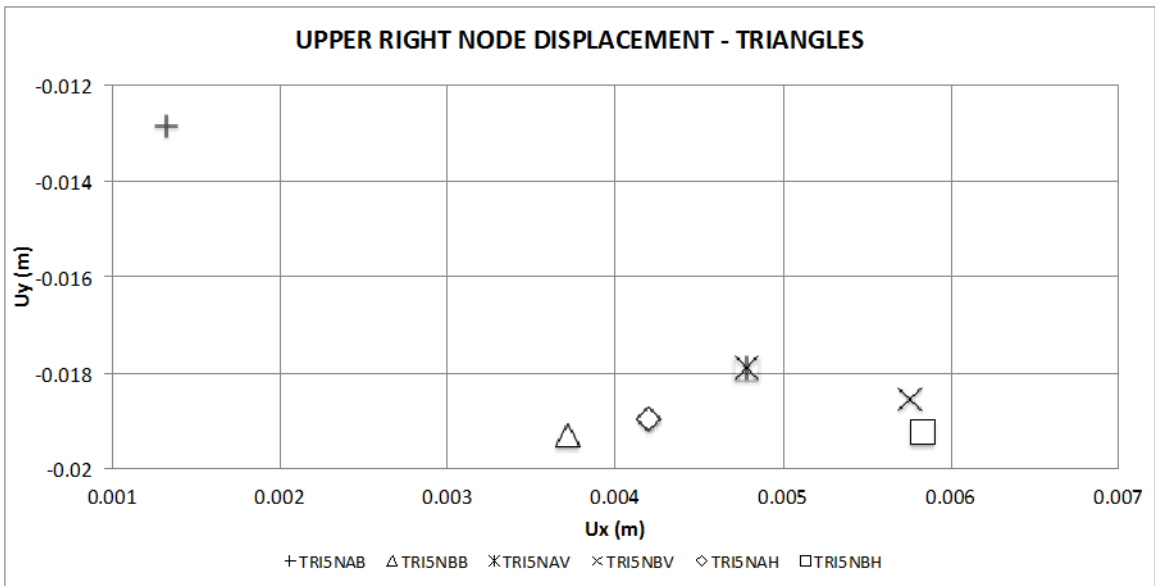
Figure 22. Models using elements with 5 nodes. Displacements at the upper edge – Right corner.

Figure 22 shows a more clustered plot, since all the models tend to have the same displacements except for the model TRI5NAB. Some of the models were not included on the plots since not every one using triangles has a node located at the middle of the upper edge. The addition of these could lead to non-representative results. The data remaining was sorted in two different plots; the first one includes models using 5-node triangles and the second one, models using 4-node and 6-node triangles.
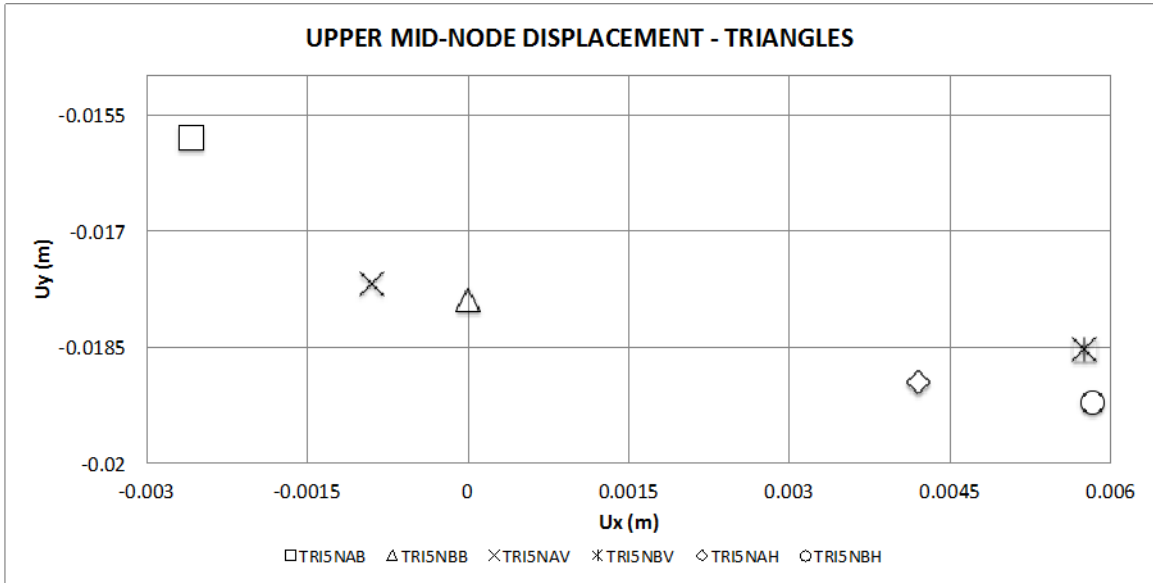
Figure 23. Models using elements with 5 nodes. Displacements at the upper edge of the models – Midside nodes (where available)
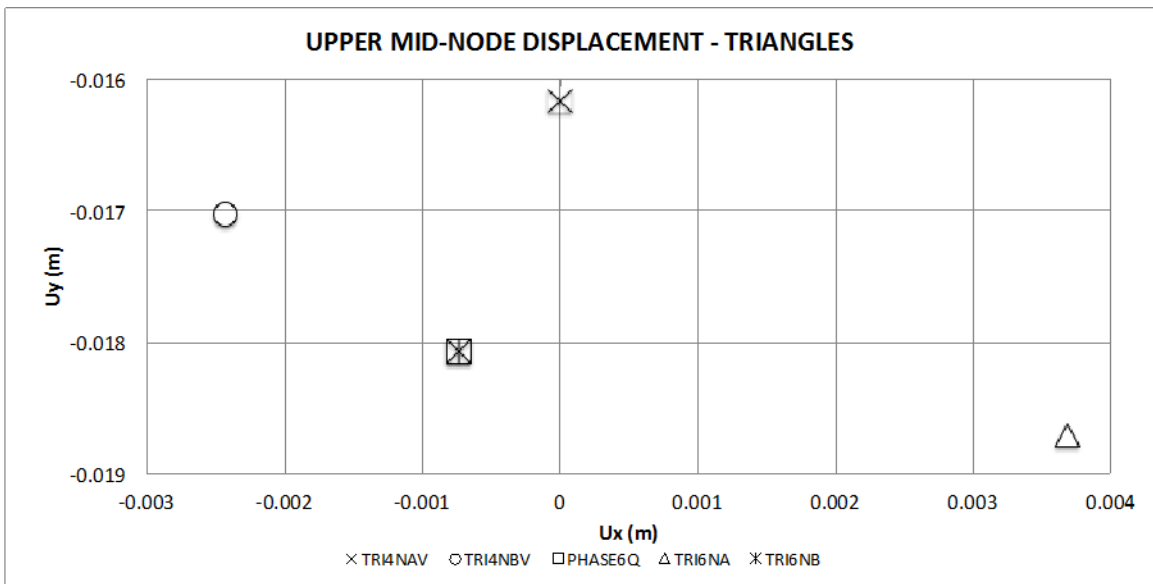
Figure 24. Models using elements with 4 and 6 nodes. Displacements at the upper edge of the models – Midside nodes (where available)

In Figure 24 models PHASE6Q and TRI6NB show the same displacements despite being modeled with different programs. Other models seem to behave according to the orientation of the diagonal edge, which was seen in mostly all the models. In the models where a diagonal comes from the lower left node towards the upper right node, the model tilts to the left and vice versa.

ELEMENTS	Ux (m)	Uy (m)
TRI5NAH	-0.006529	-0.01897
TRI5NAB	-0.006529	-0.01897
TRI4NBH	-0.002553	-0.01665
TRI4NBV	-0.006819	-0.0204
WITH RESPECT TO		
PHASE3L	-0.0062603	-0.018818
AT	UL	
	ERROR IN X	ERROR IN Y
% E TRI5NAH WRT PHASE3L	4.29%	0.81%
% E TRI5NAB WRT PHASE3L	4.29%	0.81%
% E TRI4NBH WRT PHASE3L	59.22%	11.52%
% E TRI4NBV WRT PHASE3L	8.92%	8.41%

Table 10 5-node triangular transition elements – Diagonal inverted

The tendency of displacements mainly obeys to the orientation of the diagonal edge in the triangular elements, rather than problems in the formulation of the elements, as can be seen in APPENDIX 2. TYPE I MODELS USING TRIANGULAR ELEMENTS - RESULTS; nevertheless, it is to notice, that the right upper corner node always tilts towards the negative vertical axis and the negative horizontal axis. Correspondingly, the same behavior is noticed in the upper right corner node, where all the nodes are displaced towards the positive horizontal axis and the negative vertical axis.

In the case of the upper mid-side nodes the absence of displacement in the horizontal direction is palpable. The most considerable displacements are shown in the vertical direction.

ELEMENTS	Ux (m)	Uy (m)
TRI5NBB	-0.0067612	-0.01975
TRI5NBV	-0.005754	-0.01907
TRI5NBH	-0.0067612	-0.01975
WITH RESPECT TO		
TRI6NB	-0.005064485	-0.018856
AT	UL	
	ERROR IN X	ERROR IN Y
% E TRI5NBB WRT TRI6NB	33.50%	4.74%
% E TRI5NBV WRT TRI6NB	13.61%	1.13%
% E TRI5NBH WRT TRI6NB	33.50%	4.74%

Table 11 4-node triangular transition elements

In all cases, the elements present an error approximate by 10%; except for the error in x-direction of the element TRI4NBH. Most likely, in this case, the absence of a support causes the difference. In Table 11, the errors in the y direction are almost undistinguishable. Yet, the errors in the horizontal direction obtain values around 30%. The difference is mainly caused by the location of the quadratic edges; elements with similar location of the quadratic edges show a similar behavior.

5.1.2   TYPE I MODELS USING QUADRILATERALS

The same performance evaluation applied for the models comprised by triangular elements was applied to the quadrilaterals. Several models were run in three different programs: SAP2000®, Phase^2 and SIMFEM.

ELEMENTS	Ux (m)	Uy (m)
PHASE6Q	-0.0050645	-0.018856
PHASE3L	-0.0062603	-0.018818
QUAD_SAP	-0.0061	-0.0182
WITH RESPECT TO		
QUA4N	-0.005117	-0.01705
AT	UL	
	ERROR IN X	**ERROR IN Y**
% E PHASE6Q WRT QUA4N	1.03%	10.59%
% E PHASE3L WRT QUA4N	22.34%	10.37%
% E QUAD_SAP WRT QUA4N	19.21%	6.74%

Table 12 Comparison of triangular and quadrilateral elements

In Table 12, the behaviour of quadratic and linear elements is evaluated. Some values of the percentage of error are above 15%. Nevertheless, the tilting direction of all the elements is towards the negative horizontal axis and the negative vertical axis (same direction as the load). The comparison was done between models using triangular elements and models using quadrilateral elements.

Replicating the plots shown for triangular elements, similar plots for quadrilateral elements are considered. In the next two plots, only the models using 4-node quadrilaterals and 5-node quadrilaterals are displayed. The location of the quadratic edge in the 5-node quadrilaterals is described in APPENDIX 1. TYPE I MODELS USING QUADRILATERAL ELEMENTS – RESULTS.

In Figure 25 and Figure 26, a perfect match is observed between models QUA4N and QUA5ND. Model QUA5ND has the quadratic edge located in the base, consequently, the edge carrying the load and the lateral edges remain linear, and this implies the similar conditions between these and the linear models, and the perception

of similar displacements as a result. The other models present similar displacements, due to the location of the quadratic order diagonal.
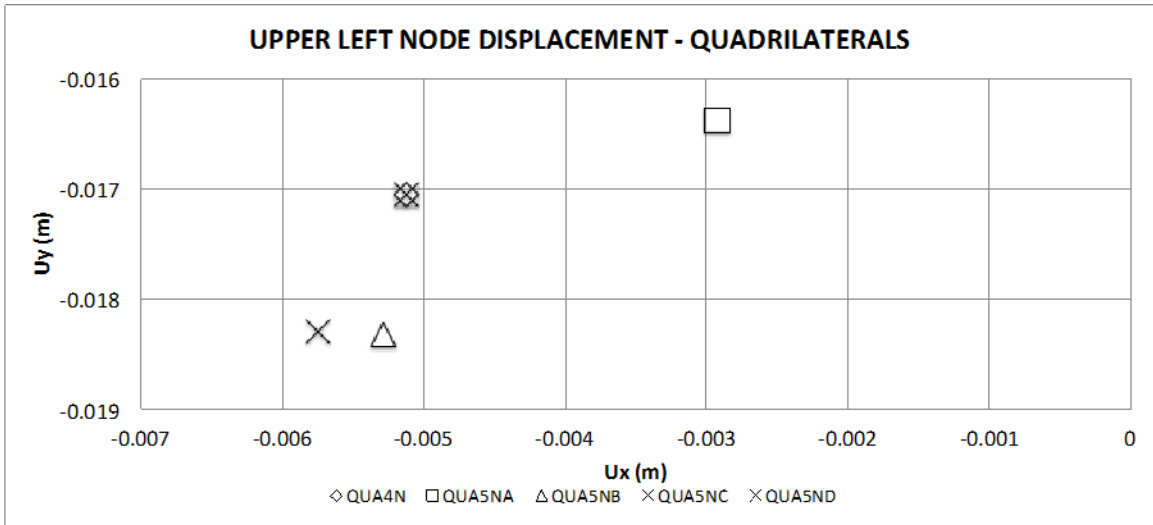
Figure 25. Models using elements with 4 and 5 nodes. Displacements at the upper edge – Left corner
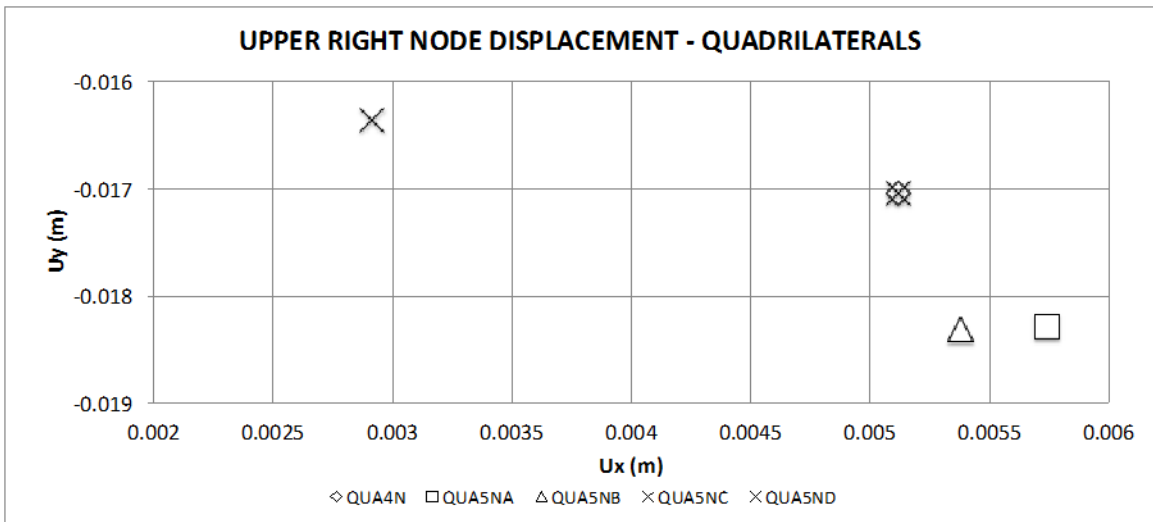
Figure 26 Models using elements with 4 and 5 nodes. Displacements at the upper edge – Right corner

ELEMENTS	Ux (m)	Uy (m)
QUA5NA	-0.0029174	-0.016381
QUA5NB	-0.0052813	-0.01832
QUA5NC	-0.005742	-0.01829
QUA5ND	-0.0051168	-0.017056
WITH RESPECT TO		
QUA4N	-0.005117	-0.01705
AT	UL	
	ERROR IN X	**ERROR IN Y**
% E QUA5NA WRT QUA4N	42.99%	3.92%
% E QUA5NB WRT QUA4N	3.21%	7.45%
% E QUA5NC WRT QUA4N	12.21%	7.27%
% E QUA5ND WRT QUA4N	0.00%	0.04%

Table 13 5-node quadrilaterals transition elements

Despite the fact that error values below 10% were reached in all the elements, in the vertical direction, these values are greater than 35% in the case of those elements that count with quadratic edges where the displacements were being measured. It is important to observe that the displacements obtained are always oriented to the predicted direction, although the influence of different types of edges in the element is noticeable.
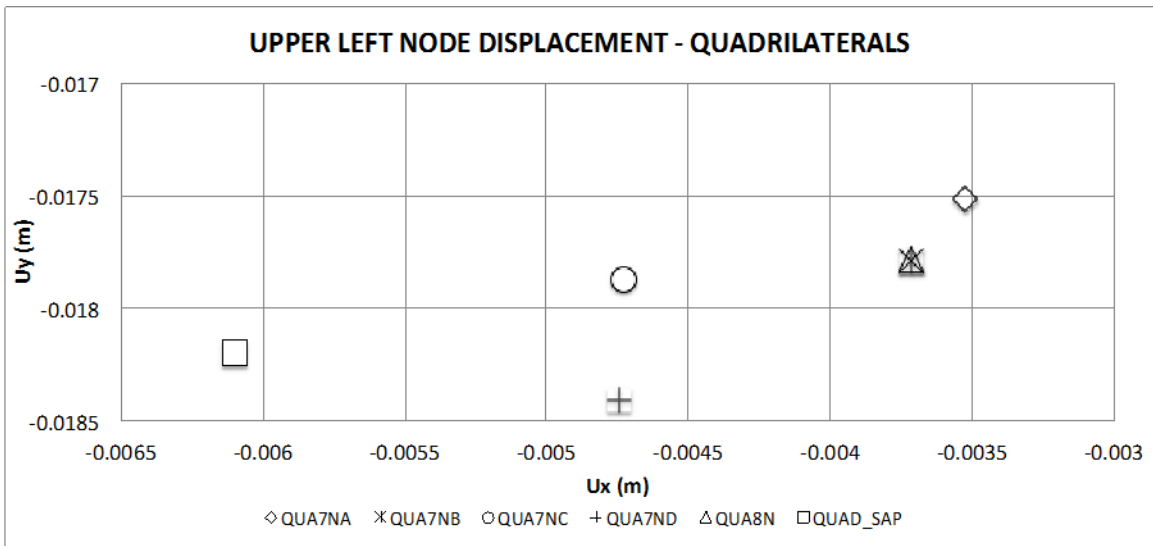
Figure 27. Models using elements with 7 and 8 nodes. Displacements at the upper edge – Left corner
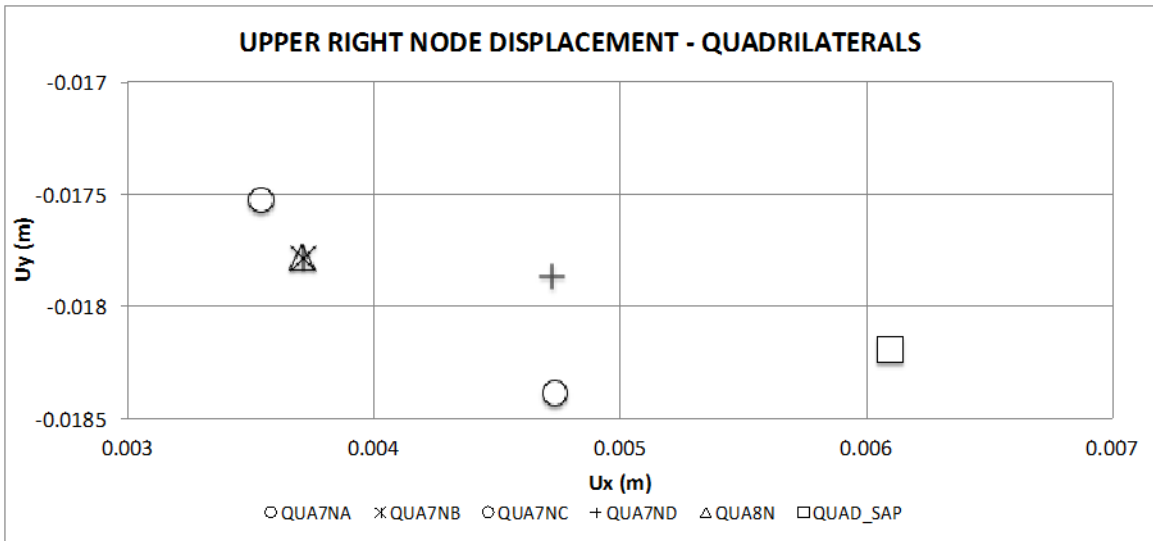
Figure 28 Models using elements with 7 and 8 nodes. Displacements at the upper edge – Right corner

In Figure 27 and Figure 28, QUA8N (quadratic) and QUA7NA (only has a linear edge located at the edge that carries the load) show the same displacements. Models QUA7NC and QUA7ND that have the linear edge at the right and left edge of the model respectively, show similar displacement in the x-axis direction. The nature of the model

44

QUAD_SAP, which has no quadratic edges, is reflected in having no similar displacements compared to its quadratic or transition counterparts.
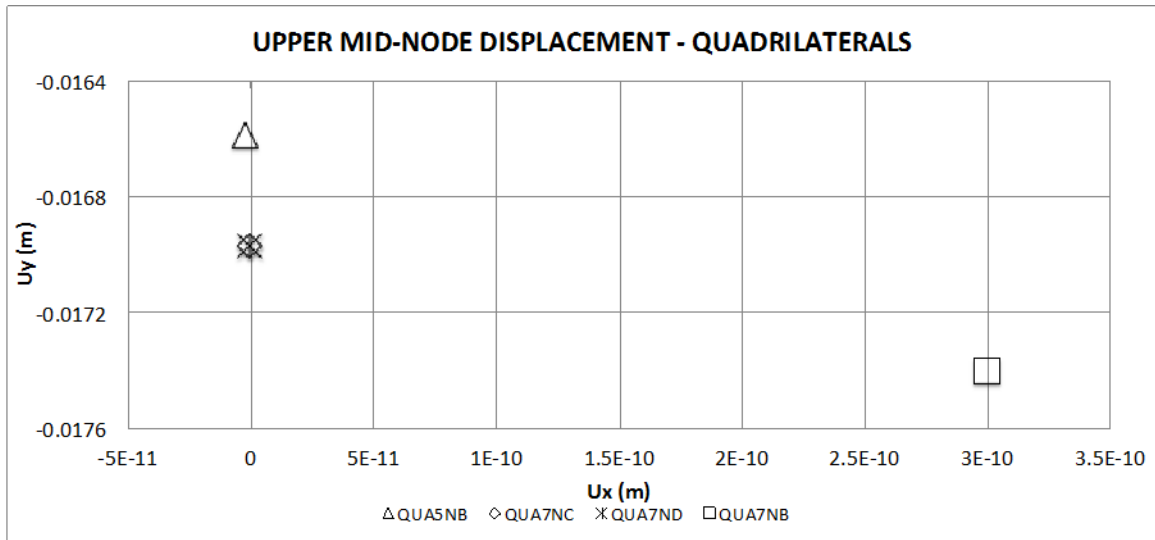
Figure 29. Models using 5 and 7-node elements. Disp. at the upper edge – Midside nodes (where available)

Similar displacements are observed in the mid-node located at the upper edge of these models. It can be said that model QUA7NB presents a different behavior, but this is only noticeable because of the scale used for the plots. The missing diagonal in these models may lead to a more uniform displaced shape compared to the models type I using triangular elements.

ELEMENTS	Ux (m)	Uy (m)
QUA7NA	-0.003524	-0.017515
QUA7NB	-0.003714	-0.017789
QUA7NC	-0.004724	-0.01787
QUA7ND	-0.004742	-0.018406
WITH RESPECT TO		
QUA4N	-0.005117	-0.01705
AT	UL	
	ERROR IN X	**ERROR IN Y**
% E QUA7NA WRT QUA4N	31.13%	2.73%
% E QUA7NB WRT QUA4N	27.42%	4.33%
% E QUA7NC WRT QUA4N	7.68%	4.81%
% E QUA7ND WRT QUA4N	7.33%	7.95%

Table 14 7-node quadrilaterals transition elements – 4-node quads.

The same analysis performed to the 5-node elements might be applied in the case of 7 node elements. The percentage of error remains within the same values as those presented in Table 13.

ELEMENTS	Ux (m)	Uy (m)
QUA7NA	-0.003524	-0.017515
QUA7NB	-0.003714	-0.017789
QUA7NC	-0.004724	-0.01787
QUA7ND	-0.004742	-0.018406
WITH RESPECT TO		
QUA8N	-0.003712	-0.01778
AT	UL	
	ERROR IN X	**ERROR IN Y**
% E QUA7NA WRT QUA8N	5.06%	1.49%
% E QUA7NB WRT QUA8N	0.05%	0.05%
% E QUA7NC WRT QUA8N	27.26%	0.51%
% E QUA7ND WRT QUA8N	27.75%	3.52%

Table 15 7-node quadrilaterals transition elements – 8-node quads.

Similar values for the percentage of error were obtained when the comparison was normalized with respect to a quadratic quadrilateral. However, values greater than 7% were reached only in the elements where the quadratic edges are located in the lower part of the model, and there is one more support located in the mid-side node.

After these results were analyzed and the performance was classified as satisfactory for presenting percent errors as similar as those related to the same model run in three different programs (SIMFEM, SAP2000® and Phase[2]). Larger scale models were developed and tested, ensuring a good performance of the transition elements when these are included systematically into a finite element mesh.

5.2 TYPE II MODELS

Once the results obtained from the type I models were analyzed and were classified as satisfactory, more comprehensive tests were carried out in order to evaluate the performance of the transition elements in larger models. Several models, including the aforementioned transition elements were developed, where the same mesh was assumed for either quadratic, linear or transition elements. The load scheme and geometry assumptions are shown in Figure 30. The material properties that were assigned to the models are shown in Table 5.

Regarding the boundary conditions of the model, roller type supports were placed in the left and lower boundaries. In the case of the lower left corner of the model, any displacement at the vertical and horizontal axis was restricted (fixed type support). The assumptions taken for the boundary conditions were the same on the type II models for both quadrilateral elements and triangular elements.
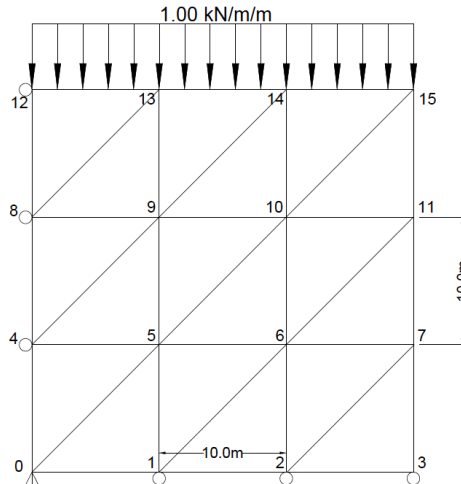
Figure 30 Type II model. Load and geometry assumptions (Using triangular elements)

5.2.1   TYPE II MODELS UTILIZING TRIANGULAR ELEMENTS

A total of 5 models utilizing triangular elements were developed. One of them was modeled in SAP2000® and the other four were modeled using the SIMFEM code, with the next specifications:

- TRI3N: The elements were assumed as 3-node linear triangles (Figure 31 left)
- TRI4N: The elements were assumed as 4-node transition triangles (Figure 31 right)
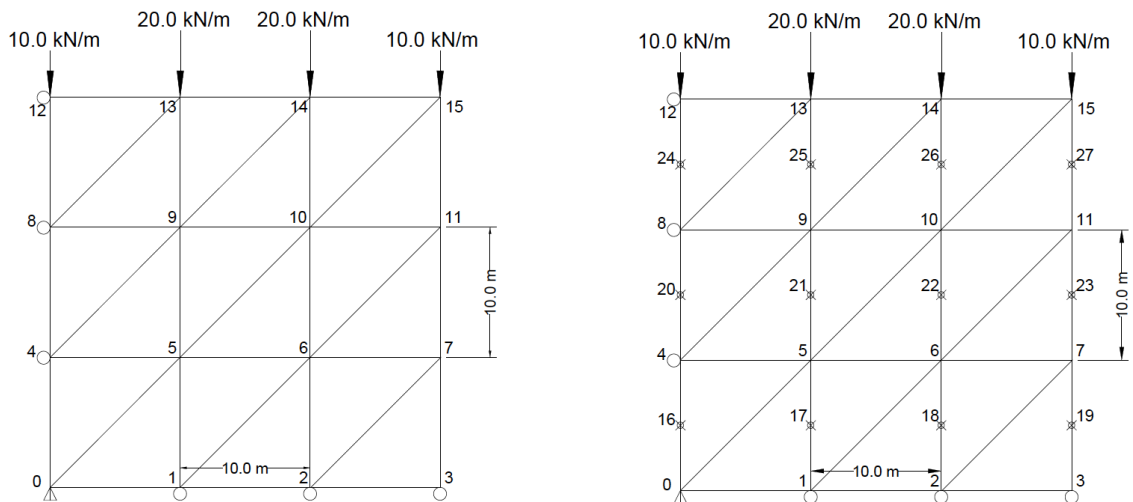
Figure 31 Type II models TRI3N and TRI4N

- TRI5N: The elements were assumed as 5-node transition triangles (Figure 32 left).
- TRI6N: The elements were assumed as 6-node quadratic triangles (Figure 32 right).
- TRI3N_SAP2000: All the elements were assumed as 3-node linear triangles. Same conditions as TRI3N model.
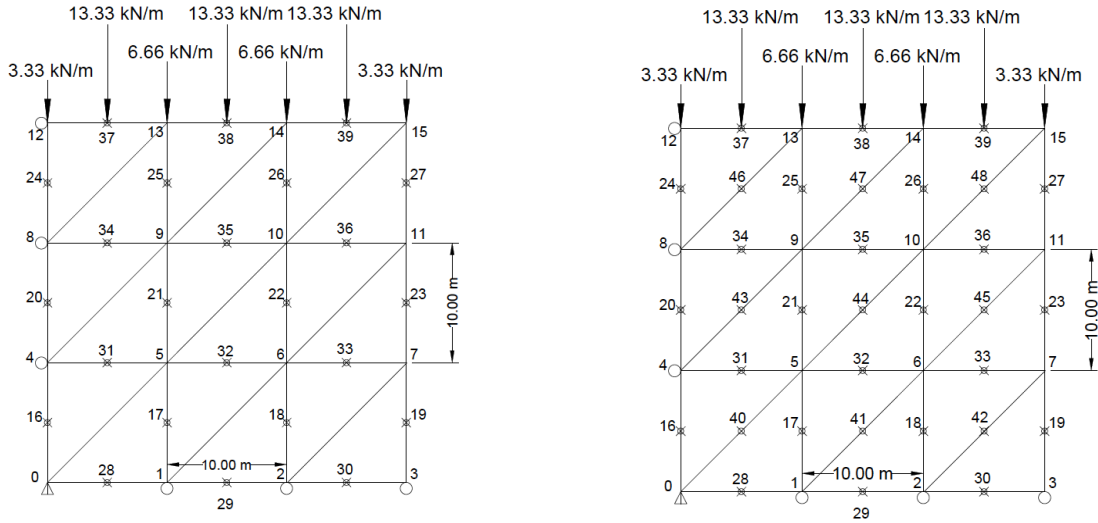
Figure 32 Type II models TRI5N and TRI6N

The results obtained exhibited a good agreement between all the models. A maximum percent error of 5.16%, was found at the upper right node of the model done using quadratic triangles run in SIMFEM with respect to the model done with linear triangles run in SAP2000®. For a better understanding of the following tables, the reader should refer to the first paragraph of this subchapter.

MODEL	Ux (m)	Uy (m)
TRI3N	0.02558	-0.06277
TRI4N	0.02566	-0.06324
TRI5N	0.02525	-0.06249
TRI6N	0.02428	-0.0614
WITH RESPECT TO		
TRI3N_SAP2000	0.0256	-0.0628
AT CORNER		
Upper Right		
%E TRI3N WRT TRI3N_SAP2000	0.08%	-0.05%
%E TRI4N WRT TRI3N_SAP2000	0.23%	-0.70%
%E TRI5N WRT TRI3N_SAP2000	1.37%	-0.49%
%E TRI6N WRT TRI3N_SAP2000	5.16%	-2.23%

Table 16 Type II models at the upper right corner normalized with respect to FEM in SAP2000®.

All the differences in the values obtained were below 6%, which corresponds to the model developed with quadratic elements. If the values were only compared between transition elements and linear elements, the results would not be greater than 1.37% in either direction (x or y axis).

48

MODEL	Ux (m)		MODEL	Uy (m)
TRI3N	0.0281		TRI3N	-0.062538
TRI4N	0.02808		TRI4N	-0.06208
TRI5N	0.0283		TRI5N	-0.06286
TRI6N	0.02892		TRI6N	-0.06329
WITH RESPECT TO			WITH RESPECT TO	
TRI3N_SAP2000	0.0281		TRI3N_SAP2000	-0.0625
AT CORNER			AT CORNER	
Lower Right			Upper Left	
%E OF TRI3N TO TRI3N_SAP2000	0.00%		%E OF TRI3N TO TRI3N_SAP2000	-0.06%
%E OF TRI4N TO TRI3N_SAP2000	0.07%		%E OF TRI4N TO TRI3N_SAP2000	-0.67%
%E OF TRI5N TO TRI3N_SAP2000	0.71%		%E OF TRI5N TO TRI3N_SAP2000	-0.58%
%E OF TRI6N TO TRI3N_SAP2000	2.92%		%E OF TRI6N TO TRI3N_SAP2000	-1.26%

Table 17 Type II models (Triangles) at the lower right corner normalized with respect to FEM in SAP2000®.

The model has a boundary condition in the x direction for the node of interest as shown in Figure 31 and Figure 32. Thus, only displacements at the vertical direction were obtained. The greatest percentage of error was 1.26% in the vertical direction and 2.92% in the horizontal direction. For better understanding of the numbers presented before, a series of plots were developed and the results are presented as follows:
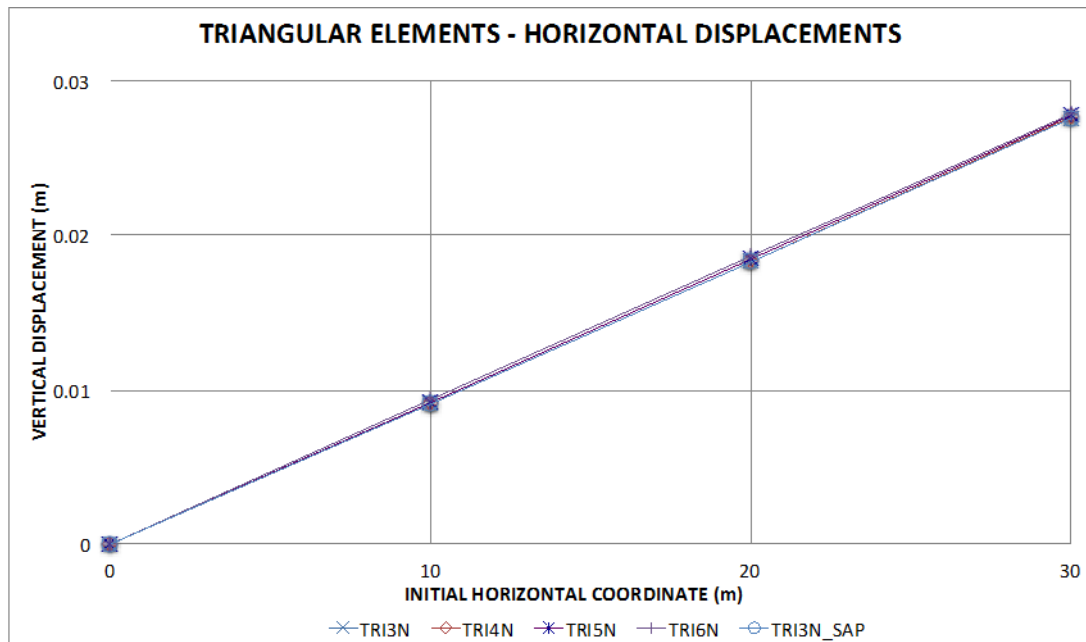
Figure 33 Horizontal displacements of corner nodes at Y = 10 m

The lines drawn in Figure 33 through Figure 38 and in Figure 41 through Figure 46 do not represent a regression of the results; only connect the data belonging to the same element facilitating the discernment of the plots.
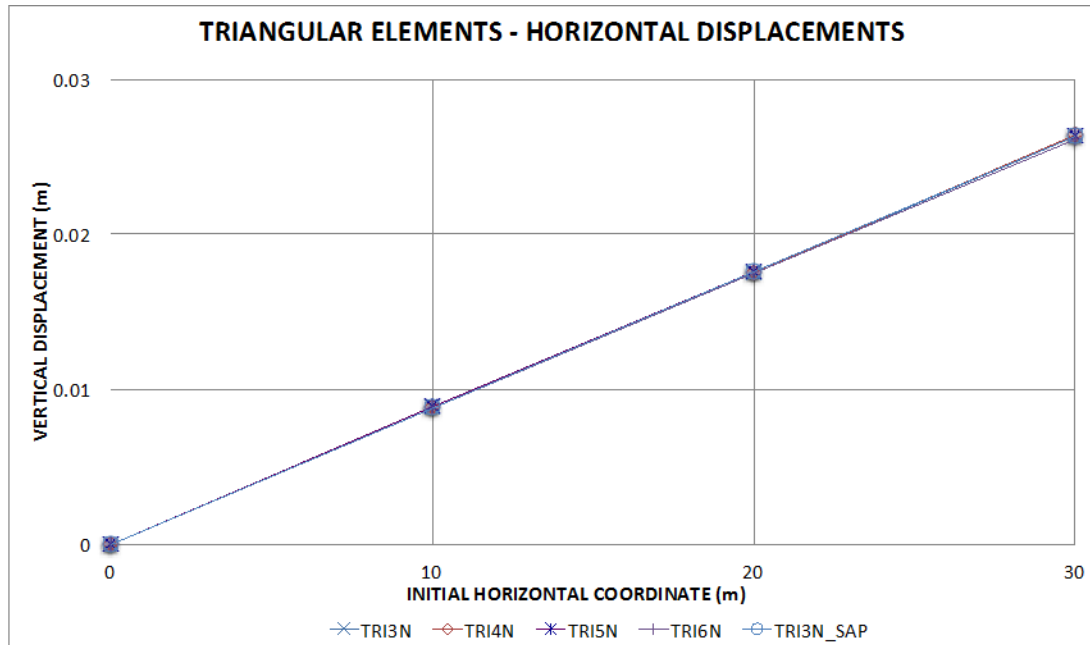
Figure 34 Horizontal displacements of corner nodes at Y = 20 m
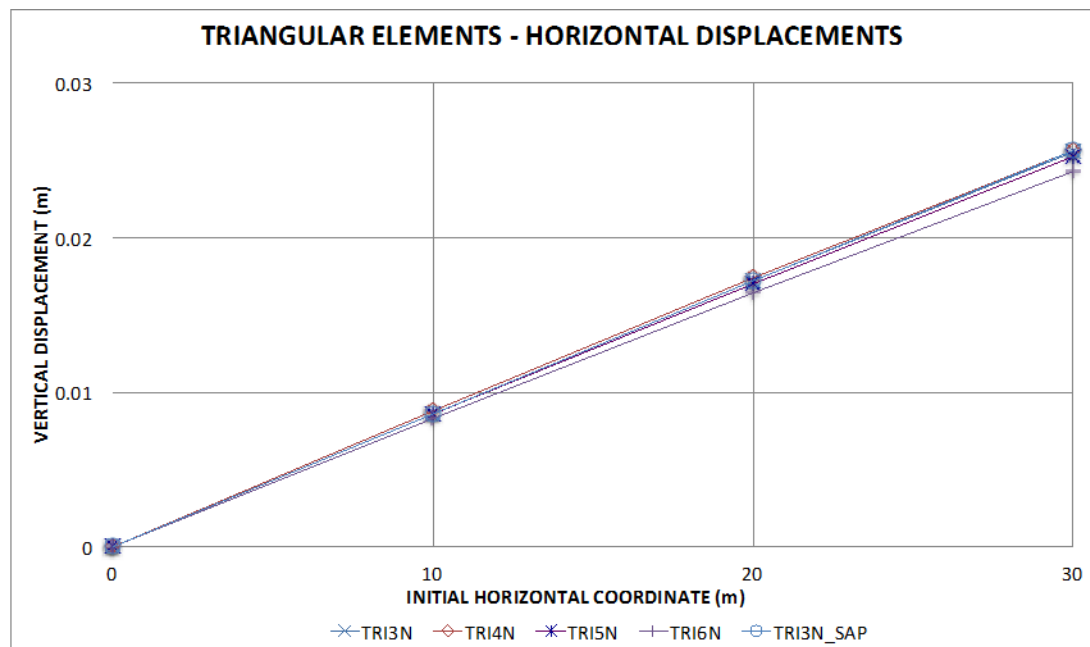
Figure 35 Horizontal displacements of corner nodes at Y = 30 m

Analyzing the displacements in the x-axis direction, the similarity is noticeable between all the models using triangles. In Figure 35, the displacements obtained from the model composed of only quadratic order elements, show greater displacements than the others. Still, its displacements only present a percentage of error of 2.92% with respect to the model built with linear order elements. The models exhibit similar displacements at different vertical coordinates (Y=10m, Y=20m and Y=30m).
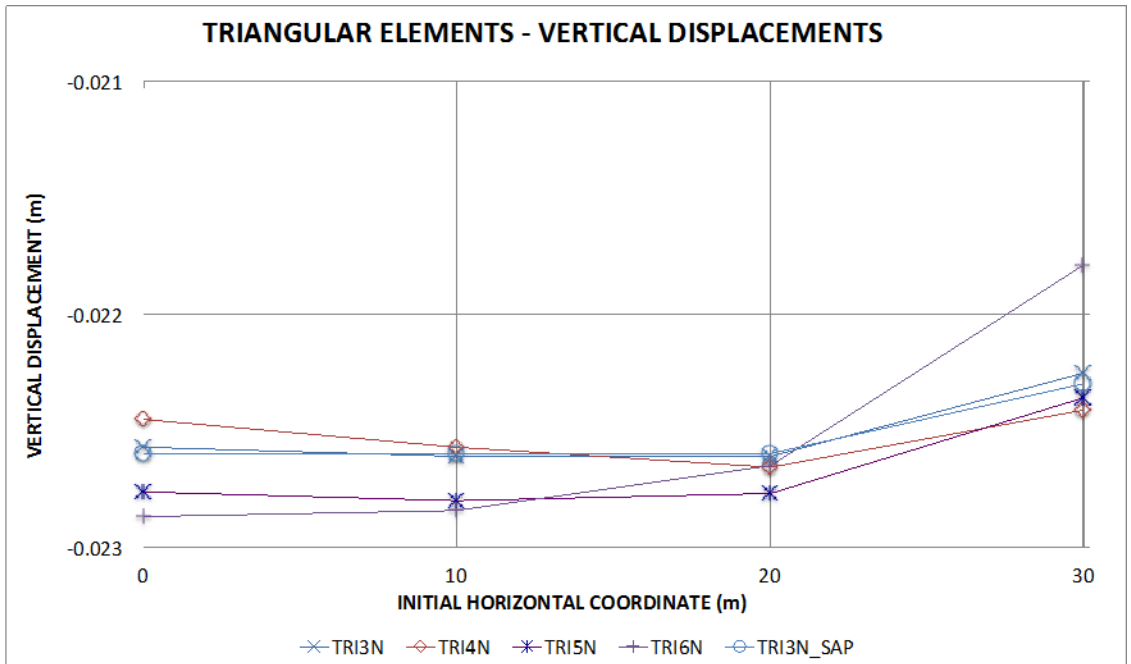
Figure 36 Vertical displacements of corner nodes at Y = 10 m
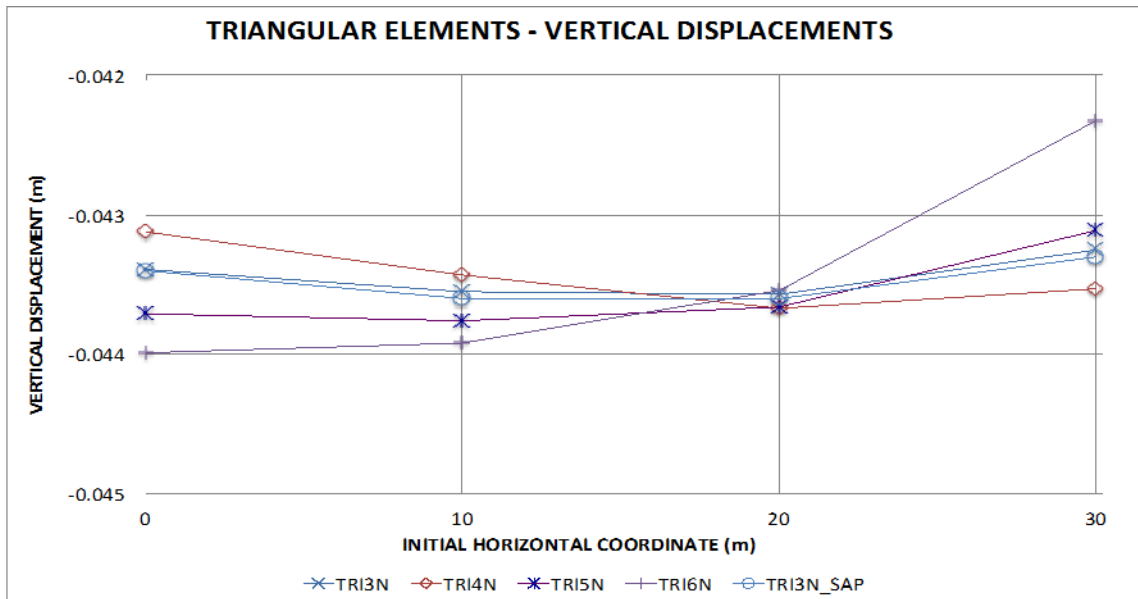
Figure 37 Vertical displacements of corner nodes at Y = 20 m
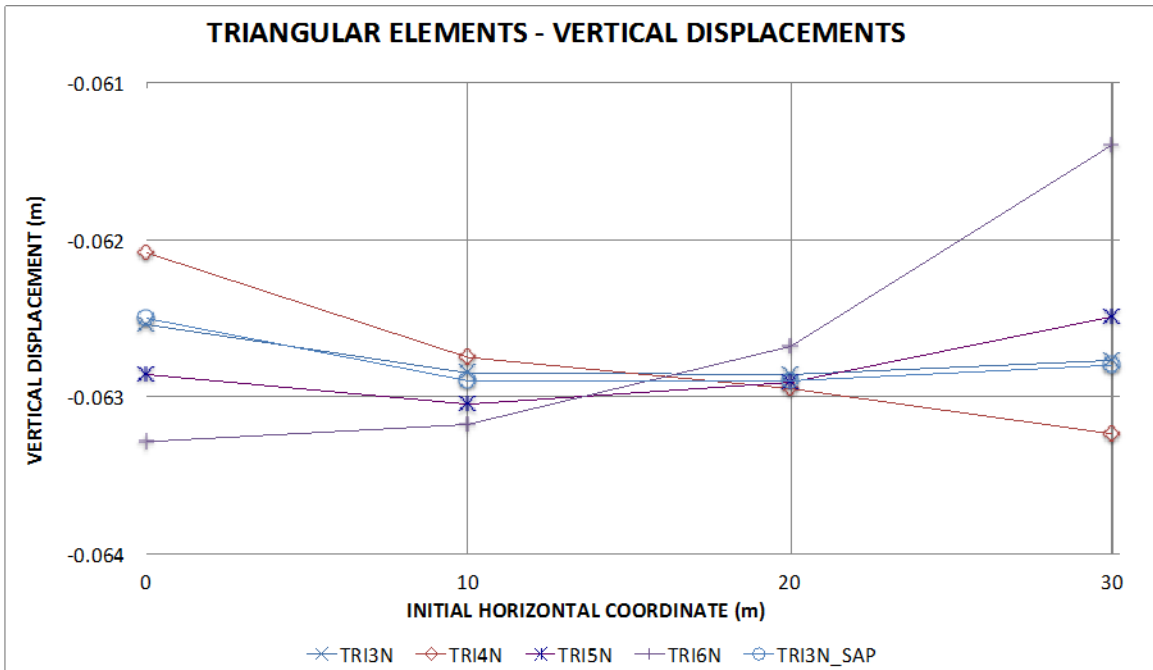
Figure 38 Vertical displacements of corner nodes at Y = 30 m

The role of the transition nodes is more noticeable on the displacements in the vertical direction; this tendency is kept with all the models plotted in Figure 36 through Figure 38 (TRI3N, TRI4N, TRI5N and TRI6N). The scale of the plots may affect the perception of the differences between the models, which show different tendencies. Once, the numerical evaluation of the displacements is carried out, the percentages of error are found in the range of 2% to 3%. As mentioned before, none of the models presented percentages of error in the vertical direction above 6%. As seen in the plots and in the data analysis, a very high equivalence of displacements was found using SIMFEM and SAP2000®.

5.2.2   TYPE II MODELS UTILIZING QUADRILATERAL ELEMENTS

Five models utilizing quadrilateral elements were developed. One of them was modeled in SAP2000® and the other four were modeled using the SIMFEM code with the next specifications:

- QUA4N: Elements assumed as 4-node linear quadrilaterals (Figure 39 left)
- QUA5N: Elements assumed as 5-node transition quadrilaterals (Figure 39 right)

Figure 39 Type II models QUA4N and QUA5N

- QUA7N: Elements assumed 7-node transition quadrilaterals (Figure 40 left)
- QUA8N: Elements assumed as 8-node quadratic quadrilaterals (Figure 40 right)
- QUA4N_SAP2000: Elements assumed as 4-node linear quadrilaterals.

Figure 40 Type II models QUA7N and QUA8N

The results show an equivalence between the models developed using SIMFEM regardless the amount of nodes in the elements, although the same differences in the percentage of error are observed among all the models run in SIMFEM and the model run in SAP2000®. This is most likely caused by the element formulation done by SAP2000®, which assumes only four integration points. Nine integration points were assumed in the models run using SIMFEM and the extrapolation necessary to recover the stresses at the nodes affected the results.

53

MODEL	Ux (m)	Uy (m)
QUA4N	0.02341	-0.05467
QUA5N	0.0239733	-0.05467
QUA7N	0.02342	-0.05468
QUA8N	0.0234	-0.05466
WITH RESPECT TO		
QUA4N_SAP2000	0.0247	-0.0616
AT CORNER		
Upper Right		
%E OF QUA4N TO QUA4N_SAP2000	5.22%	-11.25%
%E OF QUA5N TO QUA4N_SAP2000	2.94%	-11.25%
%E OF QUA7N TO QUA4N_SAP2000	5.18%	-11.23%
%E OF QUA8N TO QUA4N_SAP2000	5.26%	-11.27%

Table 18. Type II models (Quadrilaterals). Upper right corner with respect to FEM with SAP2000®.

MODEL	Ux (m)		MODEL	Uy (m)
QUA4N	0.02345		QUA4N	-0.05468
QUA5N	0.02344		QUA5N	-0.05468
QUA7N	0.02345		QUA7N	-0.05467
QUA8N	0.02345		QUA8N	-0.05468
WITH RESPECT TO			WITH RESPECT TO	
QUA4N_SAP2000	0.0287		QUA4N_SAP2000	-0.0633
AT CORNER			AT CORNER	
Lower Right			Upper Left	
%E OF QUA4N TO QUA4N_SAP2000	18.29%		%E OF QUA4N TO QUA4N_SAP2000	-13.62%
%E OF QUA5N TO QUA4N_SAP2000	18.33%		%E OF QUA5N TO QUA4N_SAP2000	-13.62%
%E OF QUA7N TO QUA4N_SAP2000	18.29%		%E OF QUA7N TO QUA4N_SAP2000	-13.63%
%E OF QUA8N TO QUA4N_SAP2000	18.29%		%E OF QUA8N TO QUA4N_SAP2000	-13.62%

Table 19 Type II models (Quadrilaterals). Lower right and upper left corners with respect to FEM with SAP2000®.

The model done in SAP2000® does not have the same displacements as those modeled using SIMFEM. All the other models work similarly.
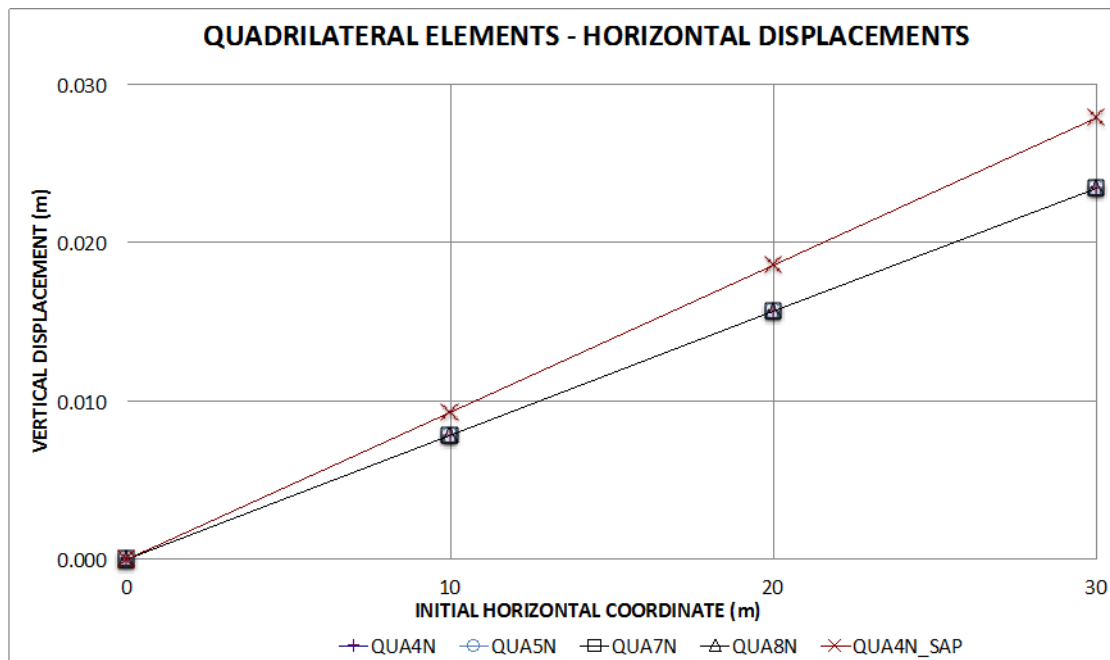
Figure 41 Horizontal displacements of corner nodes at Y = 10 m
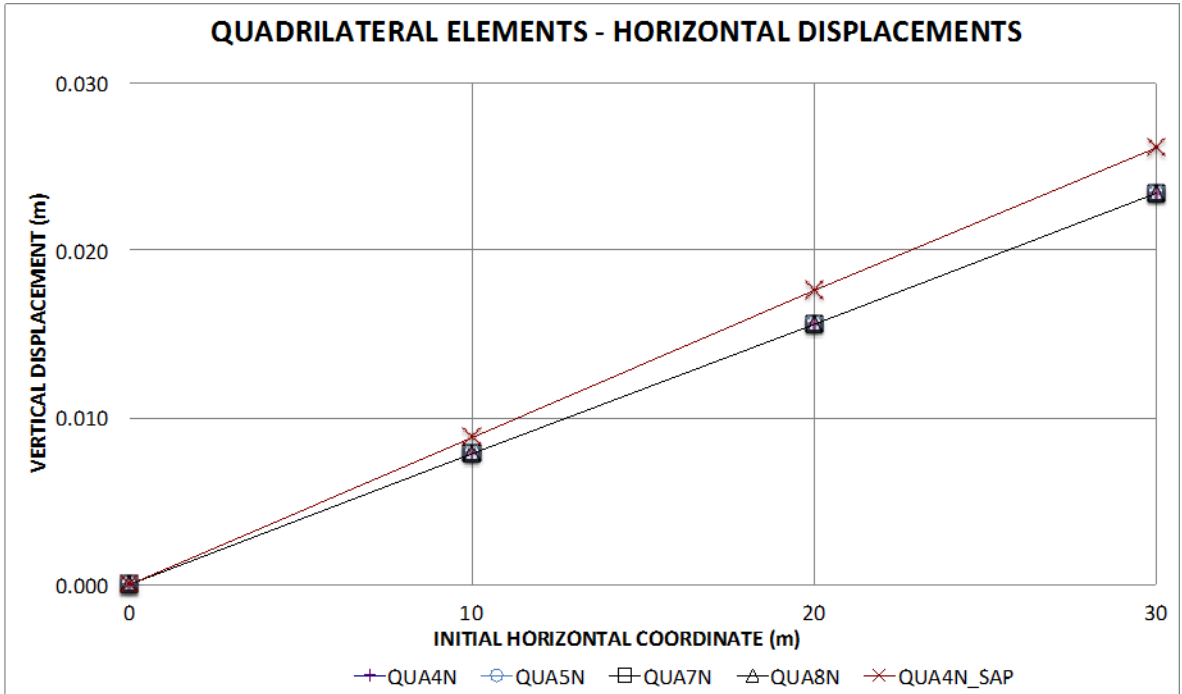
Figure 42 Horizontal displacements of corner nodes at Y = 20 m
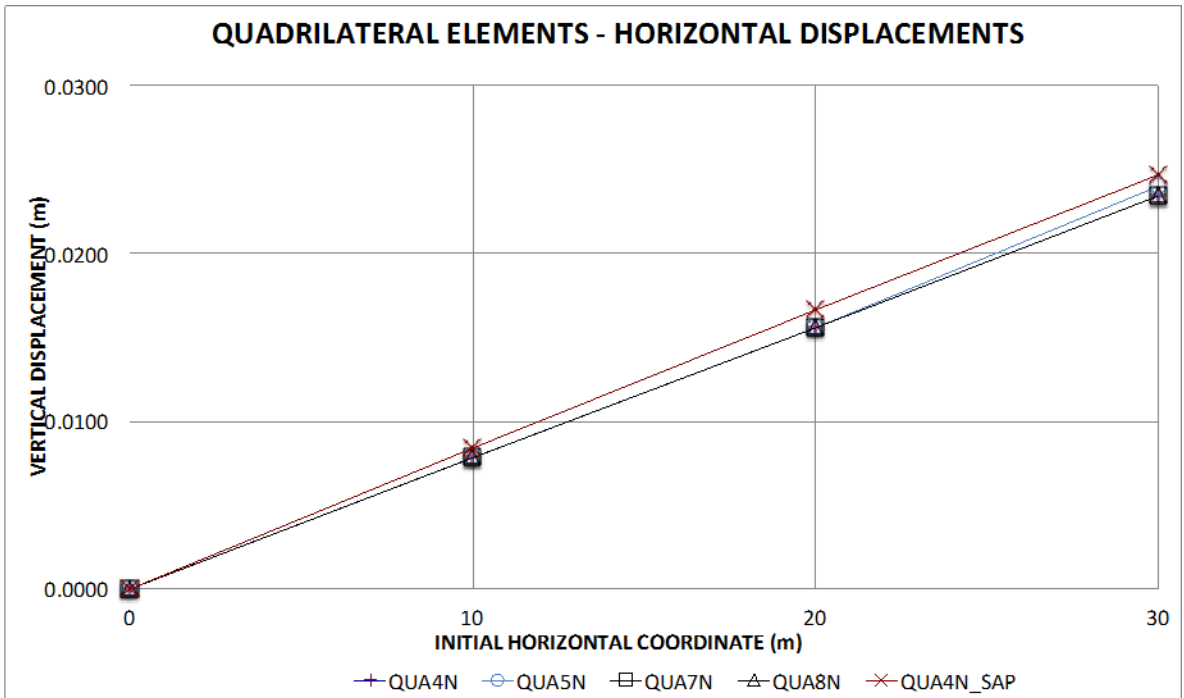
Figure 43 Horizontal displacements of corner nodes at Y = 30

As mentioned in the numerical evaluation of results, in the plots it is observed that the model developed in SAP2000® does not reflect the same behavior as the other models.
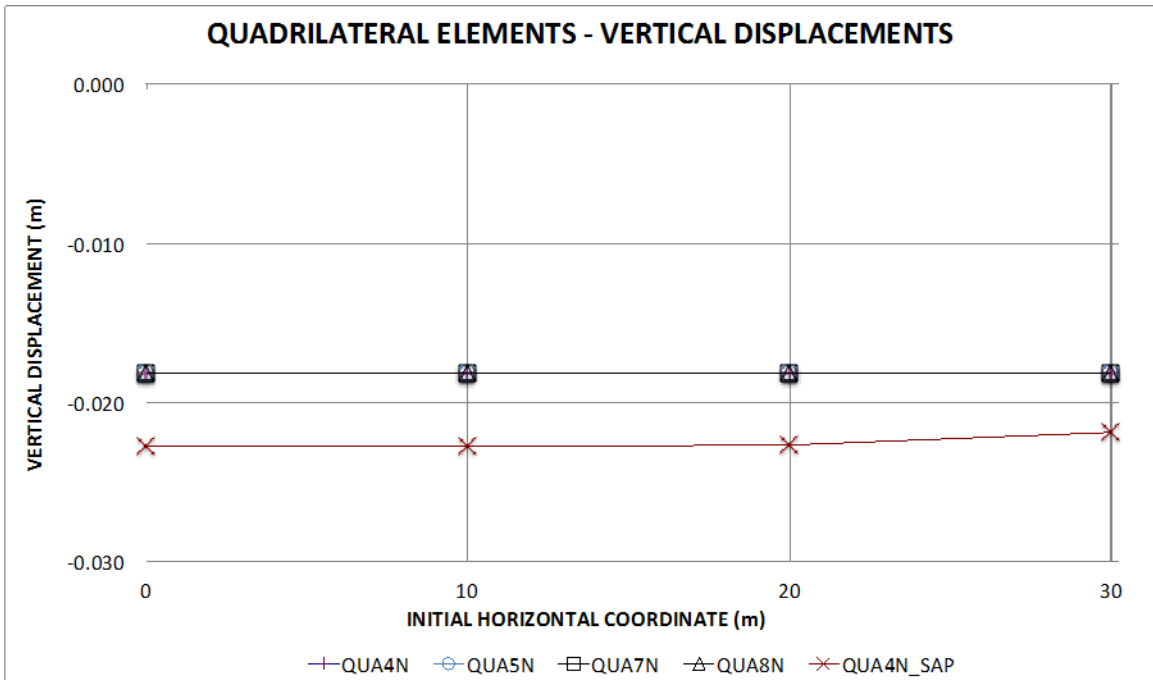
Figure 44 Vertical displacements of corner nodes at Y = 10 m
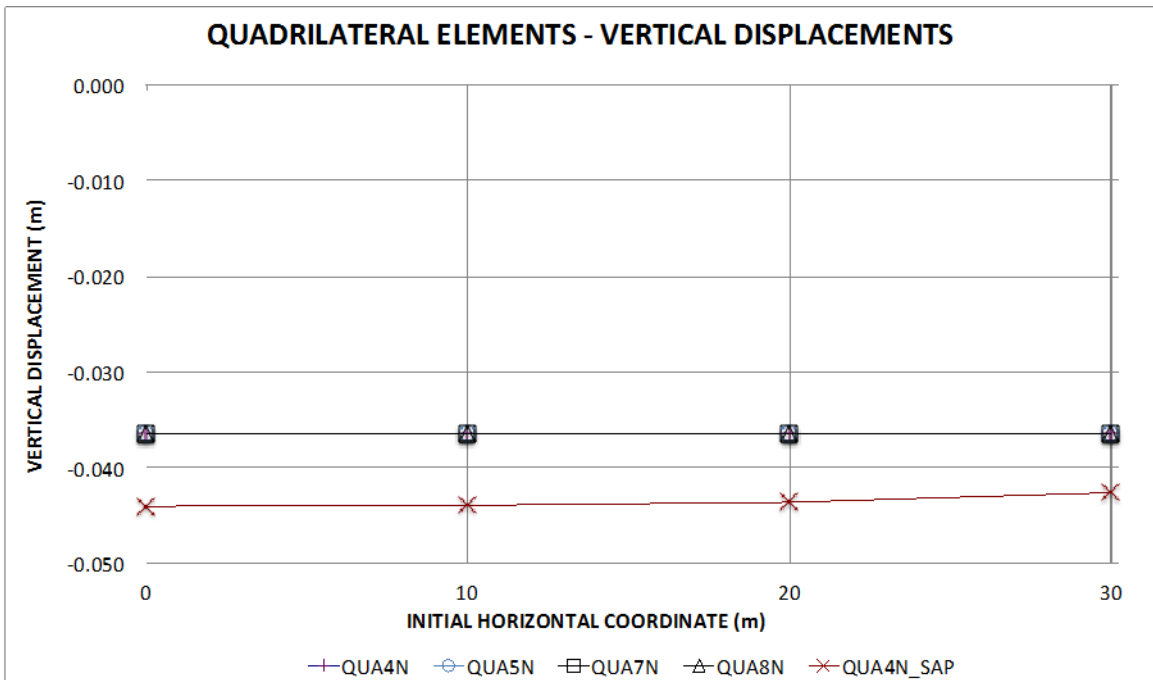
*Figure 45 Vertical displacements of corner nodes at Y = 20 m*
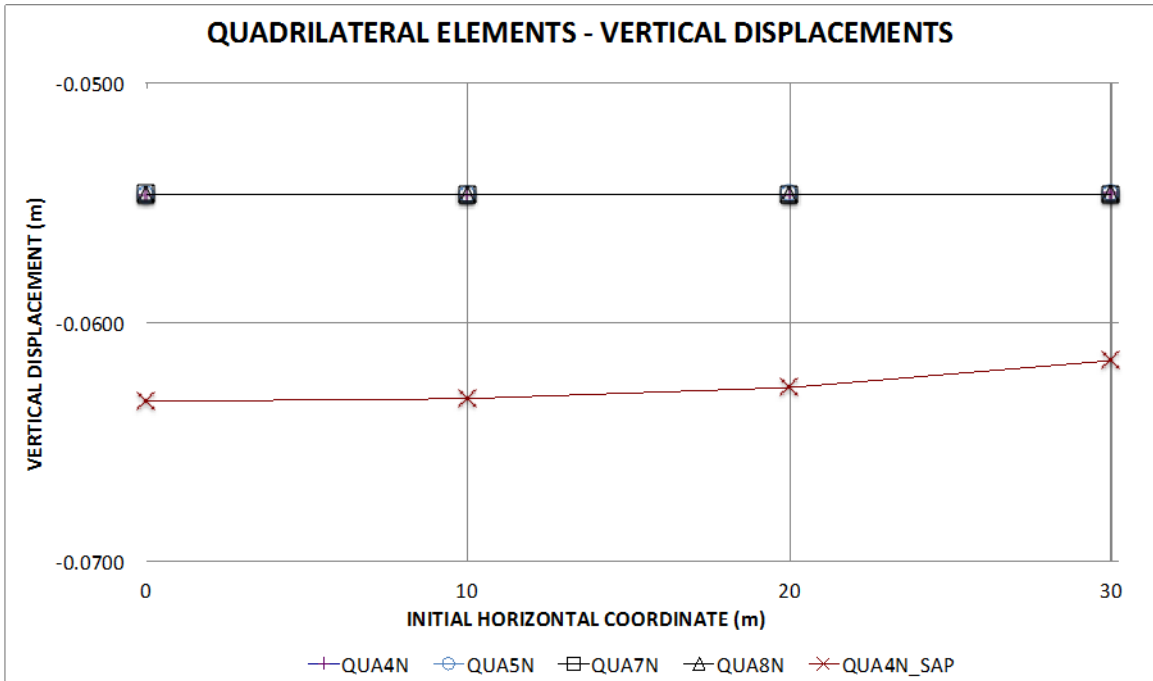
Figure 46 Horizontal displacements of corner nodes at Y = 30

Despite the performance shown by the QUA4N_SAP2000 model, all the models developed with SIMFEM presented similar behavior regardless of the presence of transition elements. Therefore, another test has to be performed successfully having as an objective the testing of different transition zones in the same model.

6. VERIFICATION OF PRACTICAL PERFORMANCE - PRESSURIZED CAVITY

For another validation of performance of the transition elements, a third test was performed on a quarter of a pressurized cavity modeled according to the load and geometric conditions shown in Figure 47. In this case the unit weight of the material surrounding the opening was neglected, while the modulus of elasticity of the material assumed was 1×10^6 kPa and its Poisson's ratio was 0.3.
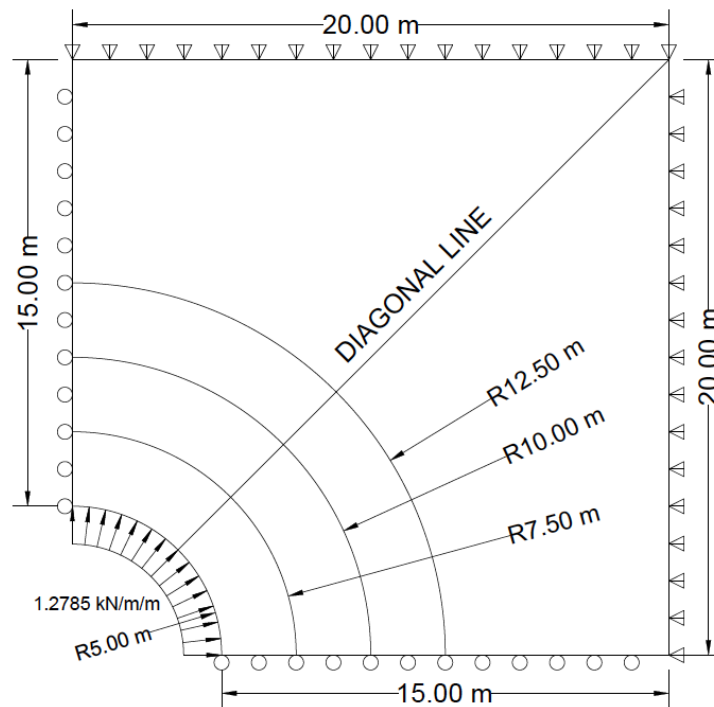
Figure 47 Load, boundary and geometric conditions for the pressurized cavity – Transition zones also shown

The main purpose of this model was to test the transition band, which was located at 3 different radii arbitrarily chosen. For each case, the criterion to determine which nodes are taken into account is quite simple. In both cases (quadrilateral and triangular elements), all the nodes inside the given radius are considered; therefore, all the elements have quadratic edges if they are located inside the radius. However, for those outside of the stated radius, only the nodes comprising the linear elements (corner nodes) are considered. The radii considered were 7.5m, 10m and 12.5m (Figure 47).
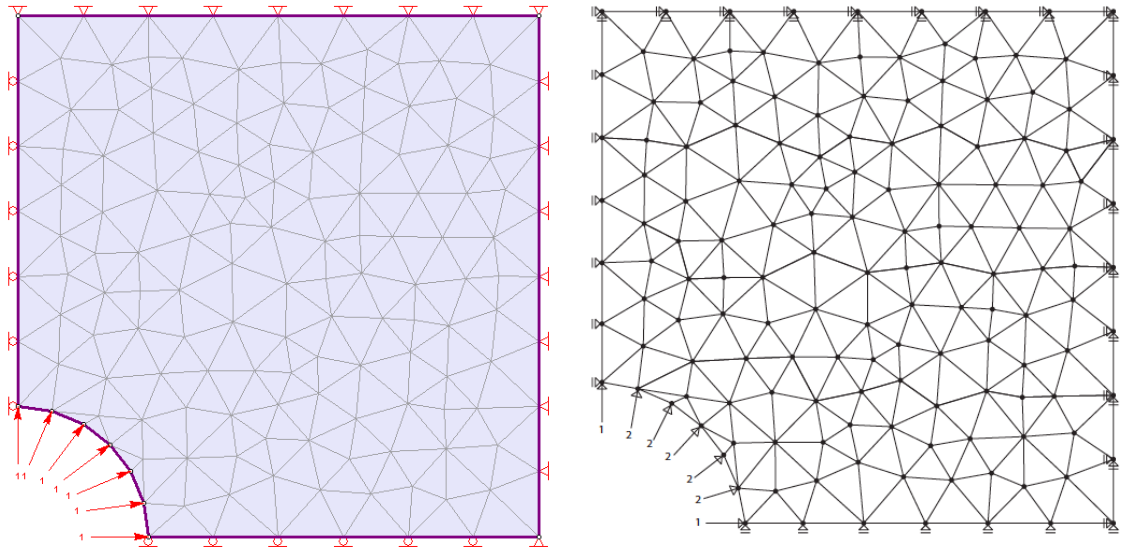
Figure 48 Pressurized cavity using linear triangles - Mesh, geometry, load and boundary conditions for Phase[2] (left) and SIMFEM (right)
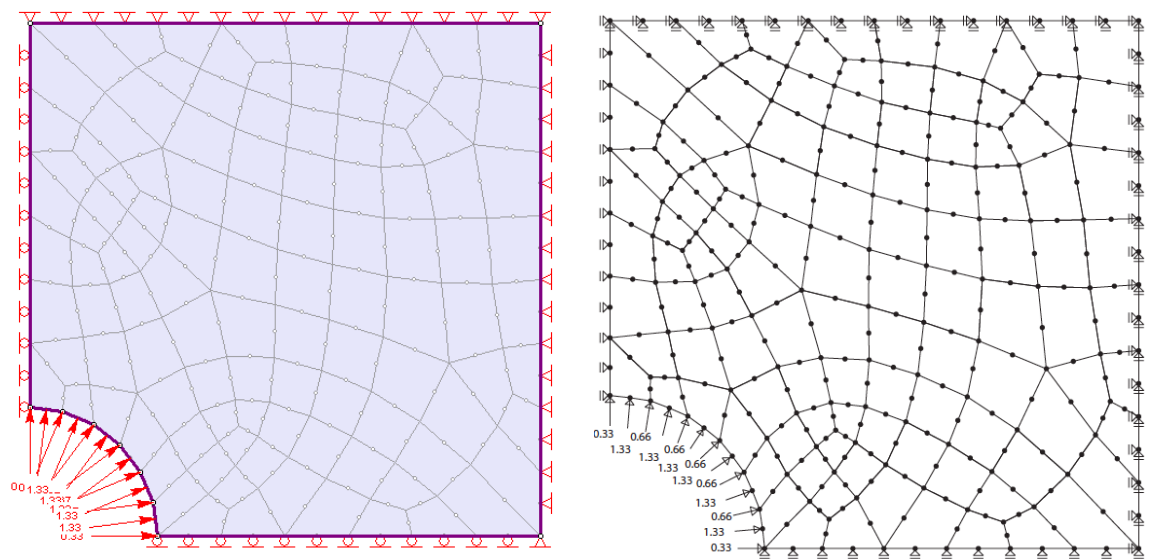
Figure 49 Pressurized cavity with quadratic quadrilaterals - Mesh, geometry, load and boundary conditions for Phase[2] (left) and SIMFEM (right)

The models composed of only quadratic or linear order elements were modeled in SIMFEM and Phase[2], and the undeformed meshes as output of the programs are shown in Figure 48 and Figure 49. The same location of nodes and elements and the boundary conditions are defined in both programs.

6.1 EQUIVALENT NODAL LOADS

The uniformly distributed load applied in the Phase² model was also transformed into a nodal equivalent load, in a similar way as it was done with the Type II models, where a uniformly distributed load at the top of the model was converted as well. In the pressurized cavity, a uniform load of 1.2785 kN/m/m was applied; depending on the order of the element where the load is applied (quadratic or linear), the load is divided in two or three fractions.
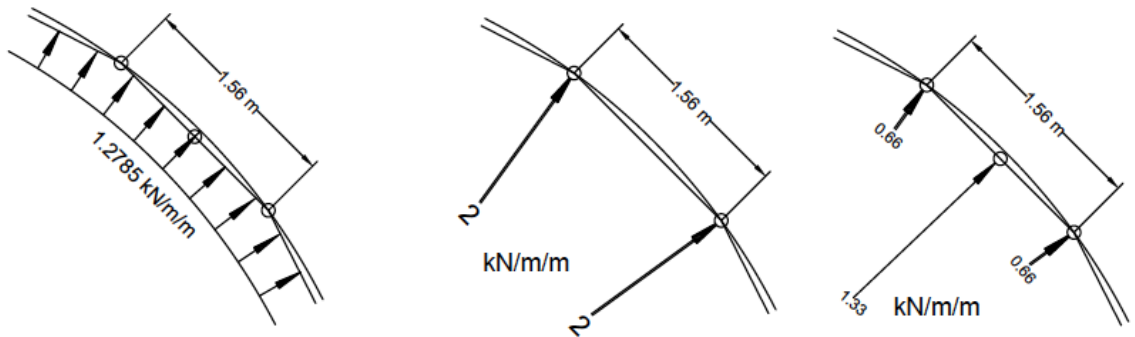
Figure 50. Equivalent nodal load in the pressurized cavity

6.2 PRESSURIZED CAVITY RESULTS ANALYSIS

In order to evaluate the behaviour of the models, a comparison of the stress contours of all the models and the displacements along both axes was performed. The displacements were compared at three different regions: the lower boundary, where due to the support condition only displacements at the horizontal direction were permitted; the left boundary, where due to the boundary conditions only vertical displacements were permitted and a diagonal axis, starting from the lower left corner of the model and projected in a direction of 45 degrees towards the opposite corner (Figure 47).

For this comparison a total of fourteen models were run. Seven models were composed by triangular elements and the remaining models were composed by quadrilateral elements.

6.3 MODELS USING TRIANGULAR ELEMENTS

Seven models were developed in SIMFEM and Phase². These models included those composed only by quadratic triangles and linear triangles, which were run in SIMFEM and Phase². The models that included linear, transition and quadratic elements were developed in SIMFEM. The models are:

3NTRI-SIMFEM: Composed of linear triangular elements. Run in SIMFEM

3NTRI-Phase: Composed of linear triangular elements. Run in Phase²

6NTRI-SIMFEM: Composed of quadratic triangular elements. Run in SIMFEM

6NTRI-Phase: Composed of quadratic triangular elements. Run in Phase²

Variable: σxx (kN/m²)

| -1.3096e+00 | -1.0012e+00 | -6.9275e-01 | -3.8432e-01 | -7.5896e-02 | 2.3253e-01 | 5.4095e-01 | 8.4938e-01 | 1.1578e+00 | 1.4662e+00 |
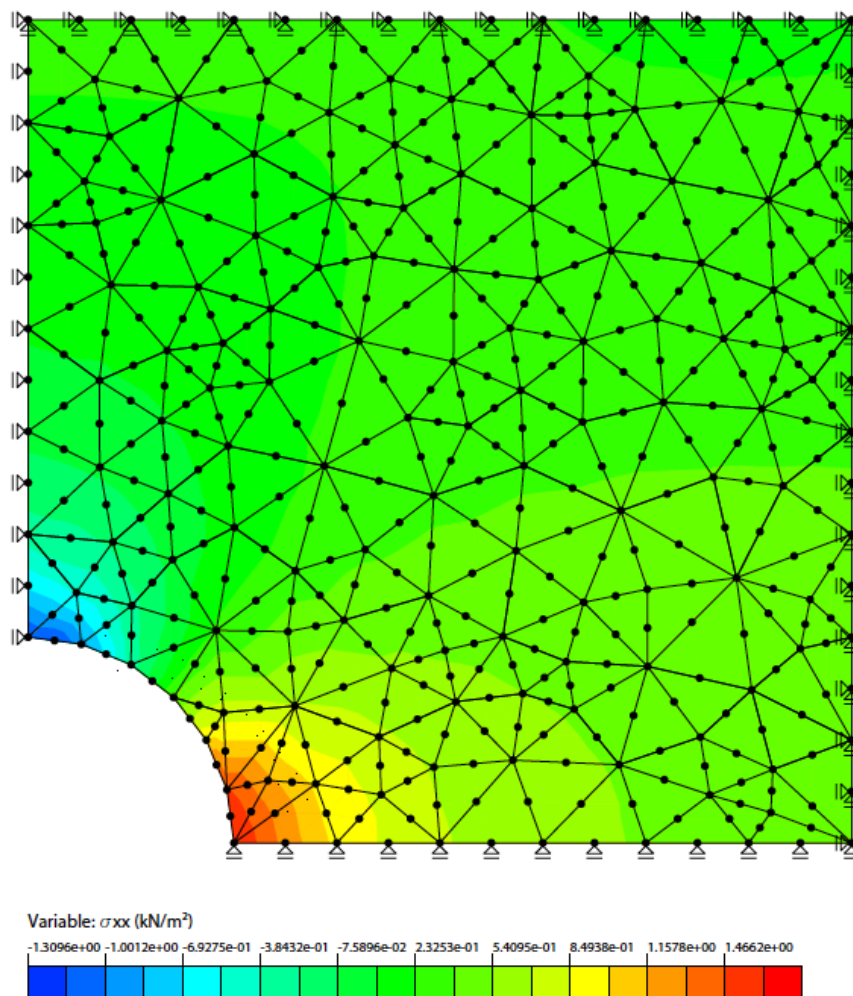
Figure 51 Model 6NTRI-SIMFEM σ_{xx} contours

TRI-TRANS1: Composed of linear, transition and quadratic triangular elements, run in SIMFEM with a transition zone located at 7.5m from the lower left corner.

TRI-TRANS2:   Composed of linear, transition and quadratic triangular elements, run in SIMFEM with a transition zone located at 10.0m from the lower left corner.

TRI-TRANS3:   Composed of linear, transition and quadratic triangular elements, run in SIMFEM with a transition zone located at 12.5m from the lower left corner.

Variable: σxx (kN/m²)

-1.3019e+00 -9.9435e-01 -6.8679e-01 -3.7923e-01 -7.1675e-02 2.3588e-01 5.4344e-01 8.5100e-01 1.1586e+00 1.4661e+00
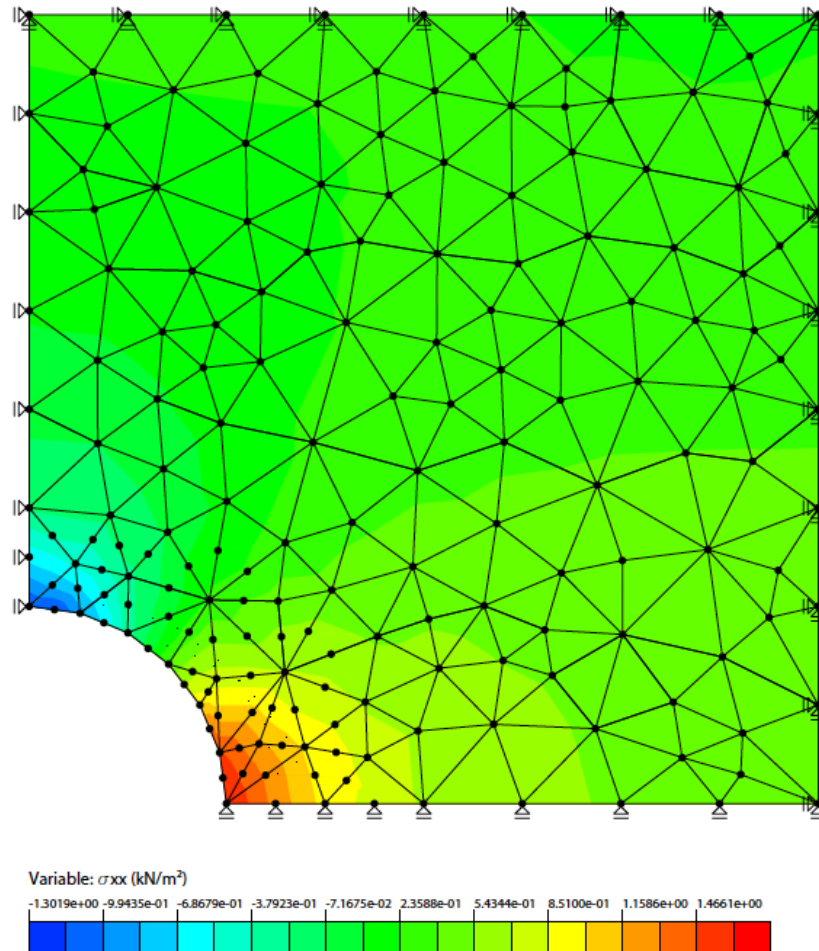
Figure 52. Model TRI_TRANS1 σ_{xx} contours

The graphic output of the program shows a close correspondence between the different models, as can be seen in Figure 51 and Figure 52. Nevertheless, for the acute eye, it is evident that not very rounded contours were achieved, which is result of a poor mesh discretization, which can be fixed either by adding elements (h-adaptivity) or by increasing the order of the elements (p-adaptivity). In this specific case, where the order of the elements was diminished in certain areas in order to evaluate their performance, a not continuous contour behaviour is observed, especially at the lower part of the model (Figure 52).

After all the models were run using SIMFEM, the displacements in the nodes were extracted and analyzed, as mentioned at the beginning of this subchapter. In this case, several plots were drawn in order to analyze all the raw data, which is also considerable in size. The displacements were evaluated by region. The first one at the left boundary of the models, the second one at the bottom of the models and the third one along the line at 45 degrees, in reference to Figure 49.
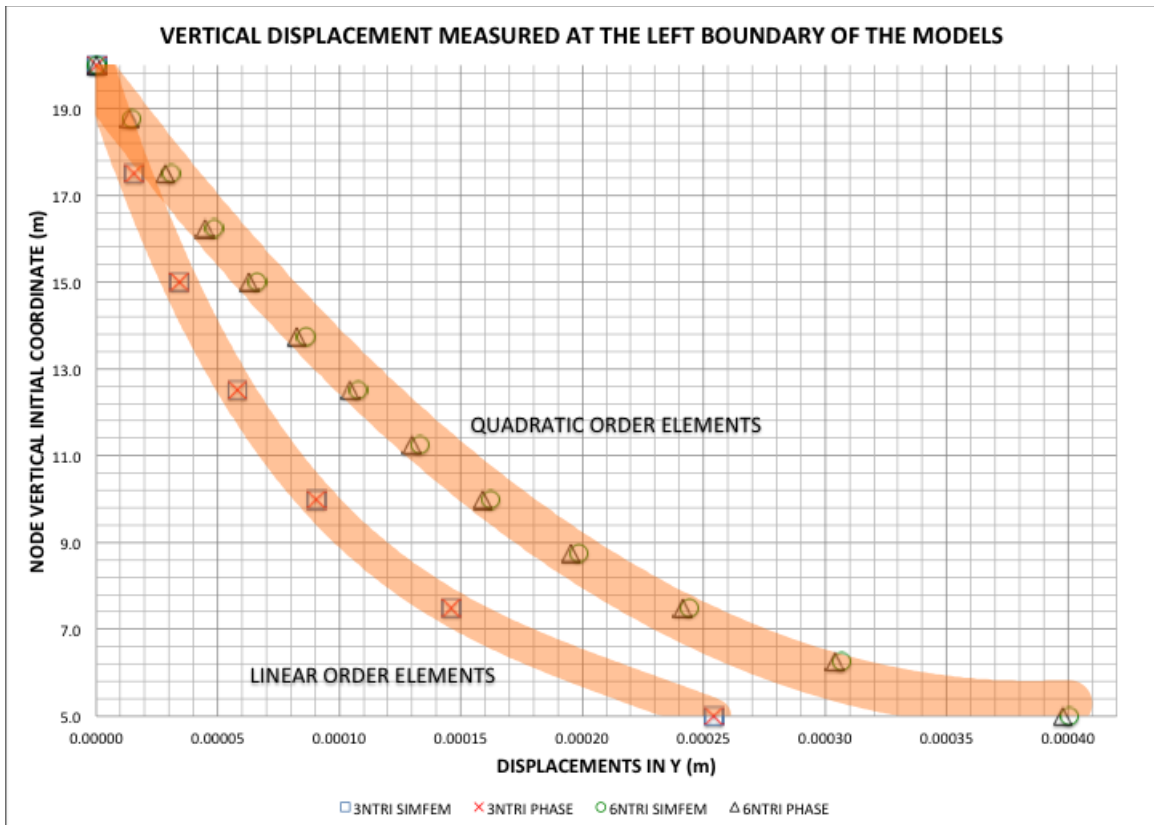
Figure 53 Displacements at left boundary of models 3NTRI SIMFEM, 3NTRI Phase, 6NTRI SIMFEM and 6NTRI Phase

The models using triangles were analyzed at their left boundary, where only vertical displacements are allowed due to the boundary conditions imposed to the model. Figure 53 presents the displacements of the models that use only quadratic or linear elements. No transition elements are present in any of the models plotted in Figure 53.

The models were run with SIMFEM and Phase[2]. The displacements presented by the quadratic models are greater than those presented by the linear elements. This tendency has been seen throughout the previous tests.
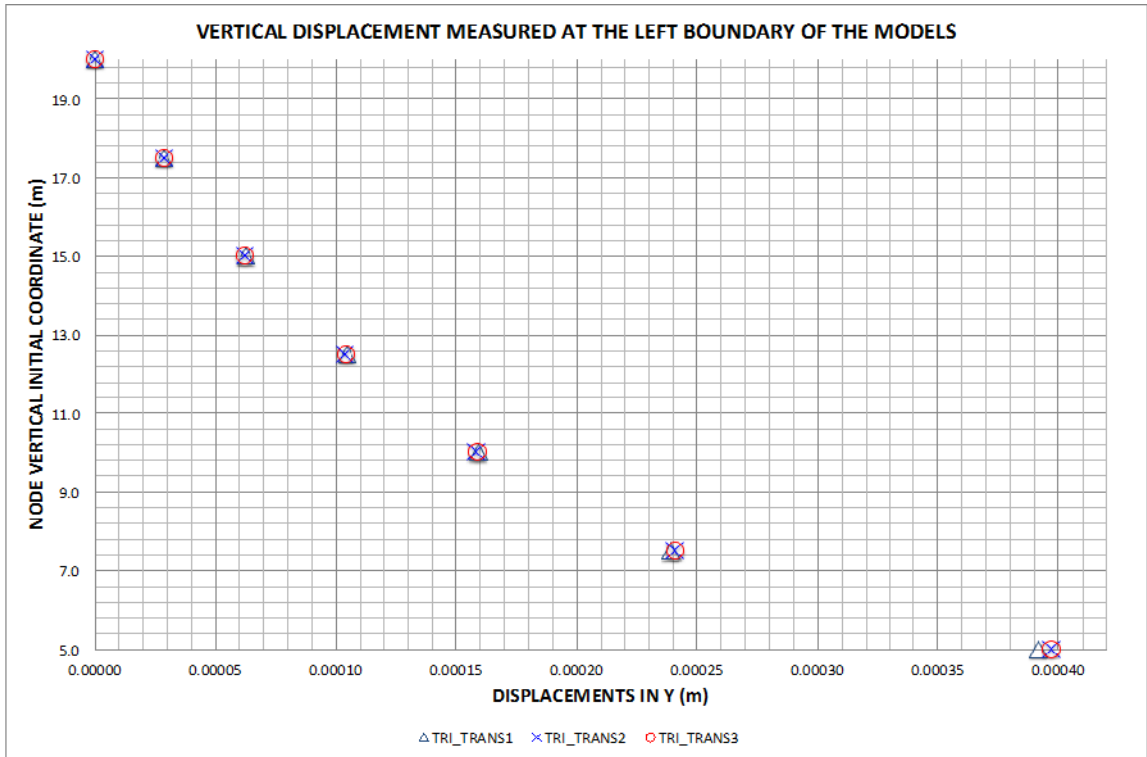
Figure 54 Displacements at left boundary of models TRI_TRANS1, TRI_TRANS2 and TRI_TRANS3
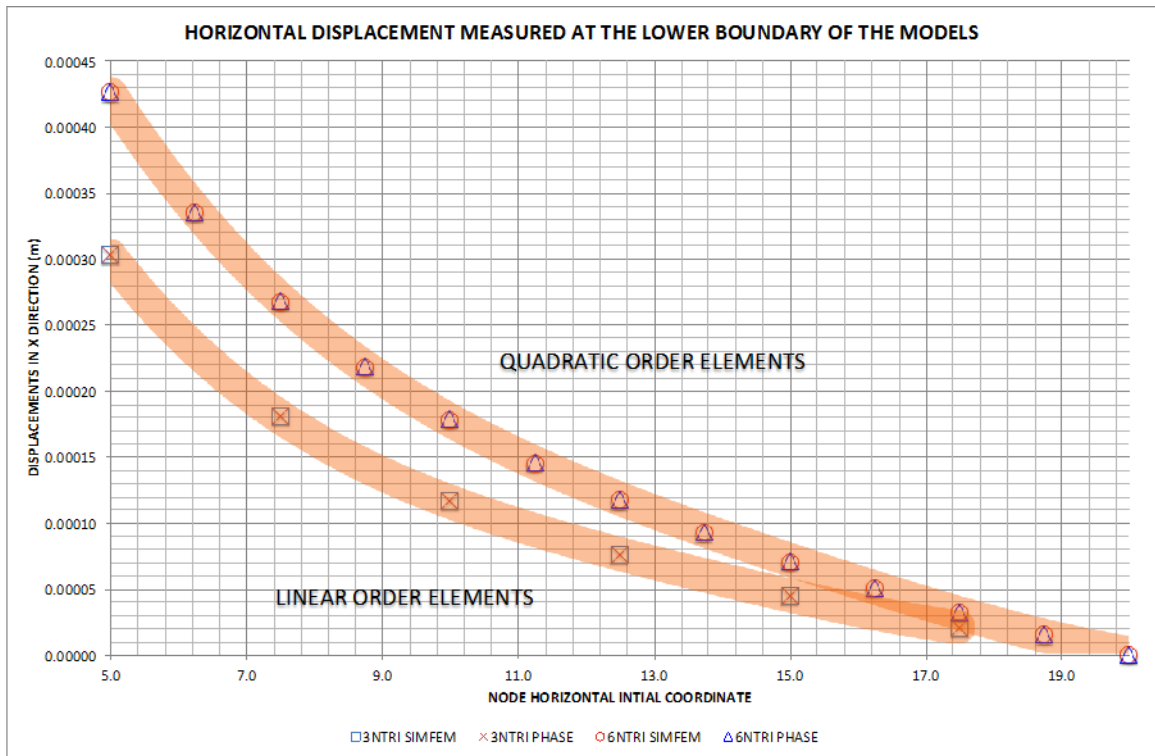
Figure 55 Displacements at lower boundary. Models 3NTRI SIMFEM, 3NTRI Phase, 6NTRI SIMFEM and 6NTRI Phase

In Figure 54, the similarity in magnitude of the displacements using transition elements is noticeable. No matter where the band of transitions elements is located (7.5m, 10m and 12.5m). Seeking neatness and clarity on the plots presented, not all the models were included in only one plot. Nevertheless, the author did plot the results merging Figure 53 and Figure 54 while analyzing the results. The results obtained from the models, including transition elements, tend to overlap the displacements obtained from the quadratic elements. In similar way, the plot merging was also performed for Figure 55 and Figure 56.
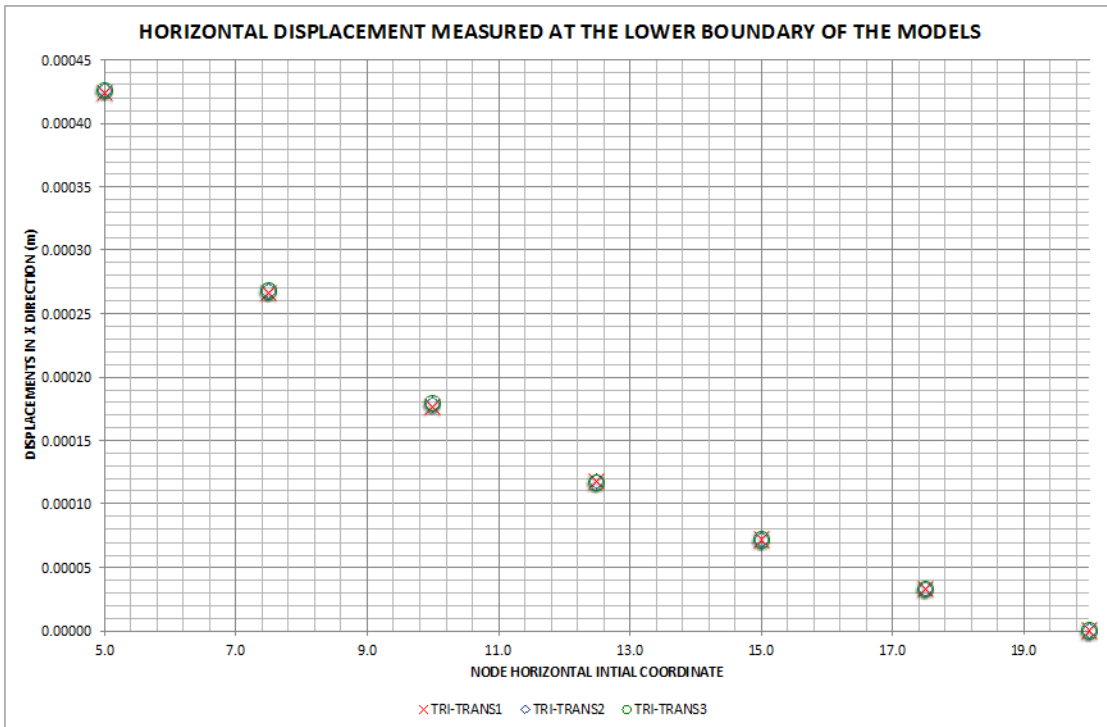
Figure 56 Displacements at lower boundary. Models TRI_TRANS1, TRI_TRANS2 and TRI_TRANS3

In case of Figure 55 and Figure 56, the same tendencies as the ones observed in Figure 53 and Figure 54 are present, where the linear and the quadrilateral models show very similar displacements. The models using transition elements also overlap the models using quadrilateral elements.
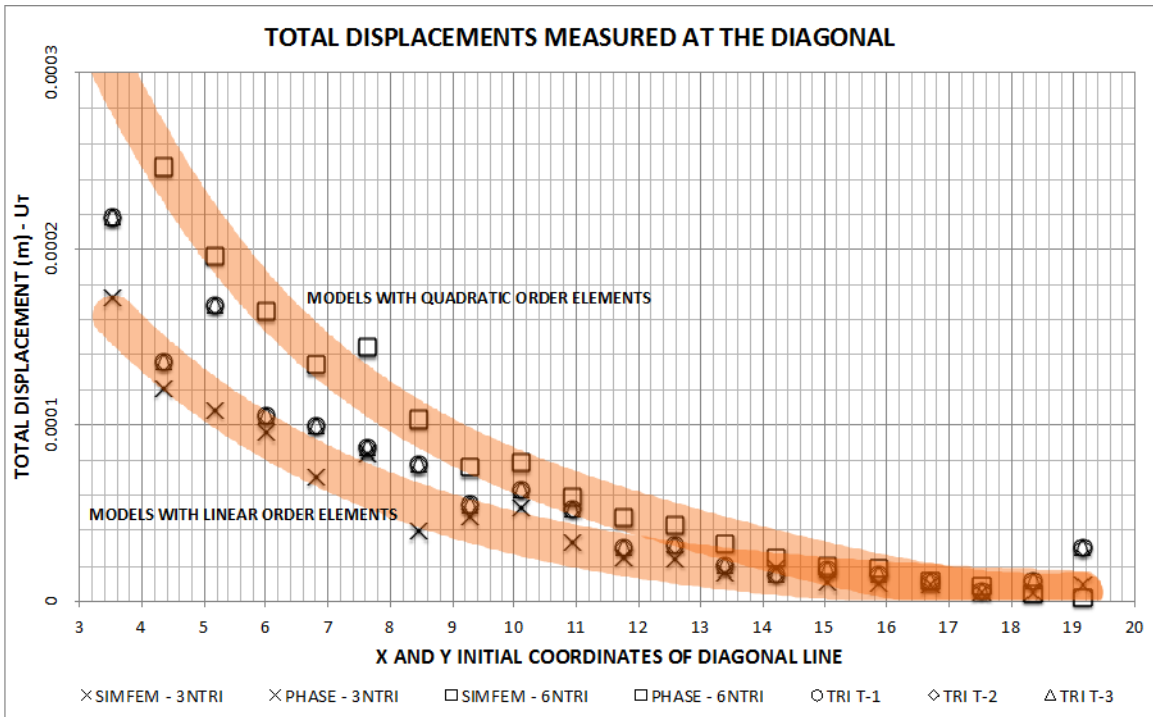
Figure 57 Total Displacements - U_T - at the diagonal. 6NTRI, 3NTRI, TRI-TRANS1, TRI-TRANS2 and TRI-TRANS3

Lastly, the analysis of the displacements along the diagonal was performed and is shown in Figure 47. The results obtained in Phase[2] are not included, so to prevent an overload of the plot. It is to recall, that the results acquired from SIMFEM and Phase[2] are remarkably close.

A tendency of the models using transition elements to behave as the models using linear order elements was observed. In this case, the displacements are not as predictable as the displacements at the left and lower boundary, where if a line were drawn joining the points it would not show any peaks along its path. Thus, the differences between the models is due to an interpolation that has to be effected to obtain the displacements at points close to those that the diagonal was crossing.

6.4 MODELS USING QUADRILATERAL ELEMENTS

Seven models were developed in SIMFEM and Phase[2] for this case. These models include those composed only by quadratic order quadrilaterals and linear order quadrilaterals, which were run in SIMFEM and Phase[2]. The models that included linear, transition and quadratic order elements were developed in SIMFEM. The models are:

66

4NQUAD-SIMFEM: Composed of linear quadrilateral elements. Run in SIMFEM

4NQUAD -PHASE: Composed of linear quadrilateral elements. Run in Phase[2]

8NQUAD -SIMFEM: Composed of quadratic quadrilateral elements. Run in SIMFEM

8NQUAD -PHASE: Composed of quadratic quadrilateral elements. Run in Phase[2]

Variable: σ_{yy} (kN/m²)

| -9.6419e-01 | -6.9418e-01 | -4.2417e-01 | -1.5415e-01 | 1.1586e-01 | 3.8587e-01 | 6.5588e-01 | 9.2590e-01 | 1.1959e+00 | 1.4659e+00 |
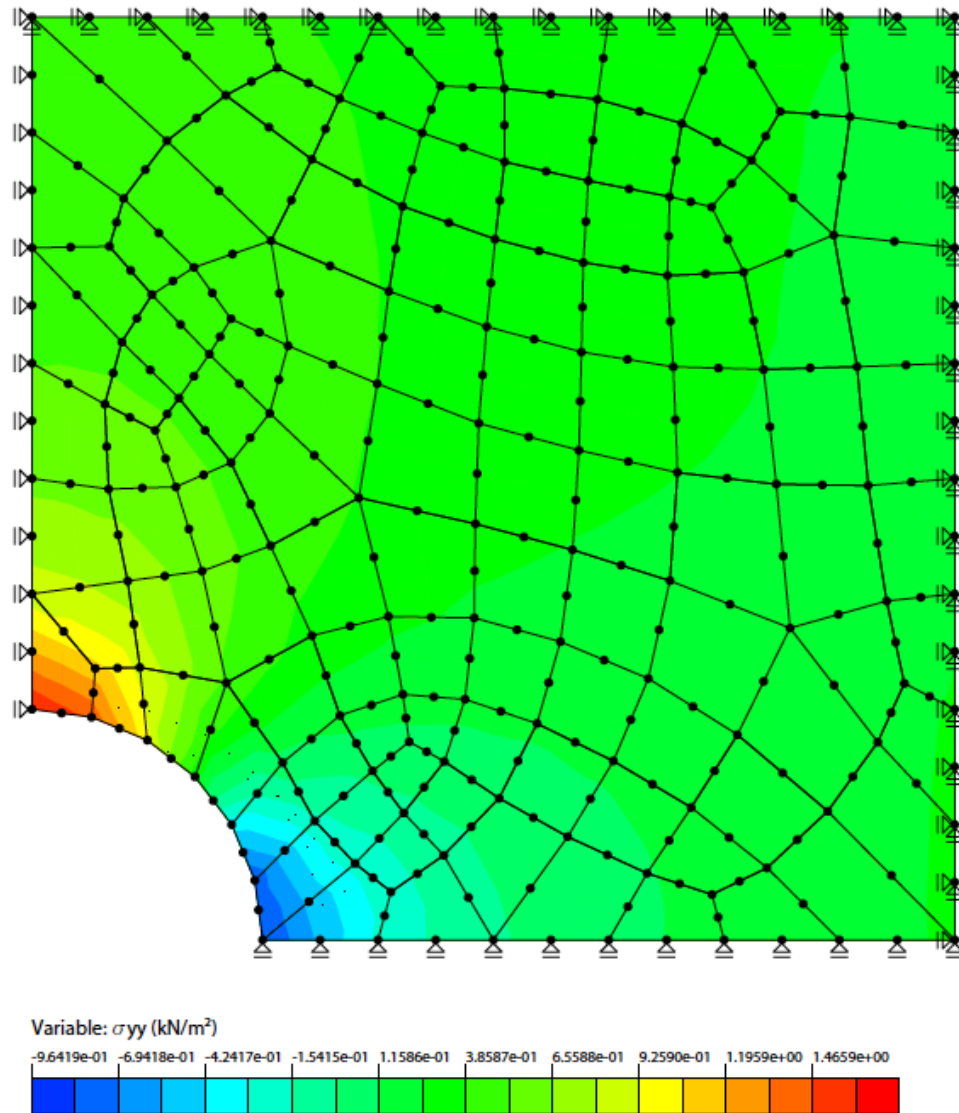
Figure 58 8NQUAD-SIMFEM σ_{yy} contours

QUAD-TRANS1: Composed of linear, transition and quadratic quadrilateral elements. Run in SIMFEM with a transition threshold located at 7.5m from the lower left corner.

QUAD-TRANS2: Composed of linear, transition and quadratic quadrilateral elements. Run in SIMFEM with a transition zone located at 10.0m from the lower left corner.

QUAD-TRANS3: Composed of linear, transition and quadratic quadrilateral elements. Run in SIMFEM with a transition zone located at 12.5m from the lower left corner.

Variable: σ_{yy} (kN/m²)

-9.6832e-01 -6.9850e-01 -4.2869e-01 -1.5887e-01 1.1094e-01 3.8076e-01 6.5058e-01 9.2039e-01 1.1902e+00 1.4600e+00
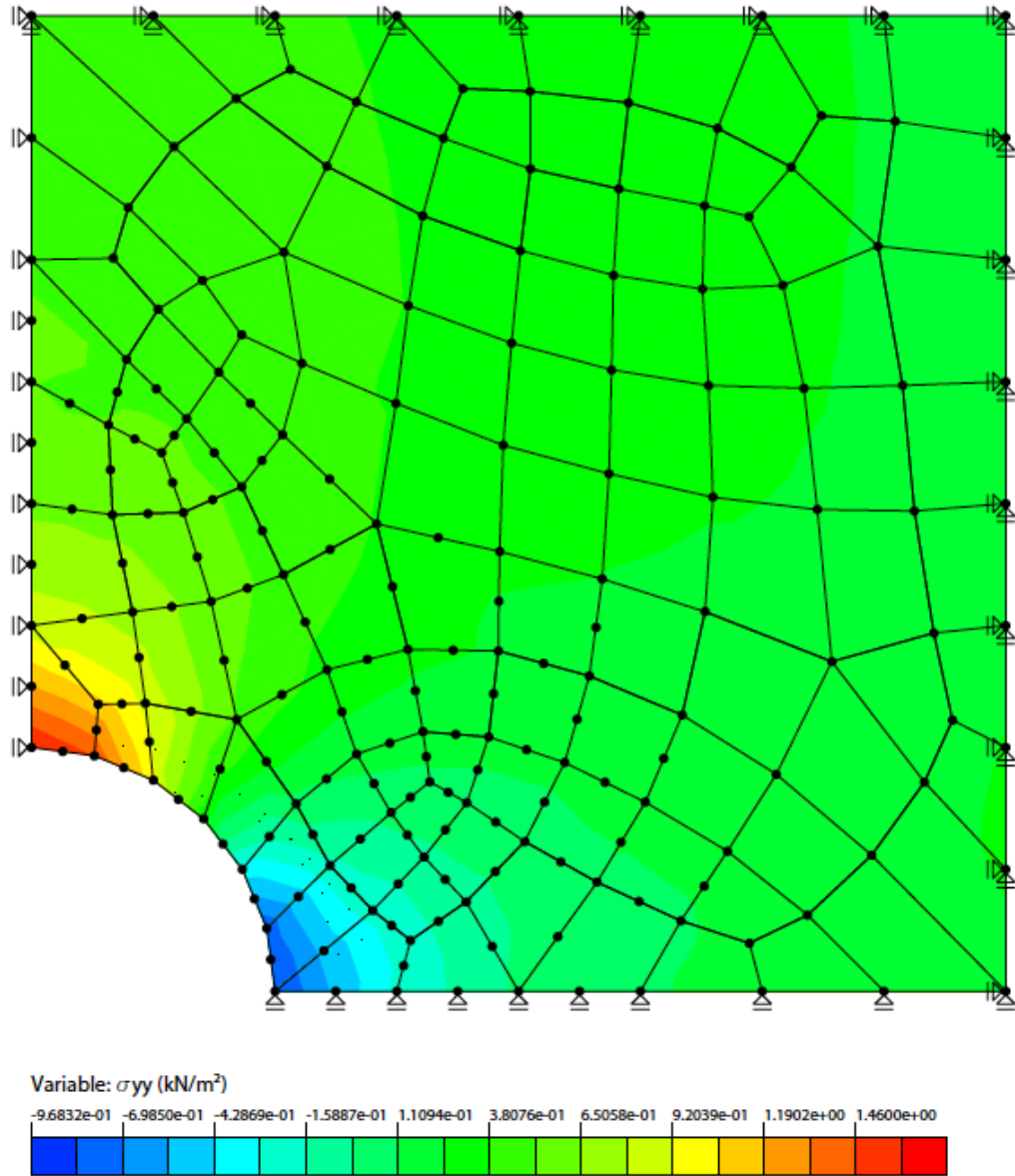
Figure 59 QUA_TRANS3 σ_{yy} contours

Replicating the analysis performed on the models made using triangular elements, the vertical displacements along the left and lower boundary were also analyzed with the quadrilateral elements.
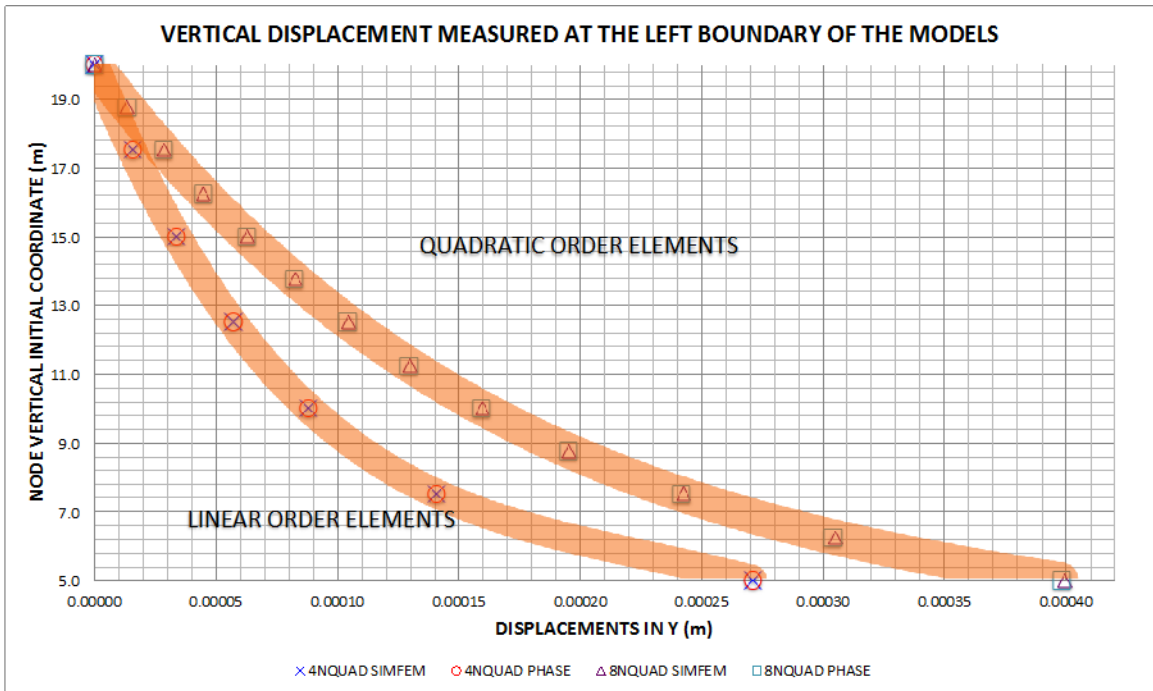
Figure 60. Uy at left boundary. Models 4NQUAD SIMFEM, 4NQUAD Phase, 8NQUAD SIMFEM and 8NQUAD Phase
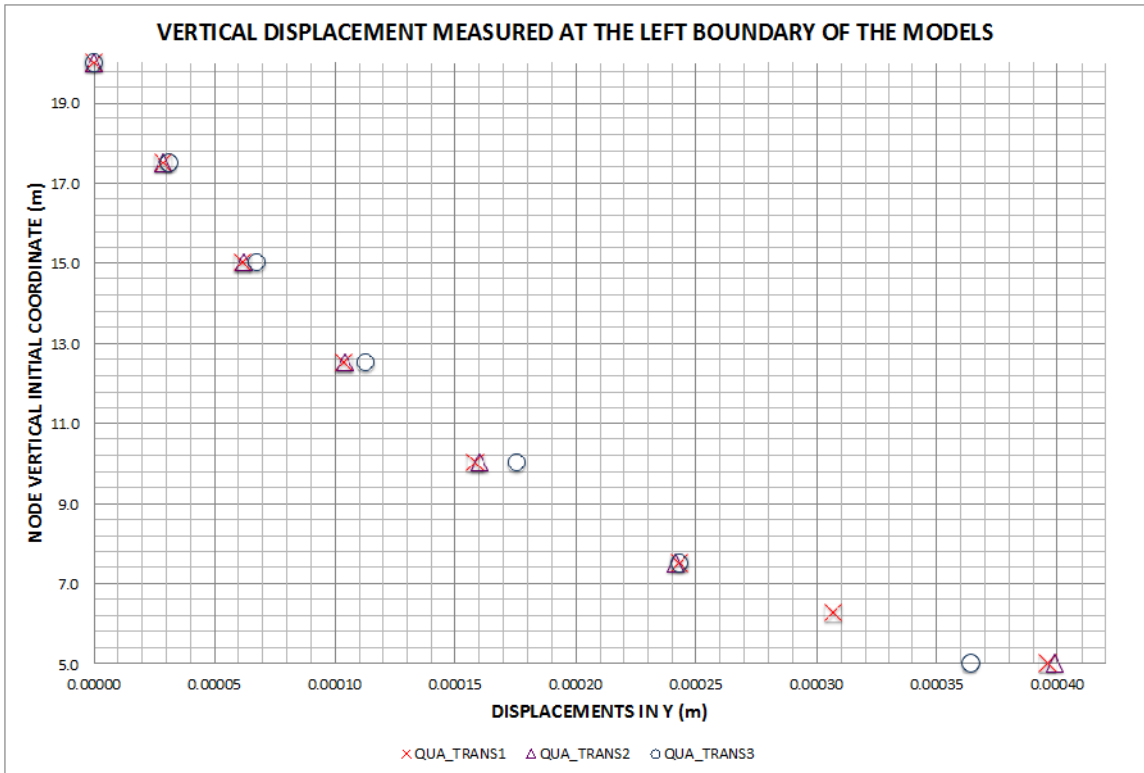
Figure 61 Displacements at left boundary of models QUA_TRANS1, QUA_TRANS2 and QUA_TRANS3
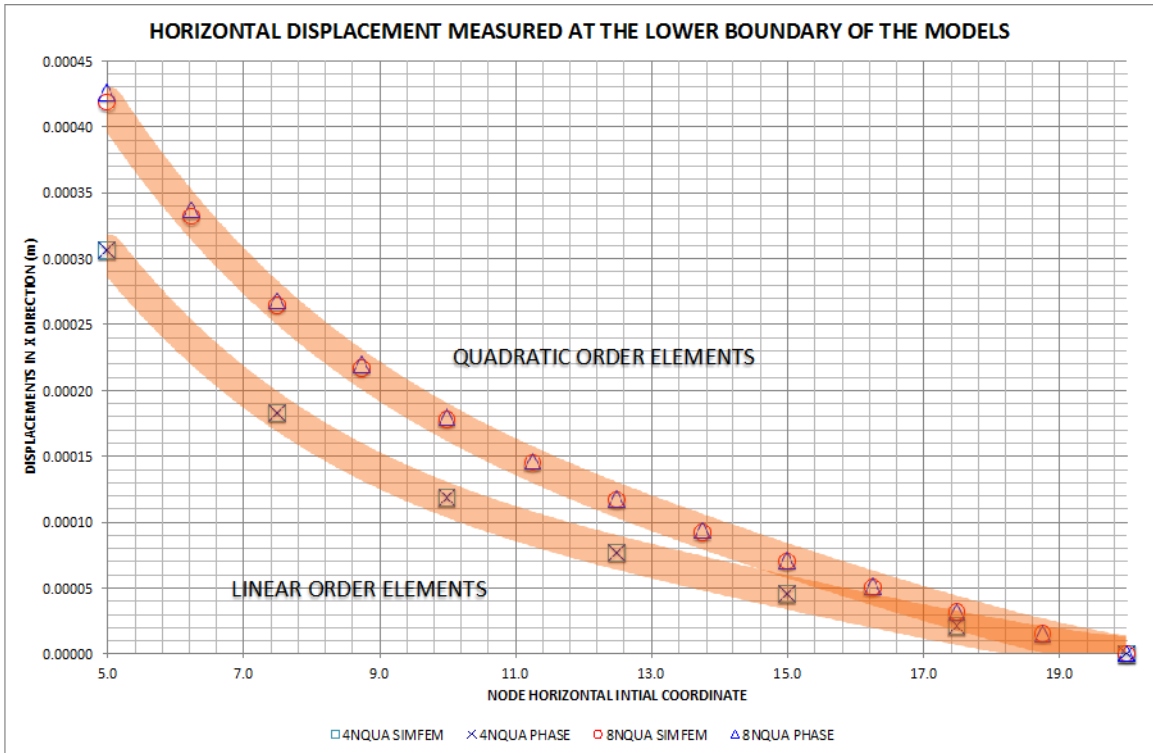
Figure 62 Displacements at lower boundary. 4NQUA SIMFEM, 4NQUA Phase, 8NQUA SIMFEM and 8NQUA Phase
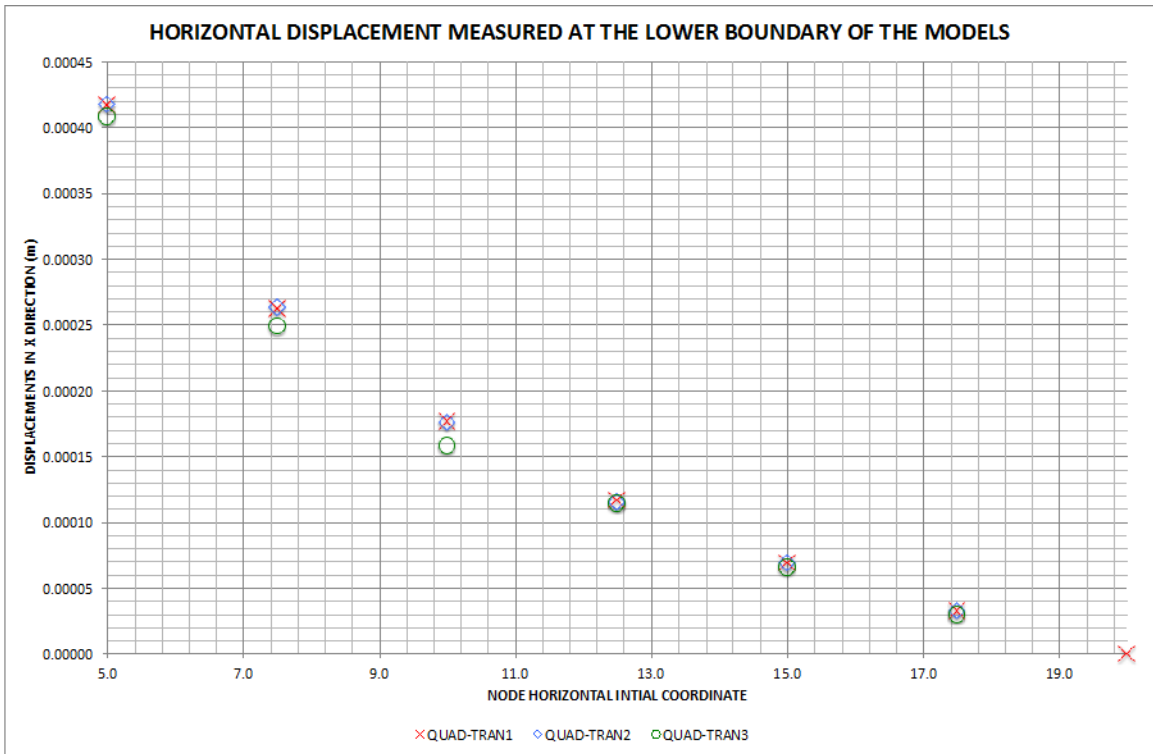
Figure 63 Displacements at lower boundary. Models QUAD_TRANS1, QUAD_TRANS2 and QUAD_TRANS3

Similarly to the results obtained from the models using quadrilateral elements, the similarities between equivalent models either linear (4NQUAD SIMFEM and 4NQUAD Phase) or quadratic (8NQUAD SIMFEM and 8NQUAD Phase) are evident. Larger displacements are also observed in the models using quadratic elements. The displacements presented by the models using transition elements also have similar behavior to the models using only quadratic elements. The results obtained from the models utilizing transition elements would also overlap the data obtained from the models utilizing quadratic elements.

All the models using transition quadrilateral elements showed similar displacements behaviour. As in the plots corresponding to the left boundary and the models using triangles, the behaviour of the transition quadrilateral elements tend to behave similarly to the quadratic quadrilateral elements.
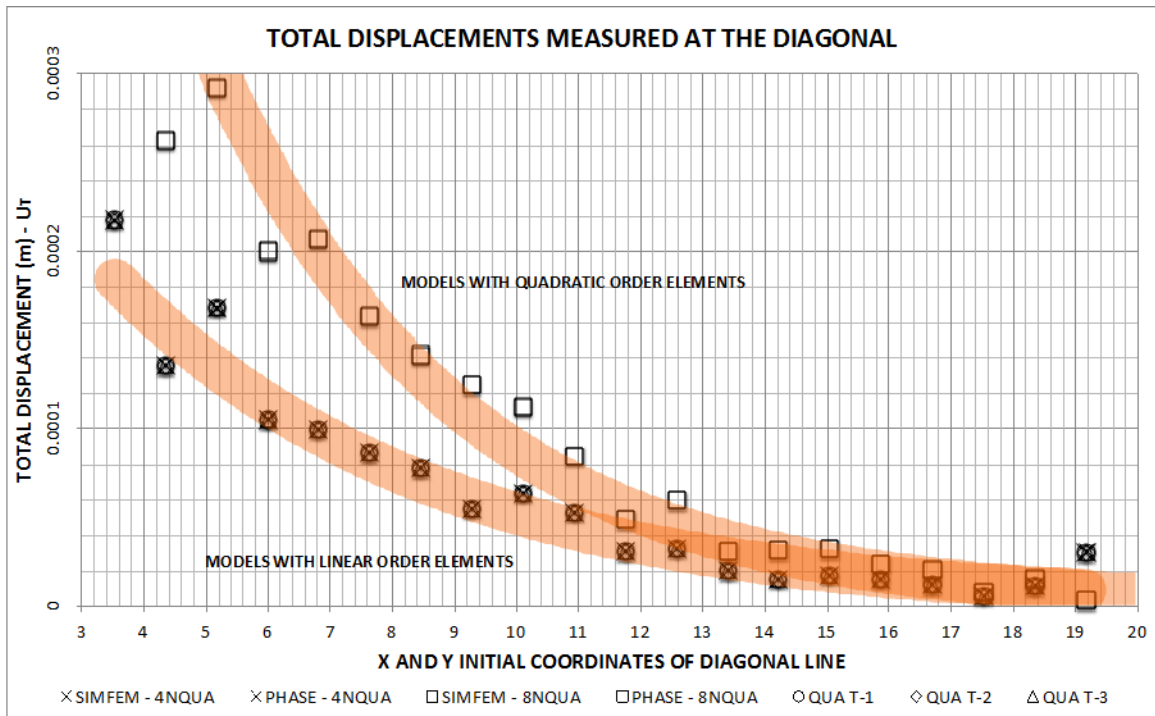
Figure 64 Total disp. – u_T - at the diagonal. 4NQUA, 8NQUA, QUATRANS1, QUATRANS2 and QUATRANS3

In Figure 64, the displacements taken at several points of a diagonal, starting from the point x = 3,53 and y = 3.53, corresponding to the intersection of a line with an angle of 45ª emerging from the origin (lower left point) of the model, and the pressurized cavity directed towards the opposite corner of the model (Refer to Figure 47). All the models that use transition elements and presented in Figure 64 were run in SIMFEM.

With these analyses from the data obtained, it is possible to conclude the good and suitable performance of the transition elements and their further applicability in the field.

6.5 RESULTS OF THE OPTIMIZATION WITH RESPECT TO TIME AND BENCHMARKS

After all the data extracted from the pressurized cavity models was analyzed and the reliability of the different types of transition elements (quadrilaterals and triangles), located at different positions was verified, it is possible to conclude that the inclusion of these in a finite element mesh is feasible. As the next step, an analysis regarding the computational resources was conducted.

The computer used to run the analyses was a Macintosh with a 2.4 GHz Intel Core Duo processor, 2 Gb in RAM at 667 MHz type DDR2 running under MAC OS X Operating System version 10.6.8. XCODE version 3.2.3 running in 64 bit mode was the software suite used to develop SIMFEM. A complete summary that indicates the different effects of the mesh optimization is presented in the next three tables. The conjugate gradient method was the algorithm used by SIMFEM to solve the system of linear equations.

MODEL	No. OF NODES	No. OF ELEMENTS	No. OF FREE DEGREES OF FREEDOM	SIZE OF GLOBAL STIFFNESS MATRIX (bytes)
3NTRI - SIMFEM	149	248	252	508,032
TRI - TRAN1	188	248	327	855,432
TRI - TRAN2	228	248	405	1,312,200
TRI - TRAN3	260	248	468	1,752,192
6NTRI - SIMFEM	531	248	972	7,558,272
4NQUA - SIMFEM	126	108	206	339,488
QUAD - TRAN1	157	108	265	561,800
QUAD - TRAN2	184	108	318	808,992
QUAD - TRAN3	215	108	377	1,137,032
8NQUA - SIMFEM	359	108	628	3,155,072

Table 20 Characteristics of the several models and the computational resources involved

In Table 22, the models 3NTRI – SIMFEM and 4NQUA – SIMFEM, are taken as the benchmark for each set of models (Set of models using quadrilaterals models and set of models using triangles).

MODEL	ITERATION STEPS	CONVERGENCE THRESHOLD	SOLUTION TIME (sec)
3NTRI - SIMFEM	414	1.00E-12	0.627
TRI - TRAN1	1,669	1.00E-12	4.239
TRI - TRAN2	2,042	1.00E-12	7.952
TRI - TRAN3	2,209	1.00E-12	11.496
6NTRI - SIMFEM	2,504	1.00E-12	56.232
4NQUA - SIMFEM	343	1.00E-12	0.348
QUAD - TRAN1	1,085	1.00E-12	1.817
QUAD - TRAN2	1,450	1.00E-12	3.478
QUAD - TRAN3	1,628	1.00E-12	5.486
8NQUA - SIMFEM	1,694	1.00E-12	15.872

Table 21 Solution computational times

MODEL	SIZE OF MATRICES RATIO (LINEAR MODEL)	ITERATION STEPS RATIO (LINEAR MODEL)	SOLUTION TIME RATIO (LINEAR MODEL)
3NTRI - SIMFEM	1.0	1.0	1.0
TRI - TRAN1	1.68	4.03	6.76
TRI - TRAN2	2.58	4.93	12.68
TRI - TRAN3	3.45	5.34	18.33
6NTRI - SIMFEM	14.88	6.05	89.68
4NQUA - SIMFEM	1.0	1.0	1.0
QUAD - TRAN1	1.65	3.16	5.22
QUAD - TRAN2	2.38	4.23	9.99
QUAD - TRAN3	3.35	4.75	15.76
8NQUA - SIMFEM	9.29	4.94	45.61

Table 22 Ratio of computational resources for the different models

After the analysis presented in the previous pages, it is depicted that there is no reason to think that the presence of quadratic, linear and transition elements in a finite element mesh would affect quality and convergence of a solution.

The user might be concerned in getting very accurate results in zones where the geometric or physical characteristics are highly changing or unpredictable, thus after setting a theoretically valid assumption to decide where to locate this zone of transition or interest the user might obtain highly reliable results, saving considerable and expensive time of engineering and resources.

The savings in computational resources in all the cases analyzed are considerable. For example, comparing the model 6NTRI (mesh composed exclusively of quadratic triangular elements) and model TRI – TRAN1 which has a band of transition elements located at 7.5m, it is possible to notice that both have the same amount of nodes located on the boundary, which allows the user to recover stresses from the circumference at twice as many points as the 3NTRI model (mesh composed exclusively of linear order triangles), and obtaining reliable results in 7.5% of the time required to run

the 6NTRI model, being the time one of the most noticeable parameters to evaluate the convenience of a calculation.

Also, the size of the global stiffness matrix is reduced in 90% and thus the size of the output files is also diminished in similar proportions. The same analysis may be applied in the case of the models with quadrilateral elements. The immediate significance of the application of the mesh optimization proposed, means an enhancement of the response capacity of an engineering team who would be able to analyze complex geometries and load conditions within shorter time without affecting the quality of the solution.

7. APPLICATION OF PARTIAL P-ADAPTIVE MESH OPTIMIZATION TO UNDERGROUND EXCAVATIONS

The application of the use of transition elements in mesh optimization to circular excavations is explained as such:

The state-of-the-art in tunnelling and mining techniques, the Tunnel Boring Machines (TBM) have been used as the most versatile and fastest technique to excavate tunnels. The machines perform these works with a circular cross section and with the last advances in engineering; these machines are able to drill through almost any geomaterials, from soft clays to hard rock.
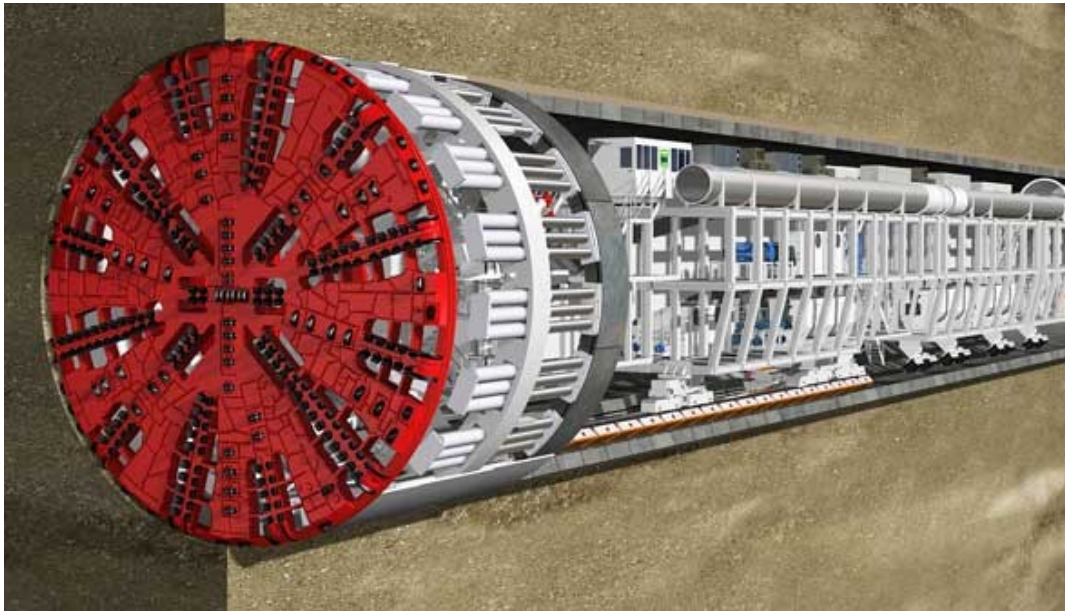
Figure 65 Scheme of an Earth Pressure Balance TBM (Herrenknecht, 2011)

Furthermore, the possibility of approximating any shape of excavation (depending on the state of stresses and the zone of influence of the excavation), to a circular/elliptical approximation in 2D or, if the problem is established in 3D any excavation might be approximated to a spherical/ellipsoidal. This is achieved by implementing an algorithm based on an object-aligned minimum-area/volume bounding rectangle in 2D or box in 3D, to fit an circle/ellipse or sphere/ellipsoid (Figure 66) to an excavation (Zsaki, 2005).
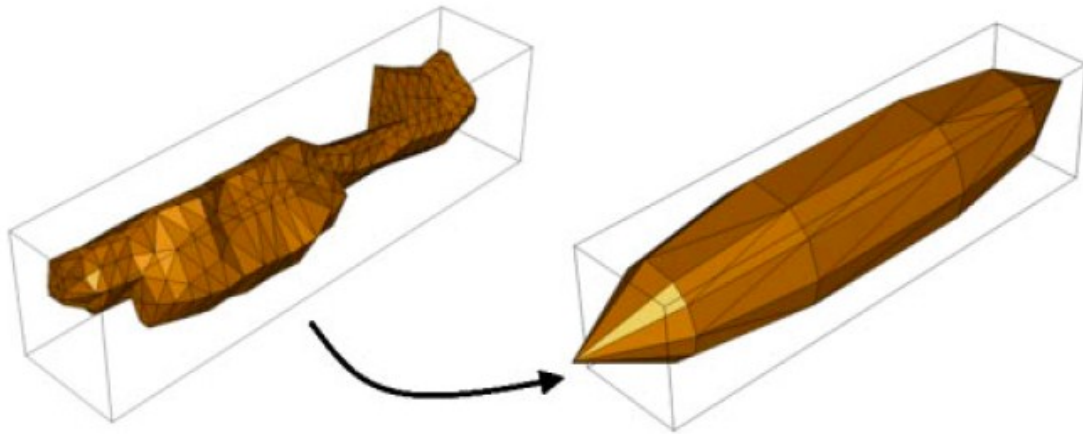
Figure 66 Ellipsoidal approximation of an excavation (Zsaki, 2005)

Thus, the final application and verification of the mesh optimization strategy is based on modelling two circular underground excavations (Chapter 3). Applying the analytical solution formulated by Kirsch (1898), which is commonly found in the bibliography as *"infinite plate with circular opening"* (Ramamurthy, 2007) (Figure 10), four models were analyzed. In the first one, quadratic triangles were used to form the finite element mesh. In the second one, quadratic quadrilaterals were assumed in the entire continuum. The last two models were used to apply the optimization, then, these models include quadratic, linear and transition triangular or quadrilateral elements. For this specific case, the excavation located at the left side of the model is called "excavation 1" and the excavation located at the right side is called "excavation 2".

7.1 RESULTS OF THE UNOPTIMIZED MODEL (UM)

A model with the geometric properties indicated in Figure 9 and the material properties listed in Table 1 is used to perform this evaluation. The material assigned to the continuum is assumed to be linear-elastic and weightless.

7.1.1 UNOPTIMIZED MODEL (UM) USING TRIANGLES

All the elements included in this model, were defined as quadratic triangles and there is no presence of transition and linear elements. With a total of 16724 degrees of freedom, this finite element mesh is composed of 4090 elements (Figure 67).
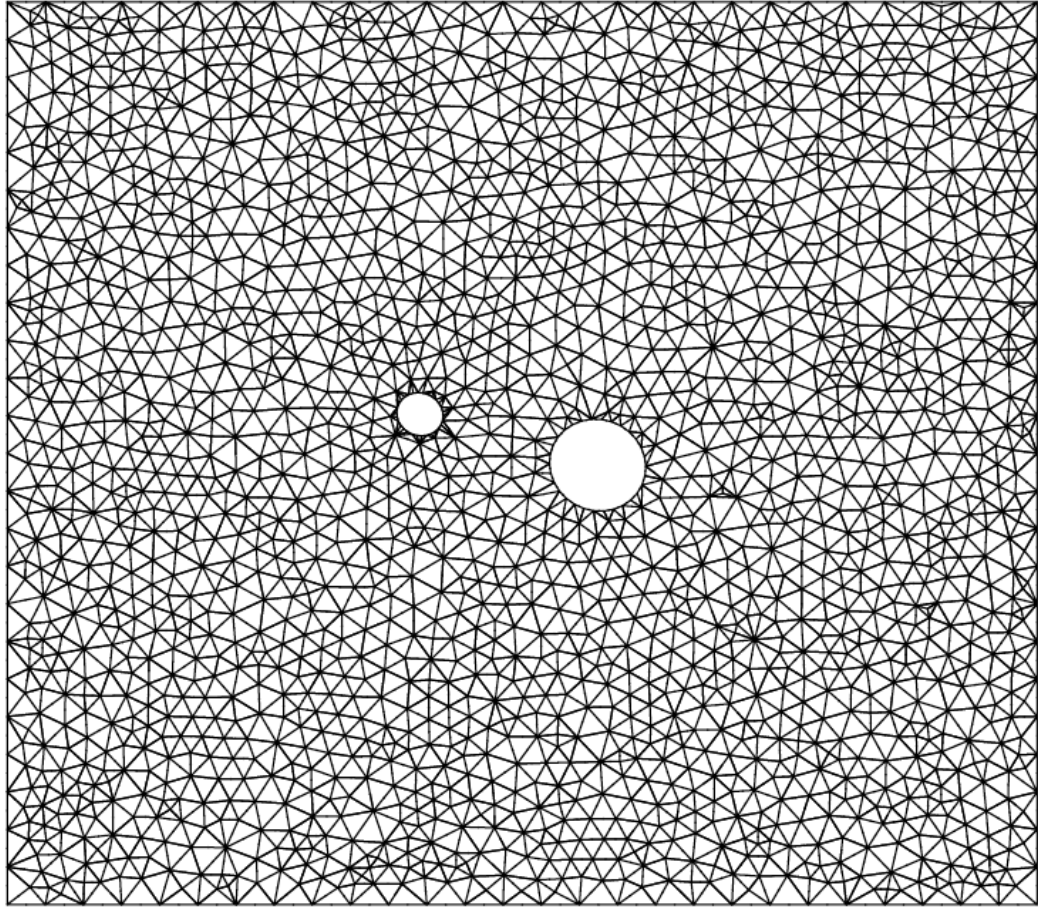
Figure 67. Finite element mesh of UNOPTIMIZED model using triangular elements
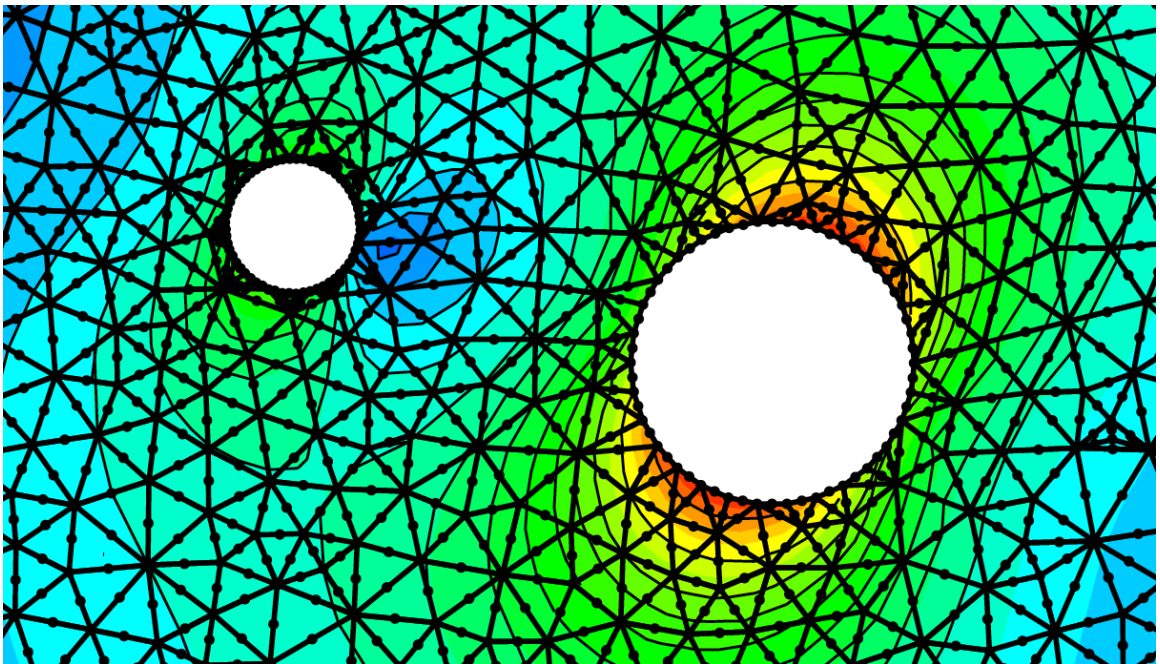
Figure 68. UNOPTIMIZED model using triangular elements - Contours u_T. Enlarged view

The boundary conditions were not plotted for appearance purposes. Phase2 was the software used to generate the finite element mesh (location of nodes and elements). This file is then manipulated to generate the input file used by SIMFEM. This process is repeated in the next three models.

An enlargement on the excavations of the unoptimized mesh is shown in Figure 68. The presence of the quadratic order elements is reflected by the presence of mid-edge nodes on every element. This figure shall be compared with Figure 72 where the elements located outside the EDZ are defined as transition and linear elements.

7.1.2   UNOPTIMIZED MODELS (UM) USING QUADRILATERALS

Replicating the process carried out with the triangular elements, a similar process was applied in the case of quadrilaterals.
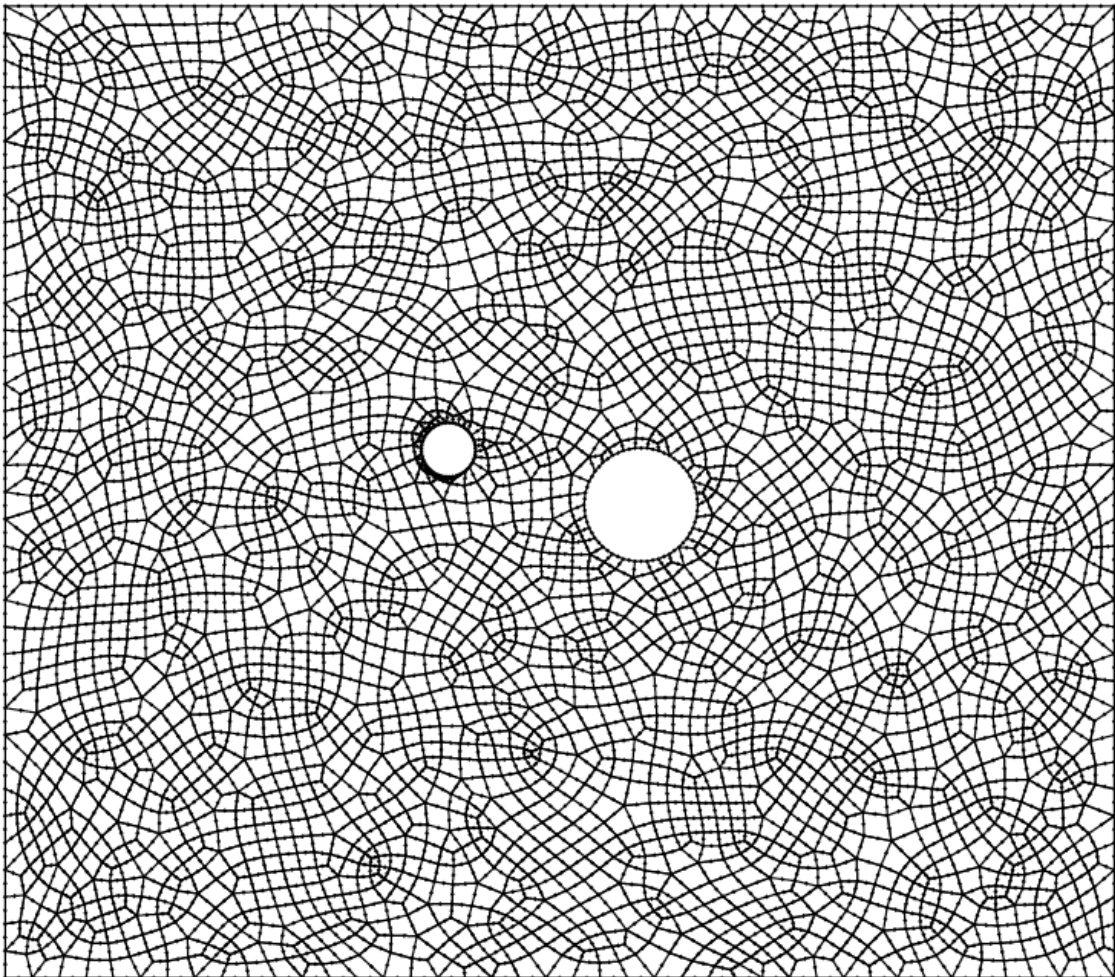
Figure 69 Finite element mesh of UNOPTIMIZED model using quadrilaterals elements

A very dense mesh comprised only by quadratic quadrilateral elements was used. With a total of 22314 degrees of freedom, the finite element mesh has a total of 3756 elements (Figure 69), where the boundary conditions were not plotted similarly to the mesh presented for the unoptimized model using triangles. The software used to generate the finite element mesh was Phase[2].
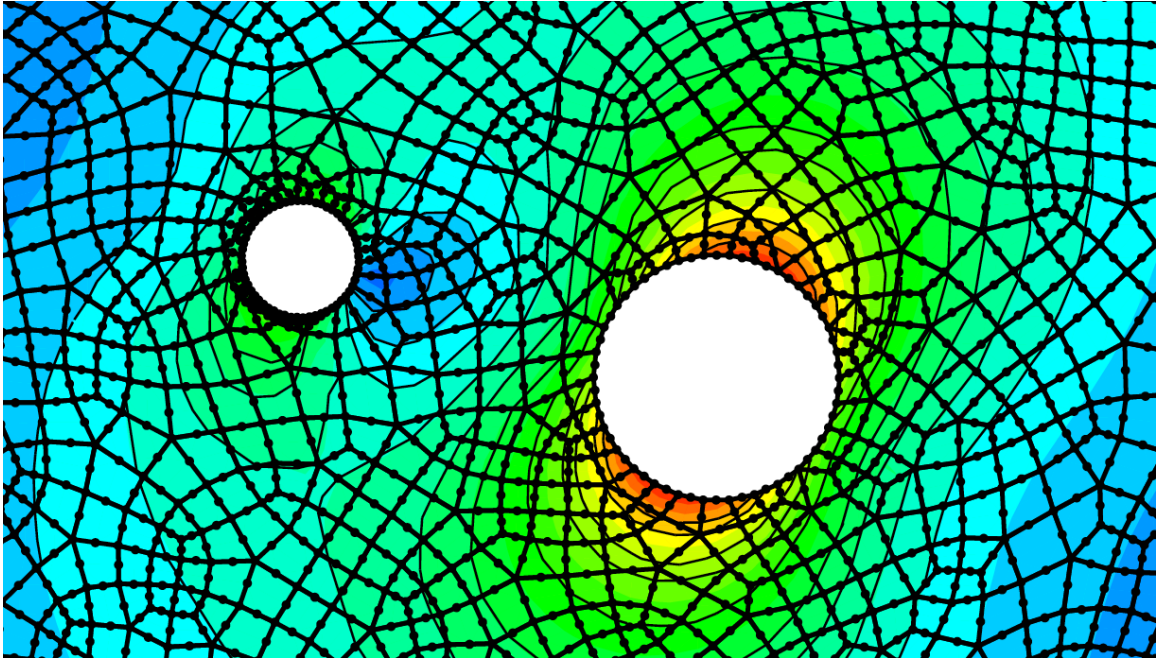
Figure 70 UNOPTIMIZED model using quadrilateral elements - Contours u_T. Enlarged view

In Figure 70, the existence of quadratic elements is depicted from the nodes located between the corners of the quadrilaterals (mid-edge nodes).

7.2 RESULTS OF THE OPTIMIZED MODEL (OM)

After running the UNDEROPT on the mesh proposed on Figure 9, which applies the concepts developed in section 3.1, two values for the location of the band of transition elements were found. Each one corresponds to the distance from the center of excavation 1 or 2, and dictates the location of the transition zone.

Transition zone from center of excavation 1: 10.4 m
Transition zone from center of excavation 2: 21.6 m

After the transitions zones were defined, both optimized models comprising quadrilateral and triangular elements were run. For the specific parameters assumed on the model,

the percentage of disturbance was found at approximately 4 times the radius of the excavation.

The general specifications of the four models run in SIMFEM are shown in Table 23. An analysis is carried out in order to evaluate the reductions in the number of nodes, the number of elements, the number of boundary conditions, the number of unrestrained degrees of freedom, the size of the global stiffness matrices and the solution time (this last variable depends on the speed of the processor, although it is included for information purposes).

MODEL	No. OF NODES	No. OF ELEMENTS	No. OF BC	No. OF FREE DOF	SIZE OF GSM (bytes)	SOLUTION TIME (sec)
TRIANGLES (UNOPTIMIZED MODEL)	8341	4090	204	16724	2,118,744,608	11121
QUADRILATERALS (UNOPTIMIZED MODEL)	11465	3756	308	22314	3,116,505,280	25193
TRIANGLES (OPTIMIZED MODEL)	3209	4090	102	6214	308,910,368	877
QUADRILATERALS (OPTIMIZED MODEL)	5171	3756	154	10034	805,449,248	4066

Table 23 Models with two circular excavations – Specifications

In terms of computational resources, the savings obtained are shown in Table 24. The ratios shown are obtained after a comparison between the models using quadrilaterals elements and the models using triangles. In the case of the models using triangular elements, the size of the global stiffness matrix was reduced by 12.68 times with respect to the matrix obtained in the unoptimized model. In a similar way, the ratio obtained in the models using quadrilaterals was 6.2.

MODEL	SIZE OF MATRICES RATIO (LINEAR MODEL)	ITERATION STEPS RATIO (LINEAR MODEL)	SOLUTION TIME RATIO (LINEAR MODEL)
TRIANGLES (UNOPTIMIZED MODEL)	6.86	1.38	12.68
QUADRILATERALS (UNOPTIMIZED MODEL)	3.87	1.13	6.20

Table 24 Models with two circular excavations - Optimization results

7.2.1 OPTIMIZED MODEL (OM) USING TRIANGLES

In the graphic output of SIMFEM, it is possible to observe the bands of transition elements and where both excavations are located. In Figure 71, the darker elements indicate the location of the bands of transition elements.
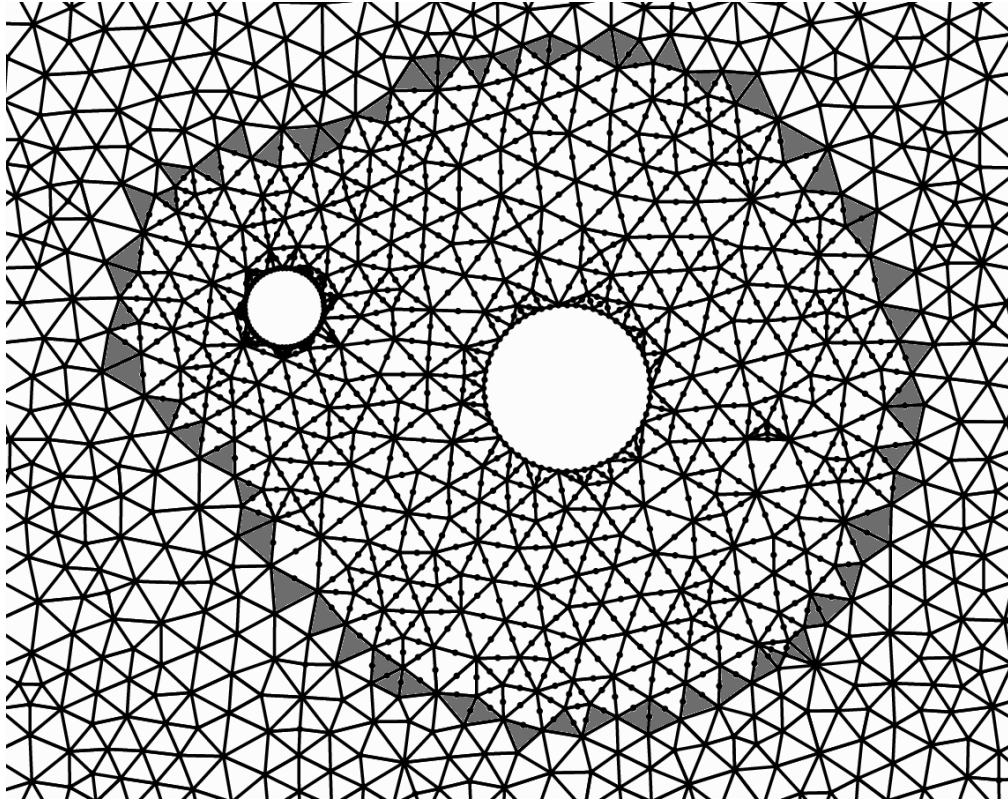
Figure 71 Finite element mesh of OPTIMIZED model using triangular elements. Enlarged view
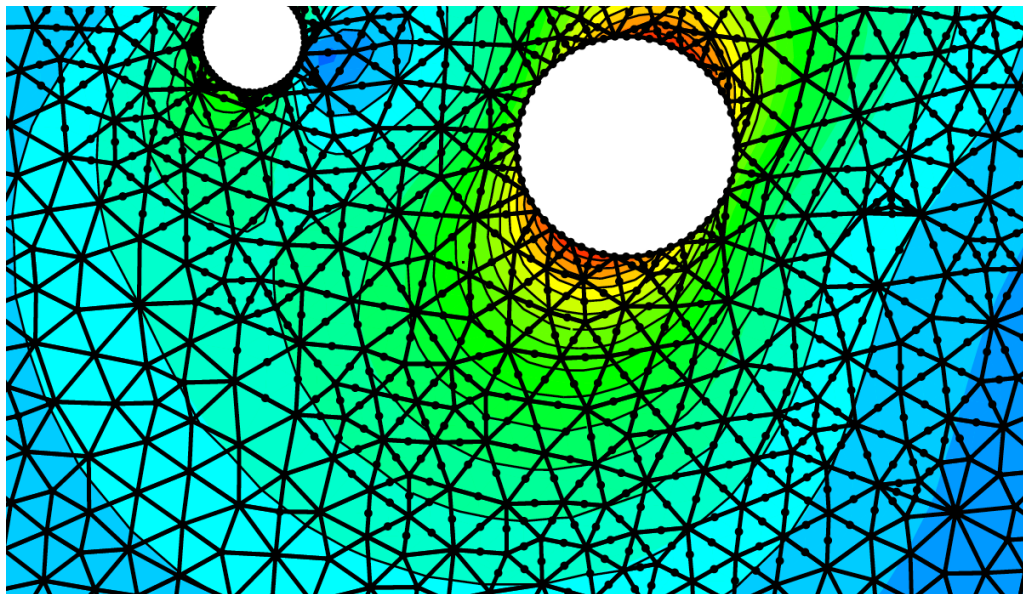
Figure 72 OPTIMIZED model using triangular elements ($variable - u_T$). Enlarged view

Figure 72 represents a fraction of the optimized model using triangles and might be compared to Figure 69, which corresponds to the unoptimized model using triangles. In both cases, the same variable u_T (total displacements) is plotted and the results are substantially similar as shown in a subsequent section.

7.2.2   OPTIMIZED MODEL (OM) USING QUADRILATERALS

In this model, the amount of nodes was reduced. On the graphic output, Figure 73, the darker elements indicate the location of the bands of transition elements, indicating the existence of a transition from quadratic to linear order elements are observed.
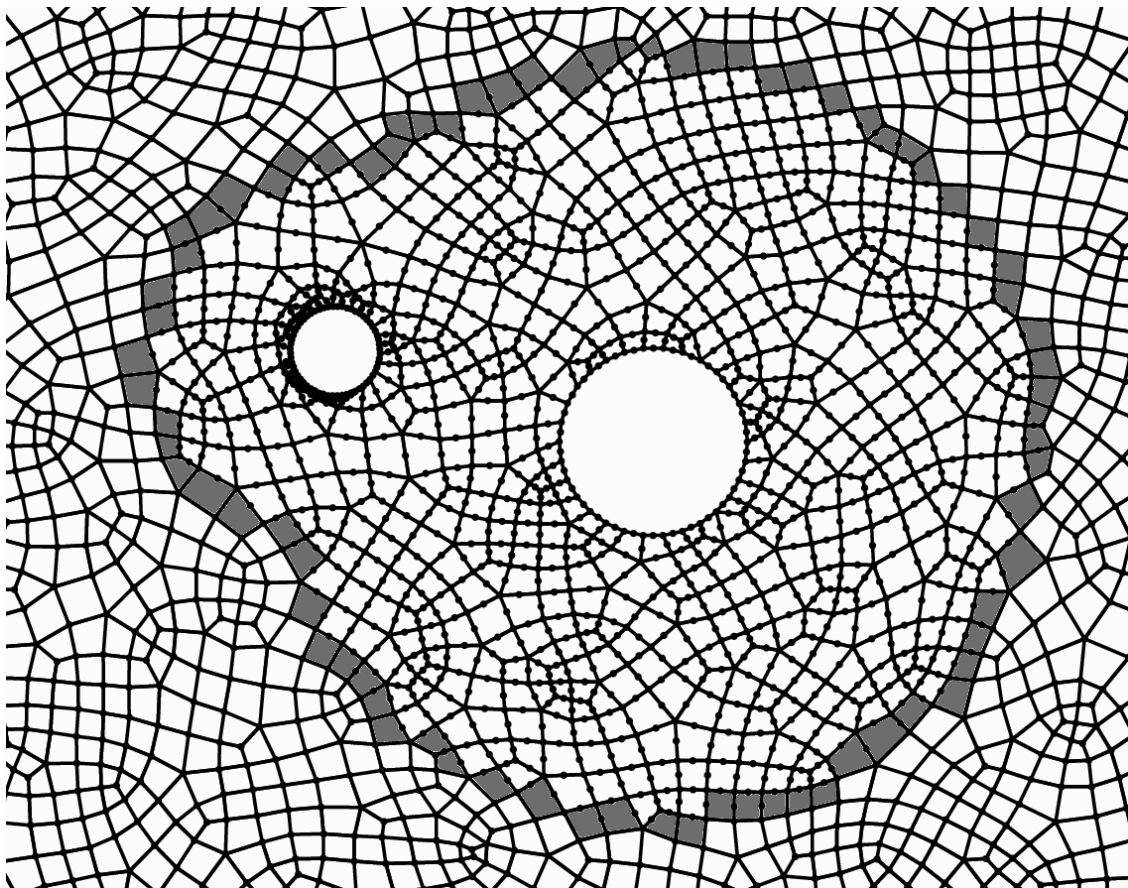
Figure 73 Finite element mesh of OPTIMIZED model using quadrilaterals elements. Enlarged view
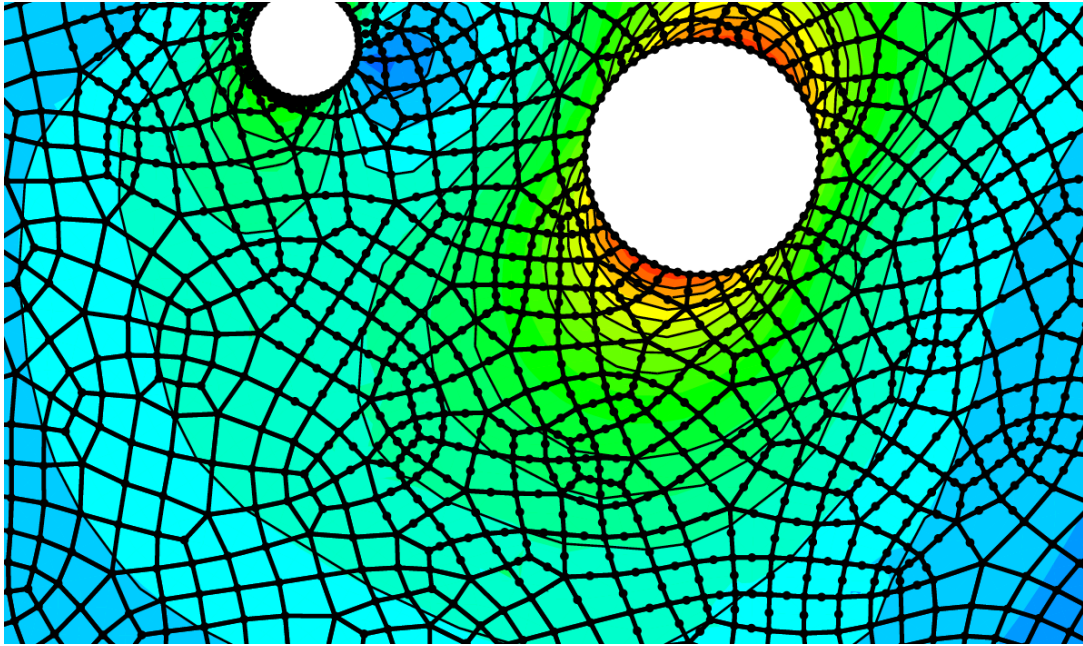
Figure 74 Zoom in on OPTIMIZED model using quadrilateral elements ($variable - u_T$)

Figure 74 can be compared to Figure 70. Despite the presence of transition elements in one of them, the contours plotted for the variable total displacements (u_T) present the same tendency, These figures might also be compared to those plotted for the models using triangular elements, where the same behavior has also been observed.

7.3 EVALUATION OF RESULTS

The reliability of the transition elements was evaluated with the analysis of results of 4 models, that assumed the same material and geometric properties including two circular excavations, having different type of elements used to form the finite element mesh (triangles or quadrilaterals) and the presence or absence of transition elements.
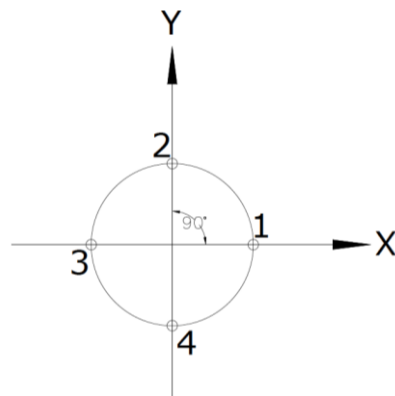
Figure 75. Points analyzed on the surface of excavations

83

When comparing the unoptimized models (using only quadratic order elements) and the optimized models (OM) (using quadratic, transition and linear elements), similar results are depicted from the graphical output. Nevertheless, in order to evaluate the quality of the solution (From Table 26 to Table 29), an assessment had to be performed. In addition, the savings in computational resources were compared.

As a comparative assessment, the displacements at 8 nodes in each model were analyzed. In each excavation, the nodes chosen to be analyzed were those located at 0° (point 1), 90° (point 2), 180° (point 3) and 270° (point 4) (Figure 75). Since Phase[2] does the mesh generation automatically, the nodes to be analyzed are not located precisely at each $\pi/2$ on the excavation. Their exact location is stated in Table 25.

NODE NUMBER IN MODEL	LOCATION IN MODEL	
	X (m)	Y (m)
0	45.5429	17.8526
8	42.8977	20.5211
15	40.4950	18.1393
23	43.1402	15.4708
30	66.2014	12.8861
37	61.4709	18.1575
45	55.6165	12.9038
53	61.4534	7.63058

Table 25 Location of analyzed nodes

Table 26 through Table 29, display the results of the mesh adaptivity process are presented. The percentage of error is calculated with respect to the unoptimized models (UM) (Equation 51). The tables show the percentage of error for each excavation and mention the type of elements forming the meshes (triangles and quadrilaterals). Firstly, the model using triangular elements is analyzed:

$$\% \ of \ error \ at \ node \ i = \left| \frac{displacement \ in \ UM \ at \ node \ i - displacement \ in \ OM* \ at \ node \ i}{displacement \ in \ UM* \ at \ node \ i} \right| \qquad (\ 51\ )$$

POINT ANALYZED	THEORETICAL LOCATION		Ux (m)	Uy (m)	% ERROR IN X AXIS	%ERROR IN Y AXIS
	X	Y				
1	45.6	18.0	-9.14E-06	-7.66E-06	0.16%	0.07%
			-9.15E-06	-7.65E-06		
2	43.0	20.6	2.89E-06	-3.73E-05	0.06%	0.07%
			2.89E-06	-3.72E-05		
3	40.4	18.0	2.99E-05	2.93E-06	0.04%	1.04%
			2.99E-05	2.90E-06		
4	43.0	15.4	1.72E-05	3.45E-05	0.27%	0.08%
			1.71E-05	3.45E-05		

Table 26 Error analyses - Models using triangles, left excavation

84

The left excavation is analyzed in Table 26. The maximum percentage of error found was 7.74% at point 1 in the vertical direction. The minimum percentage of error was 0.07% at point 3 in the horizontal direction.

POINT ANALYZED	THEORETICAL LOCATION X	THEORETICAL LOCATION Y	Ux (m)	Uy (m)	% ERROR IN X AXIS	%ERROR IN Y AXIS
1	66.4	13.0	-4.78E-05	-1.12E-05	0.00%	0.14%
			-4.78E-05	-1.12E-05		
2	61.0	18.4	-1.77E-05	-6.93E-05	0.09%	0.03%
			-1.77E-05	-6.93E-05		
3	55.6	13.0	4.60E-05	1.26E-05	0.02%	0.06%
			4.60E-05	1.26E-05		
4	61.0	7.6	6.13E-06	6.67E-05	0.17%	0.03%
			6.12E-06	6.67E-05		

Table 27 Error analyses - Models using triangles, right excavation

In Table 27, the right excavation in the models using triangles is evaluated. These nodes present a smaller percentage of error compared to the left excavation analyzed previously, exhibiting their maximum at point 4 in the vertical direction with 0.58%. The minimum percentage of error was found at point 4 in the horizontal direction with 0.01%.

POINT ANALYZED	THEORETICAL LOCATION X	THEORETICAL LOCATION Y	Ux (m)	Uy (m)	% ERROR IN X AXIS	%ERROR IN Y AXIS
1	45.6	18.0	-9.34E-06	-8.25E-06	4.89%	2.00%
			-9.79E-06	-8.42E-06		
2	43.0	20.6	2.75E-06	-3.75E-05	5.45%	1.48%
			2.90E-06	-3.70E-05		
3	40.4	18.0	2.98E-05	3.19E-06	1.69%	4.68%
			3.03E-05	3.04E-06		
4	43.0	15.4	1.72E-05	3.45E-05	1.10%	2.21%
			1.74E-05	3.37E-05		

Table 28 Error analyses - Models using quadrilaterals, left excavation

In Table 28, the displacements in the left excavation are evaluated. These show greater values than those obtained from the models using triangular elements (Table 26 and Table 27), having two important maximum values at point 1 with 10.95% in the vertical direction and at point 3 with 66.14% in the vertical direction.

POINT ANALYZED	THEORETICAL LOCATION X	THEORETICAL LOCATION Y	Ux (m)	Uy (m)	% ERROR IN X AXIS	%ERROR IN Y AXIS
1	66.4	13.0	-4.79E-05	-1.11E-05	0.28%	7.66%
			-4.78E-05	-1.03E-05		
2	61.0	18.4	-1.78E-05	-6.93E-05	1.05%	0.87%
			-1.80E-05	-6.87E-05		
3	55.6	13.0	4.62E-05	1.26E-05	1.35%	1.96%
			4.56E-05	1.23E-05		
4	61.0	7.6	6.19E-06	6.67E-05	5.29%	0.11%
			5.86E-06	6.67E-05		

Table 29 Error analyses - Models using quadrilaterals, right excavation

The values reached in the right excavation in the models using quadrilaterals are in average smaller than those obtained in the left excavation. However, these values are also greater than the average values obtained in the models using triangular elements.

With the purpose of evaluating the displacements obtained at the eight nodes aforementioned in a global context, column charts that gather all the percentages of error corresponding to the right and left excavations are presented in Figure 76 and Figure 77. The legend of these figures must be read as follows:

First fragment (X or Y): Indicates the direction (horizontal or vertical).
Second fragment (TRI or QUAD): Indicates the type of elements used in the model.
Third fragment (1, 2, 3 or 4): Indicates the point in the excavation where the percentage of error was measured. Refer to Figure 75.
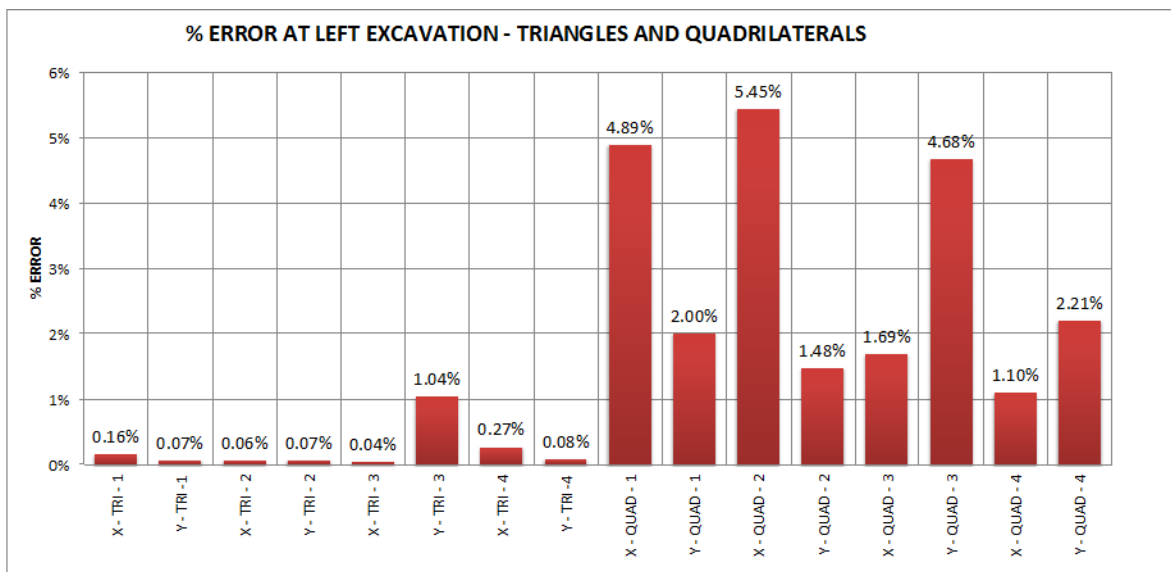
Figure 76 % of error at the left excavation. Models with quadrilaterals and triangles in the X and Y direction

In the previous figure, the percentages of error at the left excavation are plotted. Both types of elements (triangles and quadrilaterals) are included. The maximum value reached is 5.45% at point 2 in the horizontal direction, in the model using quadrilaterals. The minimum value is 0.06% at point 2, in the model using triangles, in the horizontal direction. The average percentage of error is 1.58% for both models at the left excavation. The average percentage of error for the models using triangles at the left excavation is 0.22%, and for the models using quadrilaterals is 2.94%.

% ERROR AT RIGHT EXCAVATION - TRIANGLES AND QUADRILATERALS
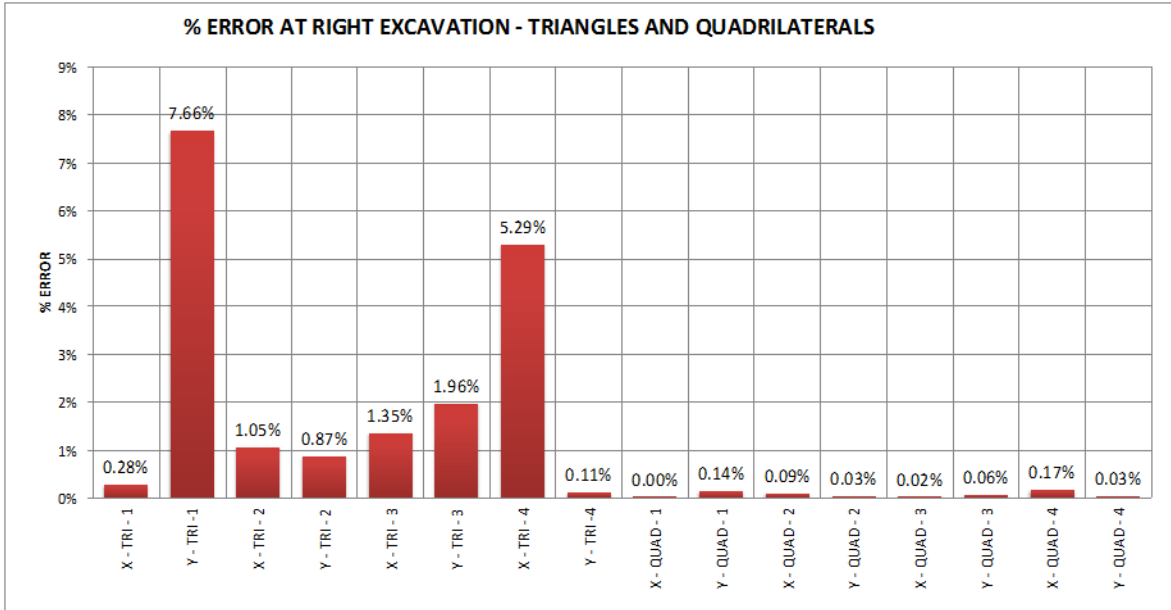
Figure 77 % of error at the right excavation. Models with quadrilaterals and triangles in the X and Y direction

In Figure 77, the percentages of error at the right excavation are plotted. Both types of elements (triangles and quadrilaterals) are included. The maximum value reached is 7.66% in the model using triangles, at point 1 and in the vertical direction. The minimum value is 0.001% in model using quadrilaterals, at point 1 and in the horizontal direction. The average percentage of error is 1.20% for both models at the right excavation. The average percentage of error for the models using triangles at the right excavation is 0.07%, and for the models using quadrilaterals is 2.32%.

The average percentage of error for all the models at both excavations using triangular elements is 0.15% and for quadrilateral elements is 2.63%.
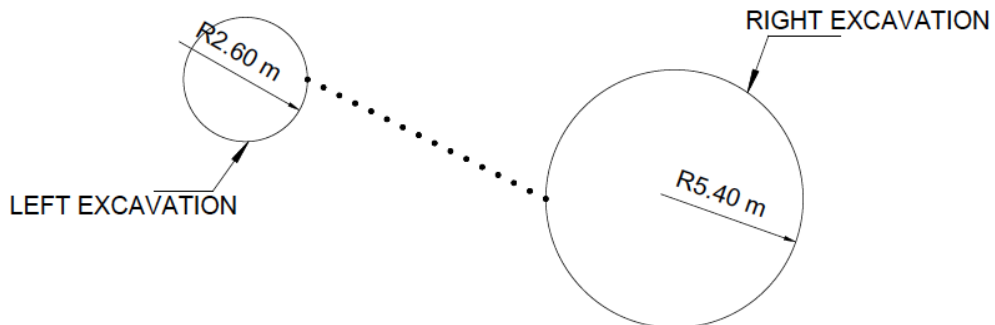
Figure 78 Diagonal connecting the excavations

In order to perform a further evaluation of the behavior of the optimized models versus the unoptimized models, the displacements between the excavations are also evaluated. For that purpose the displacements of the models were compared on 15 points located along a diagonal connecting the excavations (Figure 78). The starting point of this diagonal is at point 1 on the left excavation (refer to Figure 75), finishing on the second excavation (right excavation) at point 3. The coordinates of the 15 points chosen to evaluate the displacements are listed in Table 30.

The method implemented in sections 6.3 and 6.4, to find the displacements along a similar diagonal was also applied in the case of the diagonal connecting the excavations. A mathematical interpolation is also performed in order to find the displacements at the exact locations listed in the table below.

	X	Y	QUAD U_T	QUAD OPT U_T	%e	TRI U_T	TRI OPT U_T	%e
0	45.60	18.00	1.61E-05	1.64E-05	2.33%	1.58E-05	1.58E-05	0.03%
1	46.27	17.67	4.62E-06	4.84E-06	4.61%	8.81E-06	8.82E-06	0.17%
2	46.93	17.33	5.09E-06	4.85E-06	4.75%	3.27E-06	3.27E-06	0.15%
3	47.60	17.00	5.09E-06	4.85E-06	4.75%	6.27E-06	6.26E-06	0.19%
4	48.27	16.67	7.79E-06	7.38E-06	5.23%	9.33E-06	9.32E-06	0.15%
5	48.93	16.33	1.03E-05	9.83E-06	4.37%	9.33E-06	9.32E-06	0.15%
6	49.60	16.00	1.33E-05	1.28E-05	3.63%	1.26E-05	1.25E-05	0.10%
7	50.27	15.67	1.33E-05	1.28E-05	3.63%	1.26E-05	1.25E-05	0.10%
8	50.93	15.33	1.55E-05	1.49E-05	3.31%	1.69E-05	1.68E-05	0.07%
9	51.60	15.00	1.77E-05	1.72E-05	2.95%	1.69E-05	1.68E-05	0.07%
10	52.27	14.67	2.23E-05	2.18E-05	2.53%	2.00E-05	2.00E-05	0.05%
11	52.93	14.33	2.23E-05	2.18E-05	2.53%	2.39E-05	2.39E-05	0.04%
12	53.60	14.00	3.18E-05	3.12E-05	1.89%	2.68E-05	2.68E-05	0.03%
13	54.27	13.67	3.18E-05	3.12E-05	1.89%	3.34E-05	3.34E-05	0.03%
14	54.93	13.33	4.52E-05	4.46E-05	1.42%	3.95E-05	3.95E-05	0.03%
15	55.60	13.00	4.79E-05	4.72E-05	1.40%	4.77E-05	4.77E-05	0.02%

Table 30. Total Displacements on the diagonal connecting the excavations

The models using quadrilateral and triangular elements are treated separately. Thus, in Figure 79, only the total displacements obtained from the models composed of quadrilateral elements are evaluated.

In Figure 79, the points located along the diagonal in the optimized models show smaller displacements placing them beneath the displacements obtained in the unoptimized model. If the displacements are evaluated normalized with respect to the unoptimized model, the differences between both models fluctuate in a range of 1% and 5%. The average percentage of error in the model with quadrilateral elements is 3.20%. The displacements obtained are shown on Table 30.
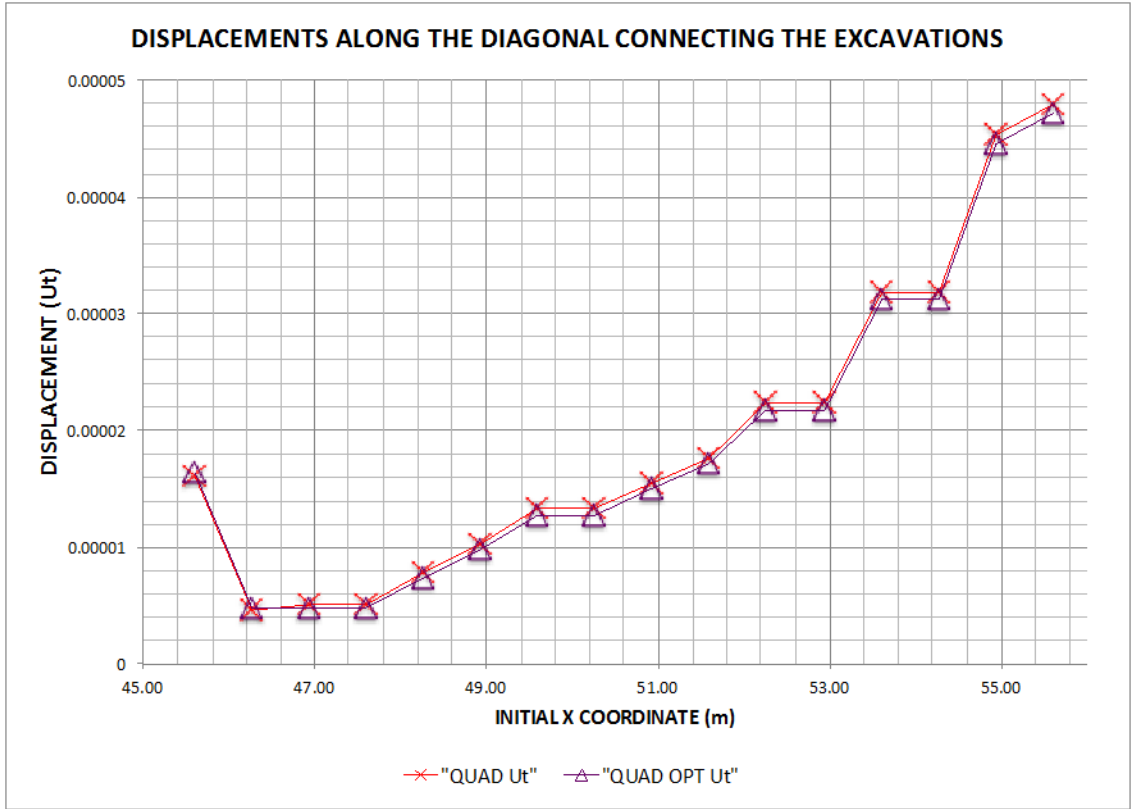
Figure 79 Displacements along the diagonal connecting the excavations - Models with quadrilateral elements
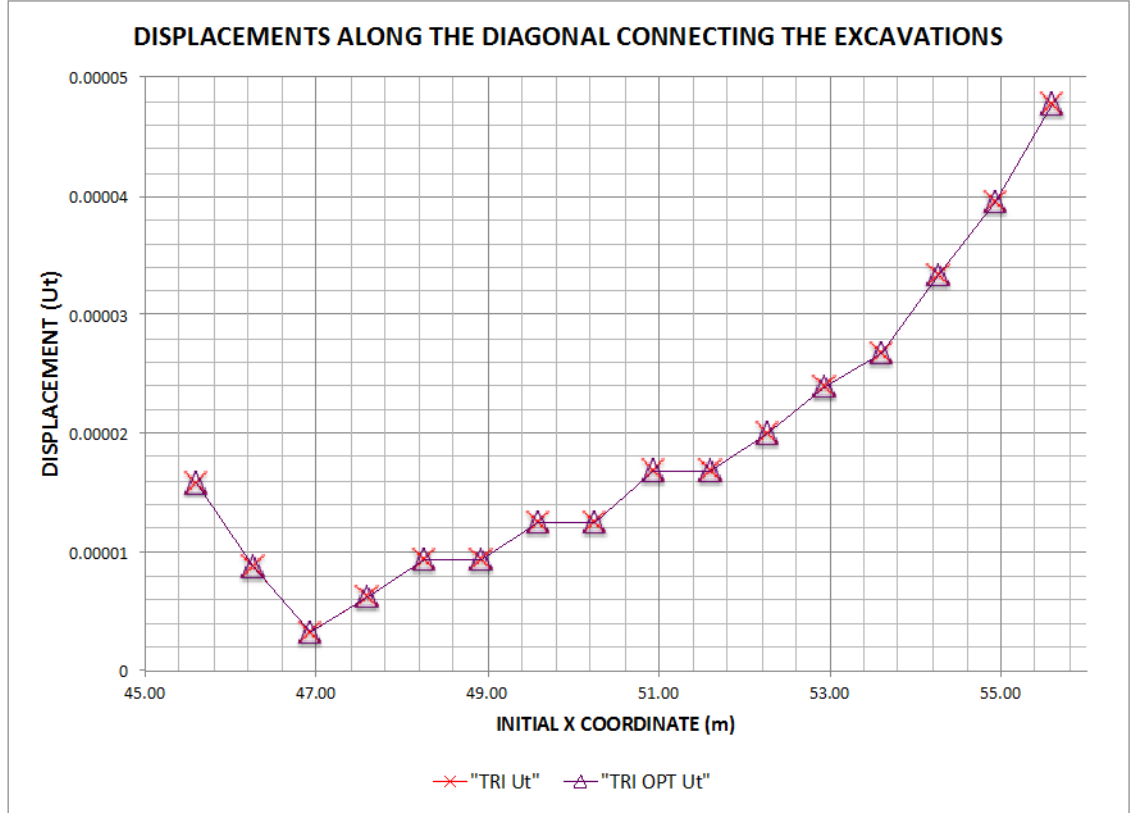
Figure 80 Displacements along the diagonal connecting the excavations - Models with triangular elements

89

The total displacements of the models composed of triangles (only linear order elements or linear, transition and quadratic elements), shown in Figure 80, present similar behavior. The percentages of error between the displacements in the optimized model and the displacements in the unoptimized model vary in small values percentages. The maximum percentage of error obtained is 0.19% and the average of the percentage of error for the 15 points evaluated is 0.09%.

The results in the numerical assessment of the points at the edge of the excavations and along diagonal traced between them (Figure 78), show smaller values of the percentage of error in the models using triangles, leading to conclude the superior behavior of triangular elements in a FEM and their better performance when mesh adaptivity methods are applied.

The tendency of quadrilateral elements to behave with less accuracy was verified by D'Azevedo (2000), where he found that *"for approximating a convex function, although bilinear quadrilaterals are more efficient, linear triangles are more accurate and may be preferred in finite element computations"*. Therefore, we can depict that the high values of percentage of error found in the models using quadrilateral elements, is a consequence of the quadrilateral element per se, rather than due to the p-adaptive mesh refinement procedure or any imprecision in the formulation of the quadrilateral transition elements.

Felippa (2010) also found a better behavior in triangular elements at the time of computing the stresses at the element nodal points. His findings showed at the time of evaluating stresses at the element nodes or at the Gauss integration points (and then extrapolating to the element nodes), that in triangular elements both approaches deliver similar results, in the mean time the quadrilateral elements deliver better results when the stresses are evaluated at the Gauss integration points and not at the elements' nodes.

8. CONCLUSIONS

After implementing and testing the formulation of transition elements and carrying out a final application to underground excavations, where a mesh optimization process has been applied with successful results without reducing the quality in the solution as documented in the previous pages.

It is possible to derive that this thesis has proposed a reliable approach to optimize the stress analysis in geotechnical problems, which leads to the next conclusions:

- The addition of transition elements allowing the combination of linear and quadratic elements, for application to geotechnical engineering problems, in one finite element mesh is a realistic possibility from the results obtained in this thesis.

- The inclusion of analytical solutions for generic and common problems in geotechnical engineering has shown to pay off with considerable savings in computational resources. It is up to the software developers to include these features or to take in the concept of a mesh with three types of elements (quadratic, linear and transitional), which potentially optimizes any software's performance.

- The amount of RAM available in a computer seldom corresponds to the total RAM installed. It is to recall that each process run by the computer occupies a certain amount of RAM, which decreases the available space to perform a calculation. Smaller models (in computational terms) also lead to reduce the possibility of having a full RAM and the chances to have a poor computer performance when a different task needs to be carried out simultaneously with the model calculation process.

- Researchers interested in the behaviour of transitional elements now can count on a work that compares the performance of state-of-the-art formulations of the elements. It might awake the curiosity of those interested in a more accurate formulation and also introduces the SIMFEM software package that they might be used to test their mathematical formulations.

- During the performance evaluation of the transition elements, especially during the test of models type I, the percentages of error (normalized to either a linear or a quadratic element) were around 30%. Nevertheless, these values were dramatically reduced when testing the models type II using triangles where the percentages of error were not greater than 6%, even modeling in 2 different programs.

- In the case of models type II using quadrilaterals; the percentage of error was around 18%. If the results created in SAP2000® were neglected, the percentage of error would be close to 0%. This difference was attributed to factors such as the amount of integration points (4 in SAP2000® and 9 in SIMFEM) or not having the option in SAP2000® to deactivate features as the thickness normal strain, displacements at the thickness direction and others.

- The savings in the time of calculation is an uncertain parameter to evaluate the effectiveness of the optimization process, since it depends on the specifications of the computer used. The most reliable parameter to measure the savings, is the size of the global stiffness matrix which was reduced more than 10 times in the case of the meshes composed of triangular elements and more than 5 times in the case of the meshes composed of quadrilaterals.

- The reduction of computer resources is not only reflected in a less memory usage and faster solution times, implications such as having smaller output files and easier numerical data to be analyzed, that implies faster visualization and transmissions of files, are features that should be also considered.

- With a reduced amount of nodes in the model, the chances to fill up the RAM in the computer used to run the models are reduced. As it is known, once the process completes the RAM capacity of the computer, this has to use part of the hard drive(s) as a RAM (disk swapping), but the accessibility to this memory is not achieved at the same speed and a remarkable increase in the calculation times is the consequence.

- Throughout the testing process of the transition elements, a tendency of the triangular elements to present smaller values of error over the quadrilateral elements was noticed.

9. RECOMMENDATIONS FOR FUTURE WORK

In this case, the application was done using percentages of disturbance based on the Kirsch theory for circular holes in infinite plates, similar concepts might be used to optimize other type of problems in FEM and not only in the geotechnical area. For example consider shallow footings, groundwater flow, stress concentration, Boussinesq approximation, slope stability, local stability problems in excavations, and similar problems.

The application of the concept of transitional elements may take an important place in mathematically more complex problems such as the FEM theory in 3 dimensions, where the sizes of the global stiffness matrices are highly increased due to presence of an extra dimension. These problems may see their calculation times reduced radically without altering the quality of the final solution.

To achieve this application, a new bibliographical compilation must be done in order to find the formulation of transition elements in 3D, which are generally tetrahedral or hexahedral elements. In this case, the work done by Brethauer (1974) in his work titled "Stress Around Pressurized Spherical Cavities In Triaxial Stress Fields" might be used to evaluate the location of a surface of transition elements.

10. BIBLIOGRAPHY

Babuška, I, Flaherty, J.E., Henshaw W. D., Hopcroft, J.E., Oliger, J.E., Tezduya. T. 1995. Modeling, mesh generation, and adaptive numerical methods for partial differential equations. Springer. Vol. 75. New York.

Becker A.A 1992. The boundary element method in engineering a complete course. McGraw Hill. New York.

Braess, D. 1938. Finite Elements: theory, fast solvers, and applications in elasticity theory; translated by Larry L. Shumaker. 2007. 3rd Edition. New York. Cambridge University Press.

Brethauer, G.E. 1974. Stress around pressurized spherical cavities in triaxial stress fields. International Journal of Rock Mechanics and Mining Science. Vol. 11 Issue 3 pp. 91 -96. Pergamon Press Inc. Oxford, England.

Ceccarelli, M. 2007. History of mechanism and machine science, Volume 20. 1st Edition. Italy. Springer.

CSI Computers and Structures Inc. 2007. CSI Analysis reference manual for SAP2000®, ETABS® , and SAFE™. Berkeley, California.

Desai, C. S., edited by Gioda G. 1990. Numerical methods and constitutive modelling in geomechanics New York. Springer.

Desai, C. S. edited by Christian, J. T. 1977. Numerical methods in geotechnical engineering. New York. McGraw-Hill.

D'Azevedo, E. F. 2000. Are bilinear quadrilaterals better than linear triangles. SIAM Journal on Scientific Computing. Vol. 22 Issue 1 pp. 198 - 217. Society for Industrial and Applied Mathematics. Philadelphia, PA, USA.

Ern, A. 1967. Theory and practice of finite elements. New York : Springer.

Felippa, C. University of Colorado Boulder website. Department of Aerospace Engineering and Center for Aerospace Structures, Introduction to Finite Element Method course. http://www.colorado.edu/engineering/CAS/courses.d/IFEM.d/Home.html (17 October, 2010)

Fish, J., Belytschko T., Hoboken, NJ. 2007. A first course in finite elements. Chichester, England. John Wiley & Sons Ltd.

Gupta, A. K. 1978. A finite element for transition from a fine to a coarse grid. International Journal for Numerical Methods in Engineering Vol. 12. Pp. 35-45. John Wiley and Sons Ltd.

Herreknetch AG. 2011. Mechanized tunneling company (12 October 2011). http://www.herrenknecht.com/news/press-section/new-record-breaking-tbm-extends-highway-network-in-italy.html.

Kattan, P. I. 2007. MATLAB guide to finite elements: an interactive approach. 2nd Edition. Berlin. New York. Springer

LaForce, Tara. (22 June, 2011) Stanford University website, "Boundary element method course notes". http://www.stanford.edu/class/energy281/BoundaryElementMethod.pdf

Logan, D. L. 2002. A first course in the finite element method. 3rd Edition. Pacific Grove. Brooks/Cole.

Martin, C.D., Kozac E.T. 1992. Rock characterization: ISRM Symposium, Eurock '92, Chester, UK. Flow measurements in the excavation disturbed zone of Room 209. Pp. 402 – 407. Thomas Telford Services Ltd.

Matsumoto, Yoshiji and Nishioka. 1991. Theoretical tunnel mechanics. 1st ed. Tokyo. University of Tokyo Press.

Nikishkov, G. P. 2007. Introduction to the finite element method. Lecture notes. University of Aizu, Japan.

Pascal J.F., Paul-Louis G. 2008. Mesh generation: application to finite elements. 2nd edition. John Wiley & Sons. Hoboken, USA.

Pepper, D. W., Heinrich J. 2006. The finite element method: basic concepts and applications. 2nd Edition. New York. Taylor & Francis.

Protas, B. (22 June, 2011) McMaster University website, "The boundary element method". http://www.math.mcmaster.ca/~bprotas/MATH745b/bem_01_4.pdf

Rao J.S. 2011. History of rotating machinery dynamics. 1st Edition. Dordrecht, NL. Springer.

Rao, S.S. 2010. The finite element method in engineering, Butterworth-Heinemann. Fifth edition. Pp. 141-169.

Ramamurthy T. 2007. Engineering in rocks for slopes, foundations and tunnels. 2nd Printing. New Delhi. PHI.

Rocscience Inc. 2007. Examine^{2D}, 2D Stress analysis for underground excavations. Verification Manual. Toronto, Ontario.

Rocscience Inc. 2007. Phase^2, 2D elasto-plastic finite element stress analysis program for underground or surface excavations in rock or soil. Verification Manual. Toronto, Ontario.

Singh, M. 1999. Object-oriented Implementation of p-adaptive finite element method. MSc Thesis. Department of Mechanical Engineering and Materials Science. Rice University.

Smith, I. M. 1982. Programming the finite element method with application to geomechanics. 1st Edition. Chichester, New York. John Wiley and Sons Ltd.

U.S. Army Corps of Engineers. 1997. Engineering and design, tunnels and shafts in rock. Engineer Manual. Washington DC. Department of the Army.

Wan, K. 2004. Transition finite element analysis for mesh refinement in plane and plate bending analyses. MPh Thesis. Department of Mechanical Engineering. The University of Hong Kong. Hong Kong.

Zsaki, A.M. and J. H. Curran. 2005. "A continuum mechanics based framework for boundary and finite element mesh optimization in two dimensions for application in excavation analysis", International Journal for Numerical and Analytical Methods in Geomechanics. Vol. 29, Issue 4, pp. 369-393. John Wiley and Sons Ltd.

Zsaki, A.M. and J. H. Curran. 2005. "A continuum mechanics based framework for optimizing boundary and finite element meshes associated with underground excavations – Accuracy, efficiency and applications", International Journal for Numerical and Analytical Methods in Geomechanics. Vol. 29, No. 13, pp. 1299-1315. John Wiley and Sons Ltd.

Zsaki, A.M. and J. H. Curran. 2005. "A continuum mechanics based framework for optimizing boundary and finite element meshes associated with underground excavations – Framework", International Journal for Numerical and Analytical Methods in Geomechanics, Vol. 29, No. 13, pp. 1271-1298. John Wiley and Sons Ltd.

Zsaki, A.M. 2010. SIMFEM. [Software] Department of Building, Civil and Environmental Engineering, Concordia University, 1455 de Maisonneuve Blvd, W., EV006.139, Montreal, Que., Canada H3G 1M8.

APPENDIX 1. TYPE I MODELS USING QUADRILATERAL ELEMENTS – RESULTS

| SCHEME | NAME | SOFTWARE | DISPLACEMENT | | |
			Ux (m)	Uy (m)	LOC
	QUA4N & QUAD_SAP	SIMFEM	0	0	LL
			0	0	LR
			0.005117	-0.01705	UR
			-0.005117	-0.01705	UL
			0	0	LL
	QUA5NA	SIMFEM	-0.0029174	-0.016381	UL
			-0.0036185	-0.007506	ML
			0	0	LL
			0	0	LR
			0.005742	-0.018293	UR
			-0.0029174	-0.016381	UL
	QUA5NB	SIMFEM	0.0053813	-0.01832	UR
			-2E-12	-0.01659	UM
			-0.0052813	-0.01832	UL
			0	0	LL
			0	0	LR
			0.0053813	-0.01832	UR
	QUA5NC	SIMFEM	0	0	LR
			0.0036185	-0.007506	MR
			0.002917	-0.016381	UR
			-0.005742	-0.01829	UL
			0	0	LL
			0	0	LR

97

SCHEME	NAME	SOFTWARE	DISPLACEMENT Ux (m)	Uy (m)	LOC
	QUA5ND	SIMFEM	0	0	LL
			0	0	LM
			0	0	LR
			0.0051168	-0.017056	UR
			-0.0051168	-0.017056	UL
			0	0	LL
	QUA7NA	SIMFEM	-0.003524	-0.017515	UL
			-0.003772	-0.00838	ML
			0	0	LL
			0	0	LM
			0	0	LR
			0.003777	-0.003891	MR
			0.003547	-0.01753	UR
			-0.003524	-0.017515	UL
	QUA7NB	SIMFEM	0	0	LR
			0.003737	-0.008498	MR
			0.003714	-0.017789	UR
			3E-10	-0.0174	UM
			-0.003714	-0.017789	UL
			-0.003737	-0.008498	ML
			0	0	LL
			0	0	LR
	QUA7NC	SIMFEM	0.004739	-0.01839	UR
			0	-0.01697	UM
			-0.004724	-0.01787	UL
			-0.004	-0.008264	ML
			0	0	LL
			0	0	LM
			0	0	LR
			0.004739	-0.01839	UR

			DISPLACEMENT		
SCHEME	NAME	SOFTWARE	Ux (m)	Uy (m)	LOC
	QUA7ND	SIMFEM	0	0	LL
			0	0	LM
			0	0	LR
			0.004002	-0.008265	MR
			0.004724	-0.01787	UR
			0	-0.01697	UM
			-0.004742	-0.018406	UL
			0	0	LL
	QUA8N	SIMFEM	0	0	LL
			0	0	LM
			0	0	LR
			0.003737	-0.008497	MR
			0.003712	-0.01778	UR
			0.00000003	-0.017402	UM
			-0.003712	-0.01778	UL
			-0.003737	-0.008497	ML
			0	0	LL
	QUAD_SAP	SAP2000®	0	0	LL
			0	0	LR
			0.0061	-0.0182	UR
			-0.0061	-0.0182	UL

APPENDIX 2. TYPE I MODELS USING TRIANGULAR ELEMENTS - RESULTS

| SCHEME | NAME | SOFTWARE | DISPLACEMENT | | LOC |
			Ux (m)	Uy (m)	
	Phase3L	Phase²	0	0	LL
			0.001787	-0.014346	UR
			-0.0062603	-0.018818	UL
			0	0	LL
			0	0	LR
			0.001787	-0.014346	UR
	Phase6Q	Phase²	0	0	LL
			-0.000281438	-0.0085912	C
			0.0036954	-0.018710024	UR
			-0.0007276	-0.018078	UM
			-0.0050645	-0.018856	UL
			-0.0040408	-0.0097888	ML
			0	0	LL
			0	0	LM
			0	0	LR
			0.0032644	-0.0087553	MR
			0.0036954	-0.018710024	UR
	TRI4NAC	SIMFEM	0	0	LL
			0	0	LR
			-0.0001026	-0.008305	C
			-0.00538	-0.01776	UL
			0	0	LL
			0	0	LR
			0.00589	-0.01827	UR
			-0.00538	-0.01776	UL
	TRI4NBC	SIMFEM	0	0	LL
			0	0	LR
			0.005382	-0.01776	UR
			0.0001026	-0.008305	C
			0	0	LL
			-0.005895	-0.01827	UL
			0.005382	-0.01776	UR

	SCHEME	NAME	SOFTWARE	DISPLACEMENT		LOC
				Ux (m)	Uy (m)	
		TRI4NAV	SIMFEM	0	0	LR
				0.004978	-0.02179	UR
				0	-0.0161645	UM
				-0.002553	-0.01665	UL
				0	0	LR
				0	0	LM
				0	0	LL
				-0.002553	-0.01665	UL
		TRI4NBV	SIMFEM	0	0	LL
				0	0	LM
				0	0	LR
				0.0011419	-0.01527	UR
				0	0	LL
				-0.006819	-0.0204	UL
				-0.002429	-0.01703	UM
				0.0011419	-0.01527	UR
		TRI4NAH	SIMFEM	0	0	LR
				0.003603	-0.010429	MR
				0.005544	-0.01948	UR
				-0.00116	-0.01674	UL
				0	0	LR
				0	0	LL
				-0.003521	-0.007827	ML
				-0.00116	-0.01674	UL
		TRI4NBH	SIMFEM	0	0	LL
				0.0014183	-0.017209	UR
				-0.00485	-0.01892	UL
				-0.00335	-0.01021	ML
				0	0	LL
				0	0	LR
				0.003726	-0.0080688	MR
				0.0014183	-0.017209	UR

			DISPLACEMENT		
SCHEME	NAME	SOFTWARE	Ux (m)	Uy (m)	LOC
	TRI4NAM1	SIMFEM	0	0	LR
			-0.0012729	-0.01548	UL
			0	0	LL
			0	0	LM
			0	0	LR
			0.003531	-0.010213	MR
			0.005862	-0.01936	UR
			-0.0012729	-0.01548	UL
	TRI4NAM2	SIMFEM	-0.0015552	-0.0169	UL
			-0.003734	-0.007964	ML
			0	0	LL
			0	0	LR
			-0.0015552	-0.0169	UL
			0.001662	-0.01768	UM
			0.005929	-0.0199	UR
			0	0	LR
	TRI5NAB	SIMFEM	0	0	LL
			0.001329	-0.01285	UR
			-0.002585	-0.015802	UM
			-0.006529	-0.01897	UL
			-0.0034017	-0.009711	ML
			0	0	LL
			0	0	LM
			0	0	LR
			0.010252	0.002562	MR
			0.001329	-0.01285	UR
	TRI5NBB	SIMFEM	-0.002866	-0.01736	UL
			-0.00443	-0.008314	ML
			0	0	LL
			0	0	LM
			0	0	LR
			-0.002866	-0.01736	UL
			0	-0.01791	UM
			0.003723	-0.0193	UR
			-0.00251	-0.01005	MR
			0	0	LR

			DISPLACEMENT		
SCHEME	NAME	SOFTWARE	Ux (m)	Uy (m)	LOC
	TRI5NAV	SIMFEM	0	0	LL
			-0.000186	-0.008244	C
			0.004786	-0.01789	UR
			-0.00089944	-0.0177	UM
			-0.0067612	-0.01975	UL
			0	0	LL
			0	0	LM
			0	0	LR
			0.004786	-0.01789	UR
	TRI5NBV	SIMFEM	0	0	LR
			0.005758	-0.01854	UR
			0	-0.01769	UM
			-0.005754	-0.01907	UL
			-0.00011907	-0.008283	C
			0	0	LR
			0	0	LM
			0	0	LL
			-0.005754	-0.01907	UL
	TRI5NAH	SIMFEM	0.004201	-0.01897	UR
			-0.00418	-0.01759	UL
			-0.003853	-0.009249	ML
			0	0	LL
			-0.0001351	-0.008675	C
			0.004201	-0.01897	UR
			0.003456	-0.00892	MR
			0	0	LR
			0	0	LL
	TRI5NBH	SIMFEM	-0.002585	-0.01733	UL
			-0.00296	-0.008145	ML
			0	0	LL
			0	0	LR
			0.000453	-0.008633	C
			-0.002585	-0.01733	UL
			0.005837	-0.01924	UR
			0.004353	-0.010108	MR
			0	0	LR

103

SCHEME	NAME	SOFTWARE	DISPLACEMENT Ux (m)	Uy (m)	LOC
	TRI6NA	SIMFEM	0.003695	-0.01871	UR
			-0.0007276	-0.0180778	UM
			-0.005064	-0.01885	UL
			-0.00404	-0.009788	ML
			0	0	LL
			-0.0002814	-0.008591	C
			0.003695	-0.01871	UR
			0.003264	-0.008755	MR
			0	0	LR
			0	0	LM
			0	0	LL
	TRI6NB	SIMFEM	0	0	LR
			-0.0002814	-0.008591	C
			-0.005064485	-0.018856	UL
			-0.0040408	-0.0097888	ML
			0	0	LL
			0	0	LM
			0	0	LR
			0.0032644	-0.0087553	MR
			0.0036954	-0.01871	UR
			-0.000727692	-0.018077876	UM
			-0.005064485	-0.018856	UL
	TRI3NA & TRIA_SAP	SIMFEM & SAP2000®	-0.0058	-0.0192	UL
			0	0	LL
			0	0	LR
			-0.0058	-0.0192	UL
			0.0019	-0.0153	UR
			0	0	LR
	TRI3NB & TRIB_SAP	SIMFEM & SAP2000®	0.0058	-0.0187	UR
			-0.0017	-0.0146	UL
			0	0	LL
			0.0058	-0.0187	UR
			0	0	LR
			0	0	LL

GLOSSARY

BEM:	Boundary Element Method
DEM:	Discrete Element Method
EDZ:	Excavation Disturbed Zone
FDM:	Finite Difference Method
FEA:	Finite Element Analysis
FEM:	Finite Element Method
PDE:	Partial Differential Equation
TBM:	Tunnel Boring Machine